Laboratory Evaluation of the AERONET and GRASP Retrieval Algorithms

G.L. Schuster[1], R. Espinosa[2], L. Ziemba[1], A. Beyersdorf[1], A. Rocha-Lima[2;3], B. Anderson[1], J. V. Martins[2], O. Dubovik[4], F. Ducos[4], D. Fuertes[5], T. Lapyonok[4], M. Shook[1], Y. Derimian[4], R. Moore[1]

1. NASA Langley Research Center; 2. University of Maryland, Baltimore County; 3. NASA Goddard Space Flight Center; 4. Universite de Lille 1/CNRS; 5. GRASP-SAS, Remote sensing developments

AERONET Cimel

angular dependence of scattering

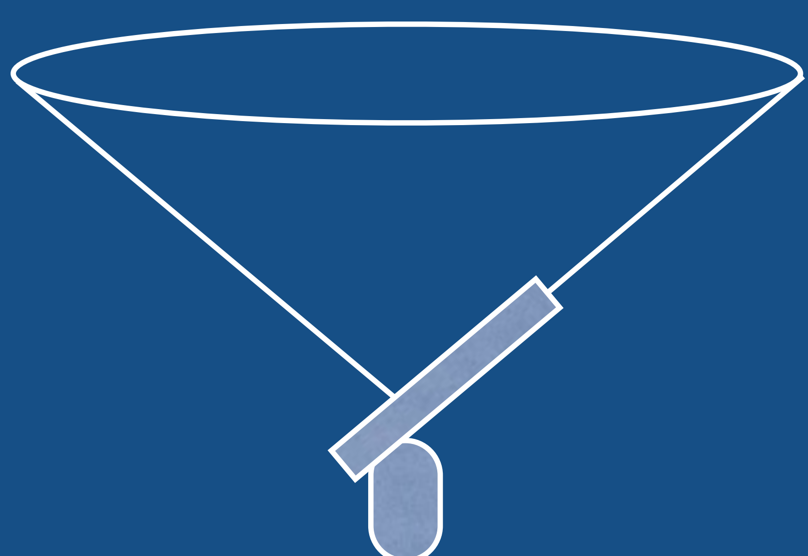

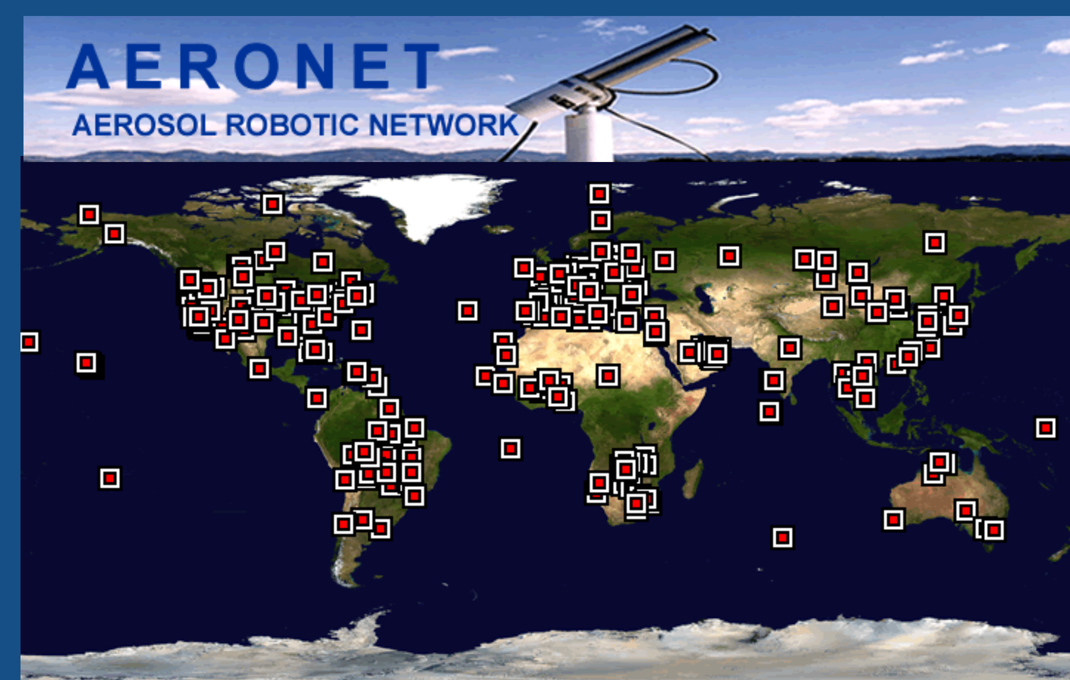

Brent Holben
P.I.
GSFC

Brent Holben, PI
Products

- Size Distribution
- Complex Refractive Index
- SSA

Laboratory Evaluation of the AERONET and GRASP Retrieval Algorithms

G.L. Schuster[1], R. Espinosa[2], L. Ziemba[1], A. Beyersdorf[1], A. Rocha-Lima[2;3], B. Anderson[1], J. V. Martins[2], O. Dubovik[4], F. Ducos[4], D. Fuertes[5], T. Lapyonok[4], M. Shook[1], Y. Derimian[4], R. Moore[1]

1. NASA Langley Research Center; 2. University of Maryland, Baltimore County; 3. NASA Goddard Space Flight Center; 4. Universite de Lille 1/CNRS; 5. GRASP-SAS, Remote sensing developments

AERONET Cimel

angular dependence of scattering

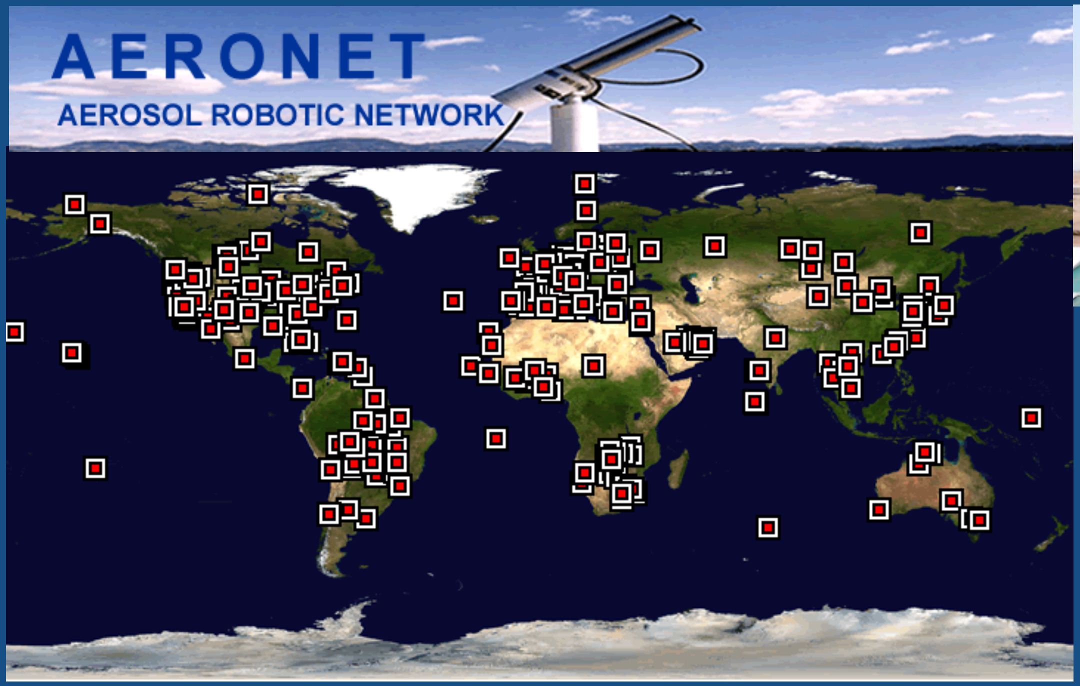

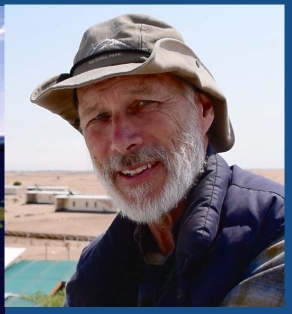

Brent Holben
P.I.
GSFC

Brent Holben, PI

Products

- Size Distribution
- Complex Refractive Index
- SSA

Simplified Schematic

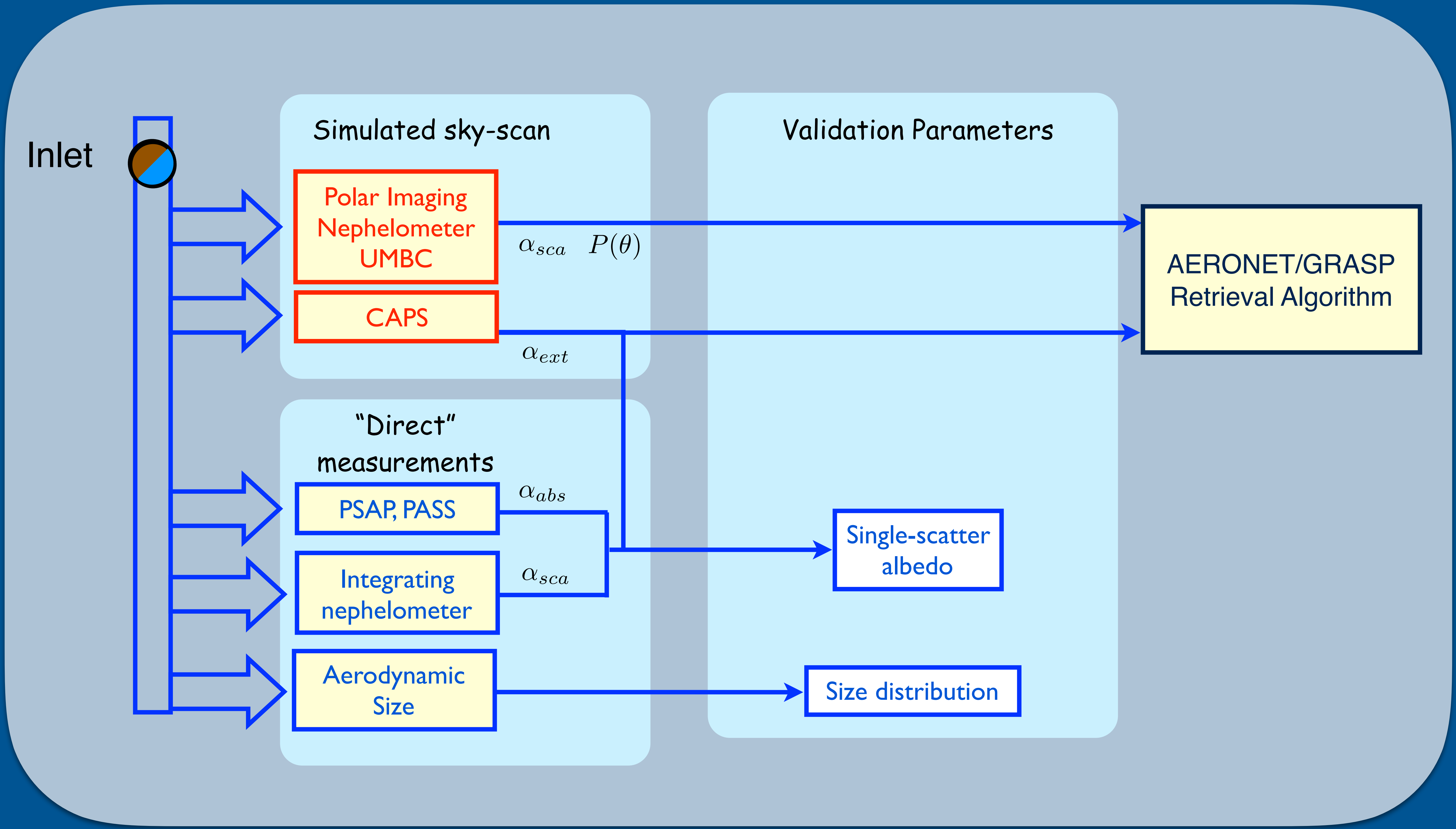

CAPS: Cavity Attenuated Phase Shift monitor
PSAP: Particle Soot Absorption Photometer
PASS: Photoacoustic Soot Spectrometer

Simplified Schematic

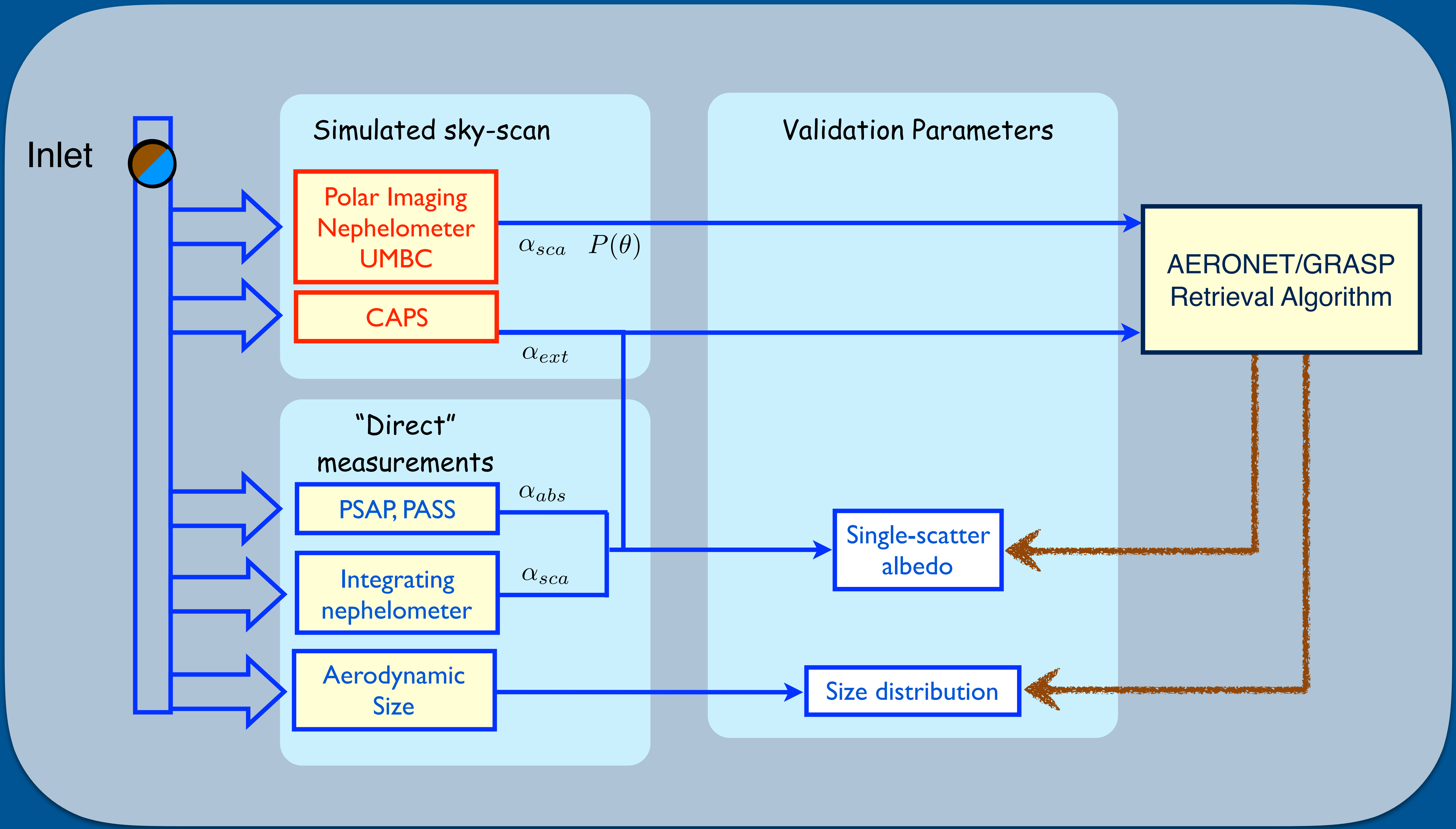

CAPS: Cavity Attenuated Phase Shift monitor
PSAP: Particle Soot Absorption Photometer
PASS: Photoacoustic Soot Spectrometer

Simplified Schematic

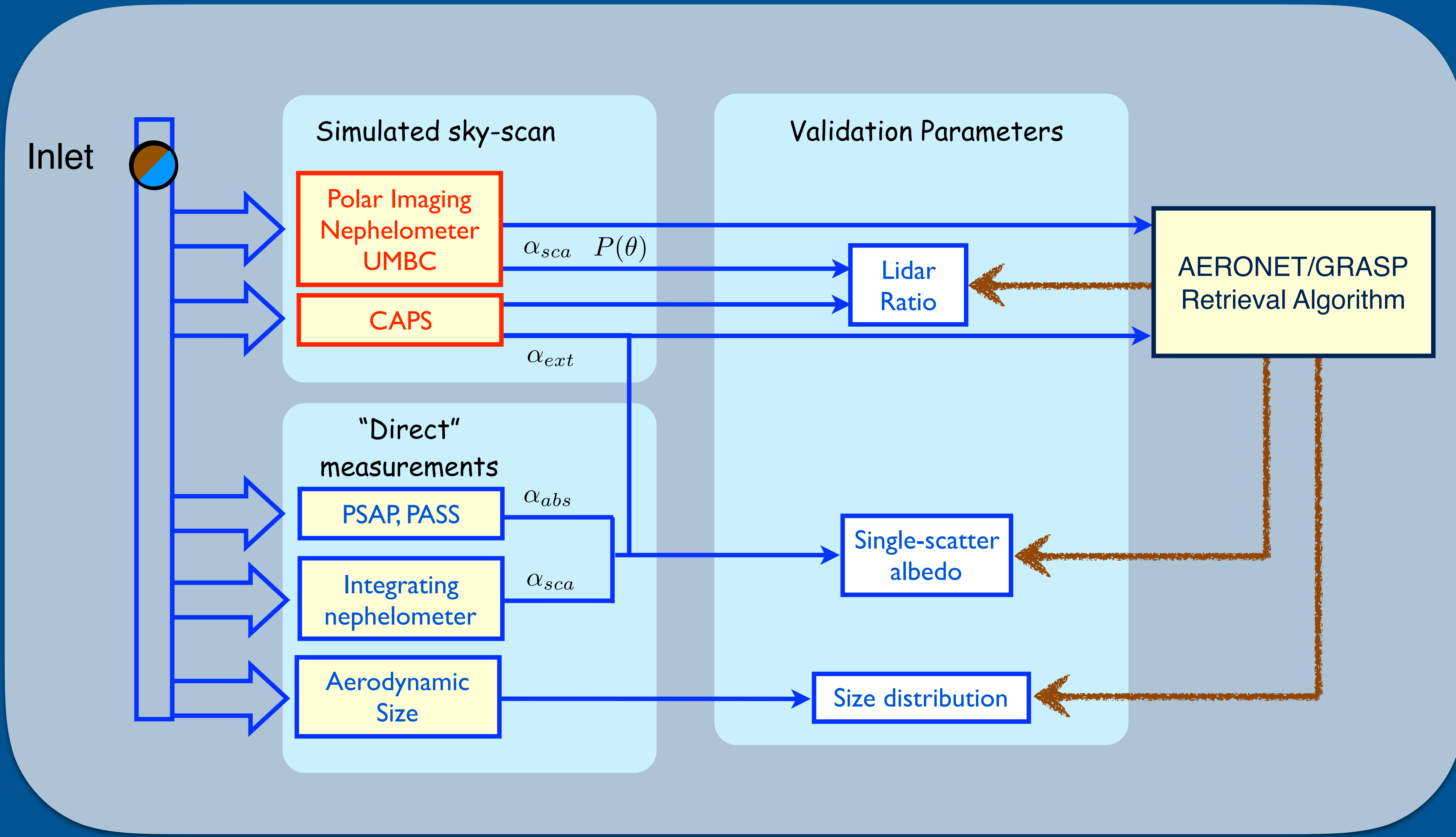

CAPS: Cavity Attenuated Phase Shift monitor
PSAP: Particle Soot Absorption Photometer
PASS: Photoacoustic Soot Spectrometer

Subsampling PI-Neph to match AERONET measurement angles

- AERONET robot pauses for measurements at fixed specified azimuth angles, ϕ.
- Thus, scattering angles (Θ) are determined by the solar zenith angle $(\theta_\circ)$ and ϕ .

$$\cos\Theta = 1 - \sin^2\theta_\circ(1 - \cos\phi)$$

193: Mt. St. Helens, PM1

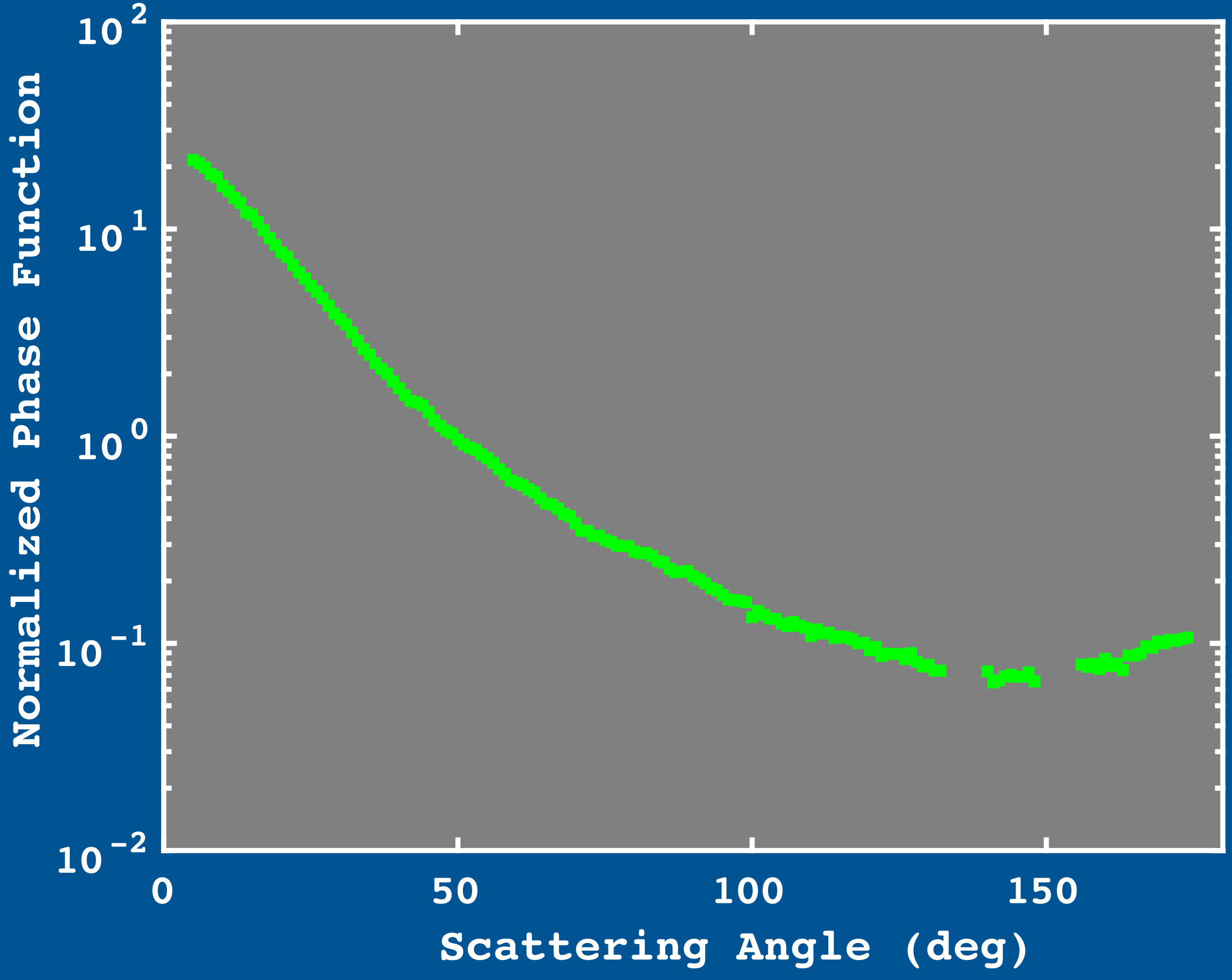

Simulating AERONET with GRASP

- Input radiances only considered at AERONET scattering angles.
- Real refr. index range: 1.33 — 1.6
- Imag. refr. index range: 0.0005 — 0.5
- Radius range: 0.05 — 15 um (22 bins)
- Residuals less than 8%

Some Inconsistencies

- PI-Neph wavelengths different than AERONET: 473, 532, 671 nm vs 440-870
- Instrument sensitivities
- No multiple scattering

"Necessary but not sufficient" experiment

Subsampling PI-Neph to match AERONET measurement angles

- AERONET robot pauses for measurements at fixed specified azimuth angles, ϕ.
- Thus, scattering angles (Θ) are determined by the solar zenith angle $(\theta_\circ)$ and ϕ .

$$\cos\Theta = 1 - \sin^2\theta_\circ(1 - \cos\phi)$$

193: Mt. St. Helens, PM1

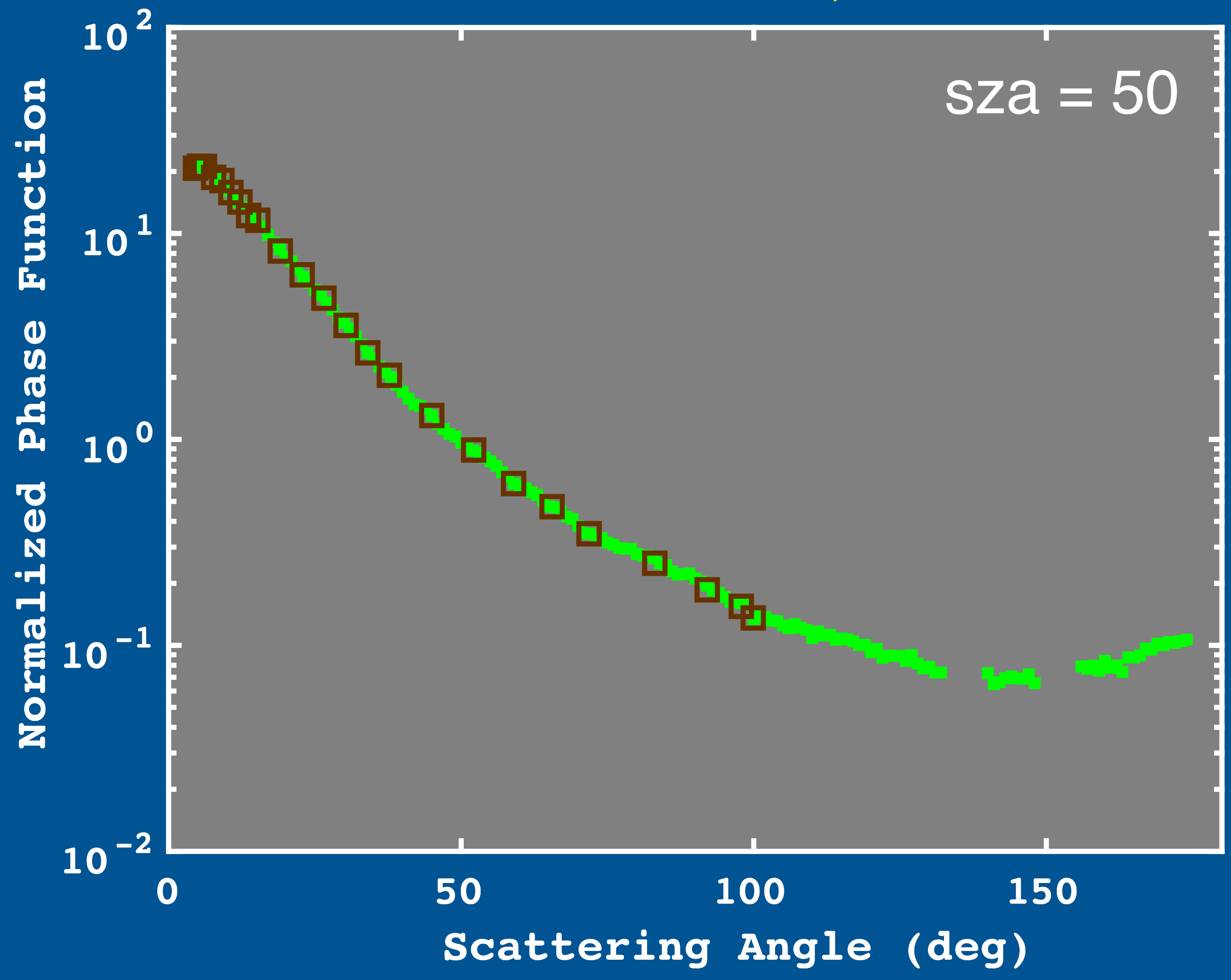

Simulating AERONET with GRASP

- Input radiances only considered at AERONET scattering angles.
- Real refr. index range: 1.33 — 1.6
- Imag. refr. index range: 0.0005 — 0.5
- Radius range: 0.05 — 15 um (22 bins)
- Residuals less than 8%

Some Inconsistencies

- PI-Neph wavelengths different than AERONET: 473, 532, 671 nm vs 440-870
- Instrument sensitivities
- No multiple scattering

"Necessary but not sufficient" experiment

Subsampling PI-Neph to match AERONET measurement angles

- AERONET robot pauses for measurements at fixed specified azimuth angles, ϕ.
- Thus, scattering angles (Θ) are determined by the solar zenith angle $(\theta_\circ)$ and ϕ .

$$\cos\Theta = 1 - \sin^2\theta_\circ(1-\cos\phi)$$

193: Mt. St. Helens, PM1

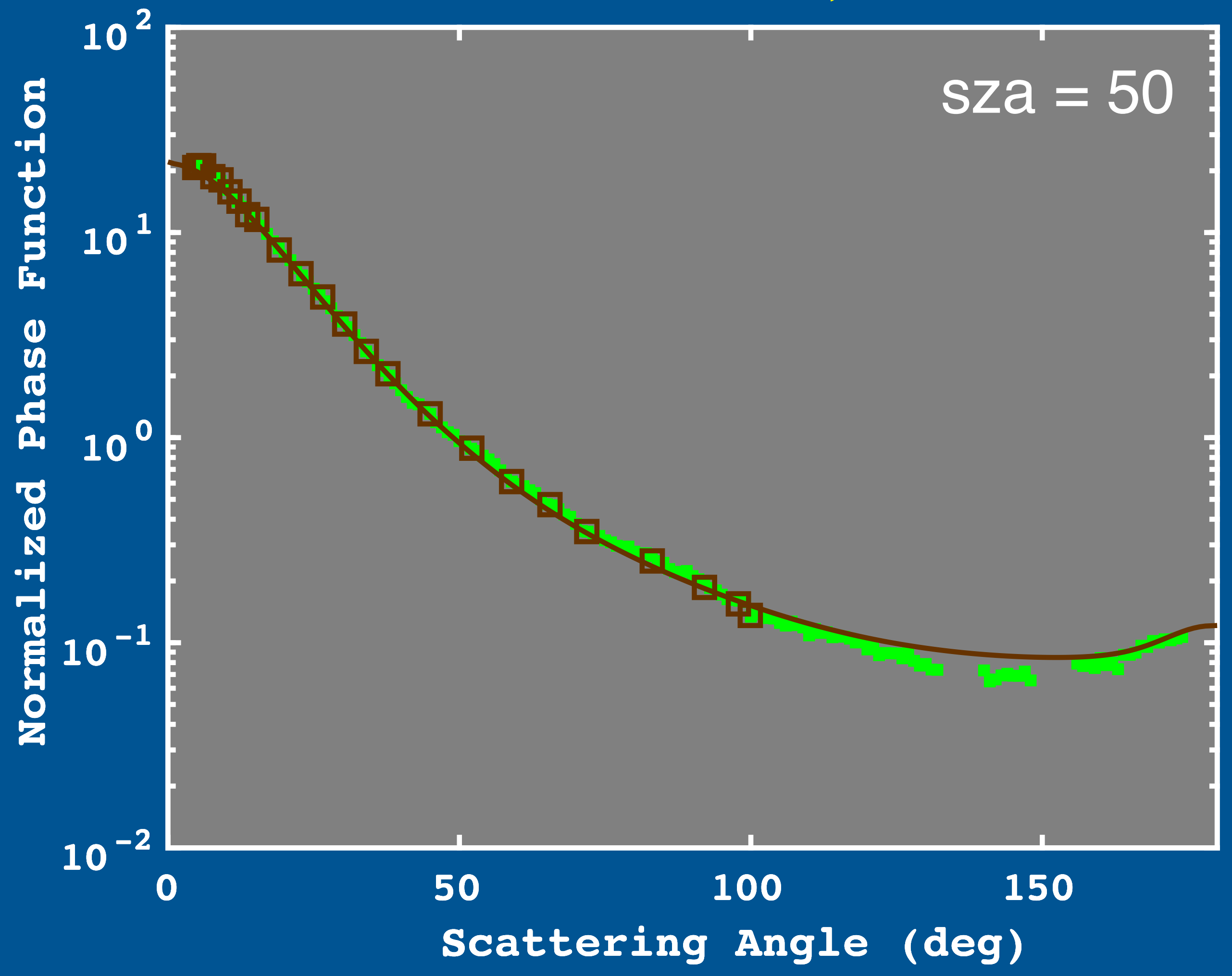

Simulating AERONET with GRASP

- Input radiances only considered at AERONET scattering angles.
- Real refr. index range: 1.33 — 1.6
- Imag. refr. index range: 0.0005 — 0.5
- Radius range: 0.05 — 15 um (22 bins)
- Residuals less than 8%

Some Inconsistencies

- PI-Neph wavelengths different than AERONET: 473, 532, 671 nm vs 440-870
- Instrument sensitivities
- No multiple scattering

"Necessary but not sufficient" experiment

Tested 285 samples

Tests include humidified and dried runs for both PM1 and PM2.5.

Minerals
Hectorite
Hematite
Arizona Test Dust
Cambrianshale Imt-2
Saz-2 Ca-rich Montmorillonite
Illite-smectite
Na-Montmorillonite
Montmorillonite, STx-1b
Montmorillonite SCa-3
Israel, Negev Desert
Senegal
Ripidolite CCa-2
Palygorskite
Arginotec NX Europe
A1 ultrafine test dust
Silica Dust

Artist Pigments
Lemon Ocher
Yellow Ocher Light
Blue Ridge Hematite
Brown Ocher (Goethite)
Nicosia Yellow Ocher
Ambrogio Yellow Earth

Volcanic Ash
Mt. St. Helens
Fuego Volcano
Pinatubo
Iceland Volcano
Mt. St. Helens
Puyeheu
Spurr
Gulagong

Soot
Ashrae #2
120 nm soot
105 nm Soot
60 nm soot
25 nm soot
70 nm soot
Fullerene soot

Spheres
600 nm PSL
900 nm PSL
100 nm PSL

Standards
Ammonium Sulfate
Ammonium Nitrate
Adipic Acid

Mixtures
Mont STx + 5% Goethite (by mass)
Mont STx + 10% Goethite (by mass)
Amm Sulf + Goethite (9—26% of scat)
Amm Sulf + Amborgio Yellow Earth (11-30% of scat)
Amm Sulf + Italian Yellow Earth (11-38%)
Amm Sulf + Soot (0.78–0.97 SSA)
Internal Silica+AS
Internal Silica+fullerene
Internal Hematite+AS
Internal Goethite+AS
Internal Goethite+AS
Internal Hematite+AS
AS + Soot - 0.87–0.98 SSA
AN/Full_Int #1 + 7-15% Arginotec
AN/Full_Int #2 + 9-17% Mont. Sca-3
Mont. STx, 150–1000 Mm-1
Mont. STx, APS=0.63, 19LPM
Mont. STx, APS=0.73, 12LPM
Mont. STx, APS=0.94, 8LPM
Mont. STx, APS=1.38, 5LPM
Mont. STx, APS=1.57, 2LPM
600 (60/Mm) + 900 nm (100/Mm) PSL
600 (110/Mm) + 900 nm (100/Mm) PSL
Mont. SCa-3 + Amm. Nit. (~61%)
Mont. SCa-3 + Amm. Nit. (9–80%)
Fullerene + Amm. Nit. (external, 0.86–0.96 SSA)
Silica + Fullerene
Silica + AS (Ext, 16% Dust)
Blue Ridge Hematite + AS (Ext, 19% Dust)
Blue Ridge Hematite + AS (Ext, 16% Dust)
Arginotec + AS (Ext, 24% Dust)
Arginotec + AS (Ext, 21% Dust)
AN+Full (Ext, SSA = 0.92)
Argintoc + AN/Full_Ext (18% Dust, SSA = 0.92)
Mont. Sca-3 + AN/Full_Ext (18% Dust, SSA = 0.92)
Mont. Sca-3 + AN/Full_Ext (18% Dust when dry, SSA = 0.92)
Argintoc + AN/Full_Ext (18% Dust when dry, SSA = 0.92)

Comparing Retrieved Size Distributions to Aerodynamic Size

Evaluate size distribution retrievals using the effective variance and effective radius.

$$r_{eff} = \frac{\int r \times \pi r^2 n(r) dr}{\int \pi r^2 n(r) dr}$$

$$v_{eff} = \frac{\int (r - r_{eff})^2 \times \pi r^2 n(r) dr}{r_{eff}^2 \int \pi r^2 n(r) dr}$$

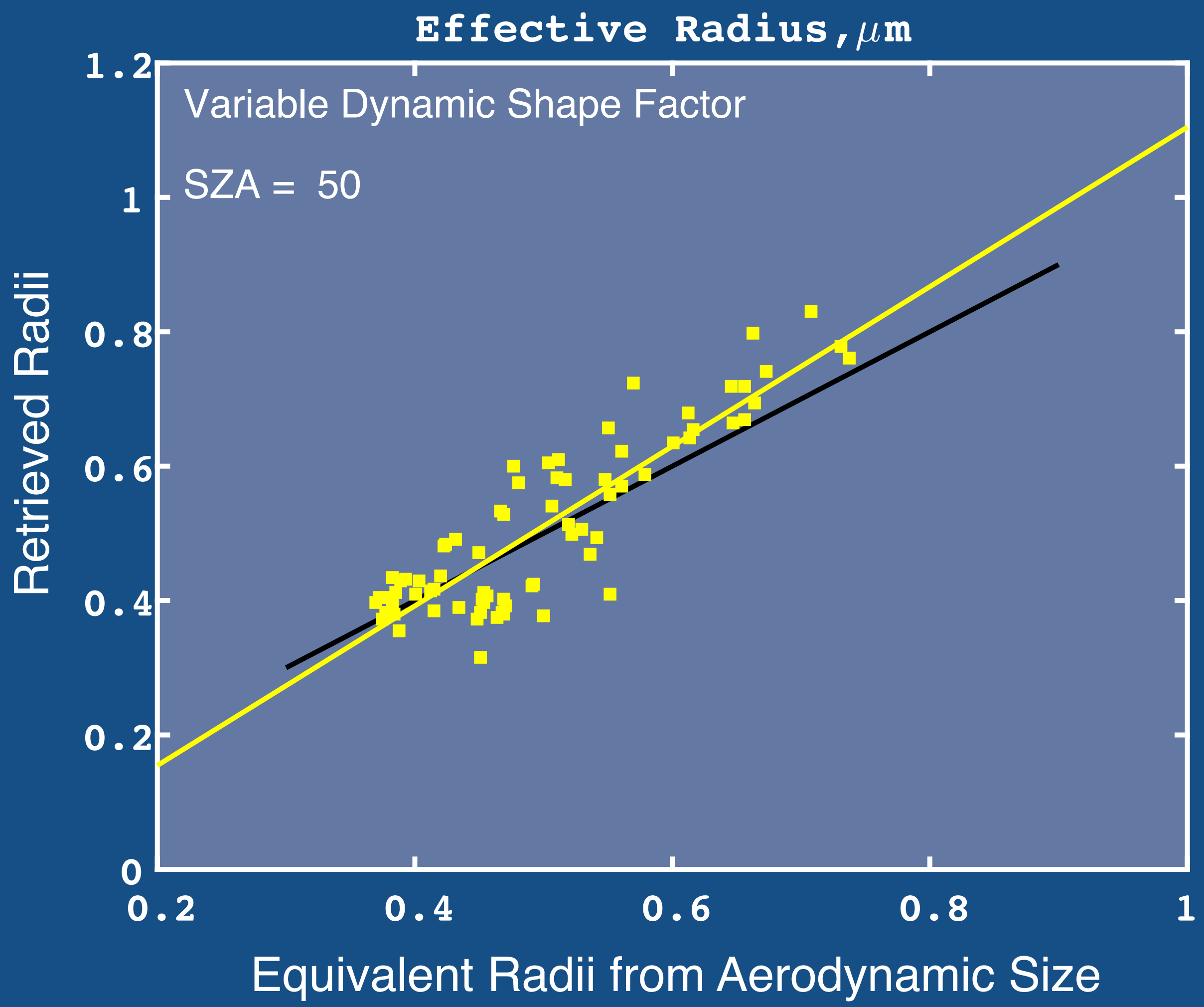

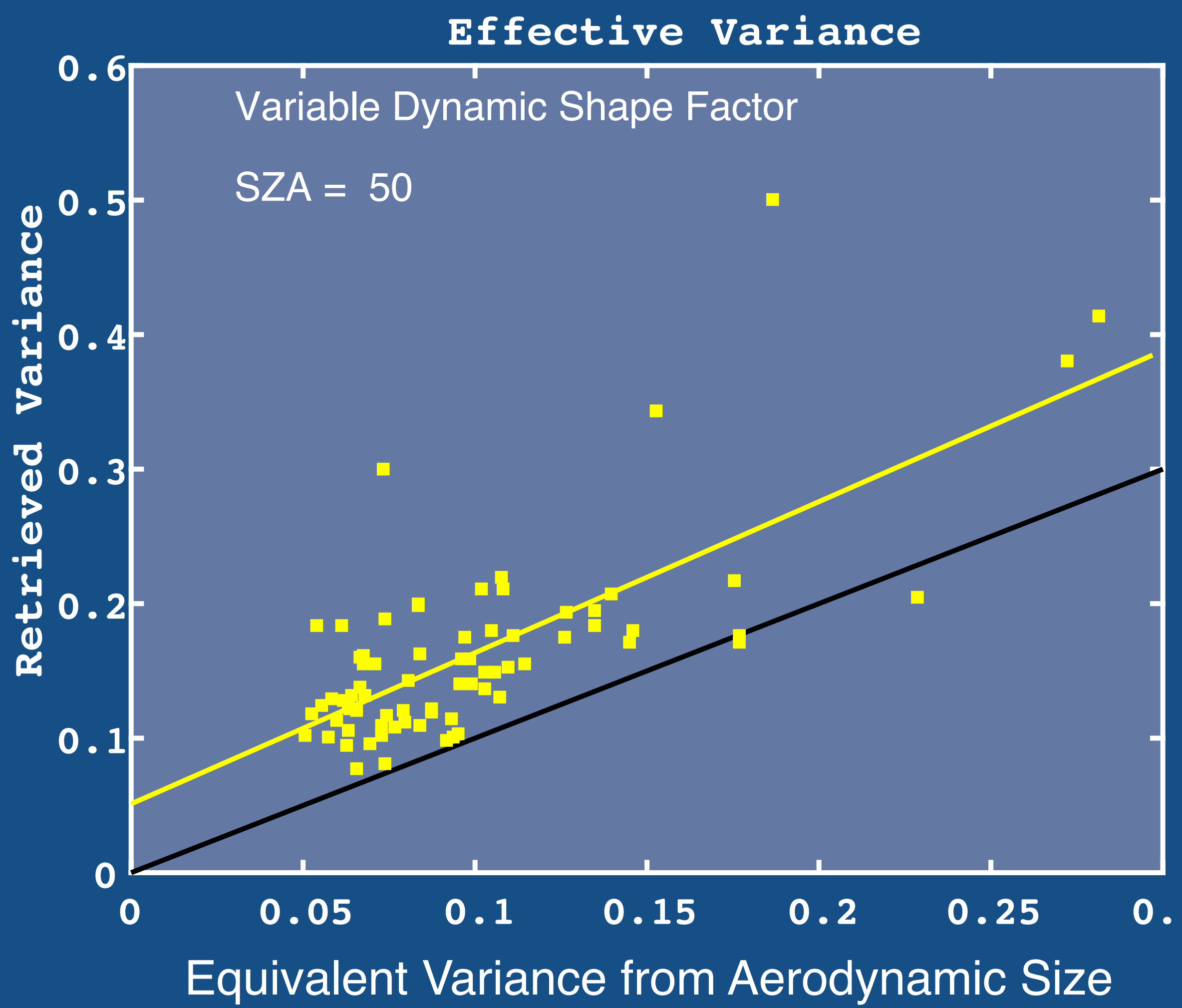

	slope	intcpt	cc	Absolute Bias	Relative Bias (%)	RMS	N	SZA	DSF
R_eff	1.1876	-0.0830	0.8796	0.0108	1	0.0566	74	50	vrbl
V_eff	1.1231	0.0512	0.7161	0.0634	116	0.0710	74	50	vrbl

Single Scatter Albedo

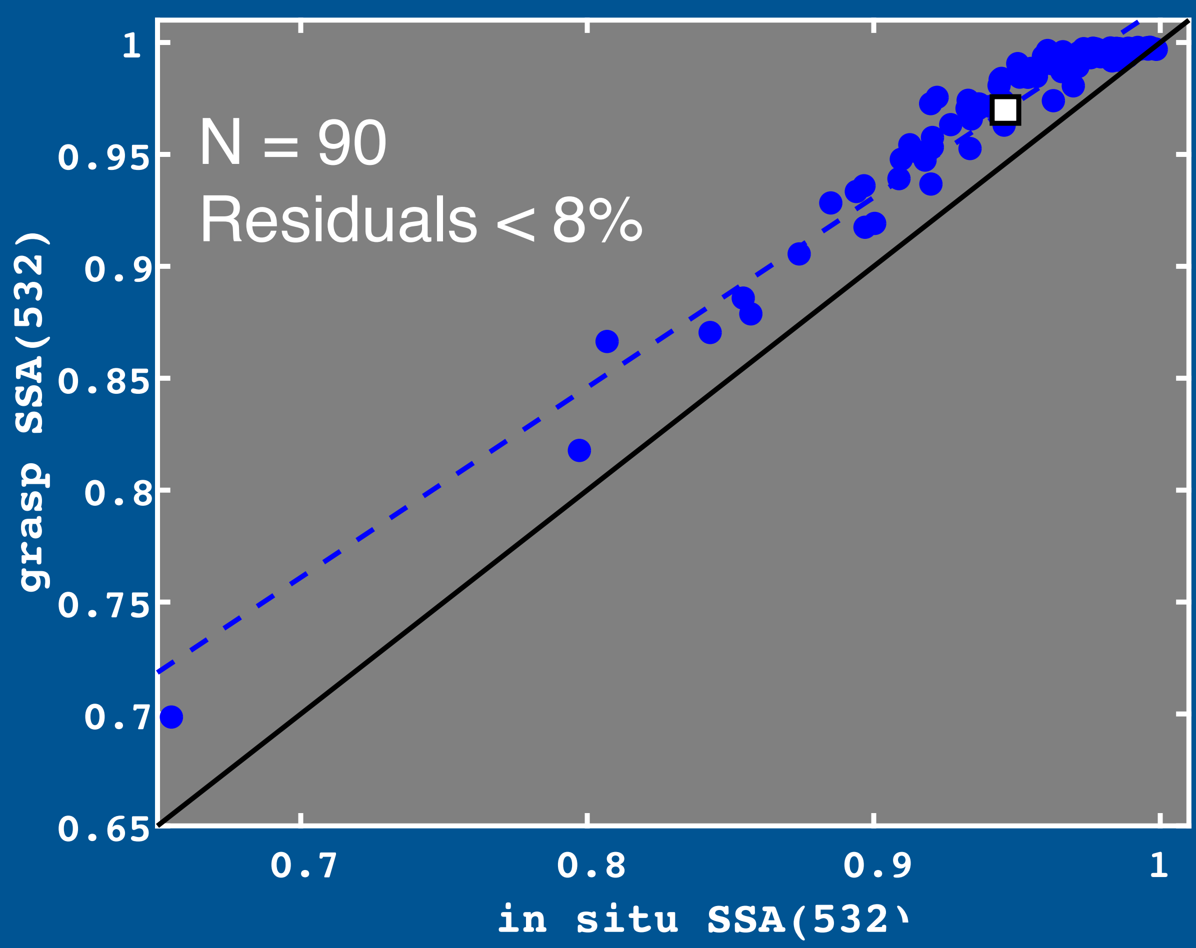

PSAP

	(EXT - ABS_{psap}) / EXT
corr. coef.	0.973
slope	0.860
intercept	0.155
abslt bias	0.023

EXT:
Extinction via Cavity Attenuated Phase Shift Spectrometer (CAPS)

Single Scatter Albedo

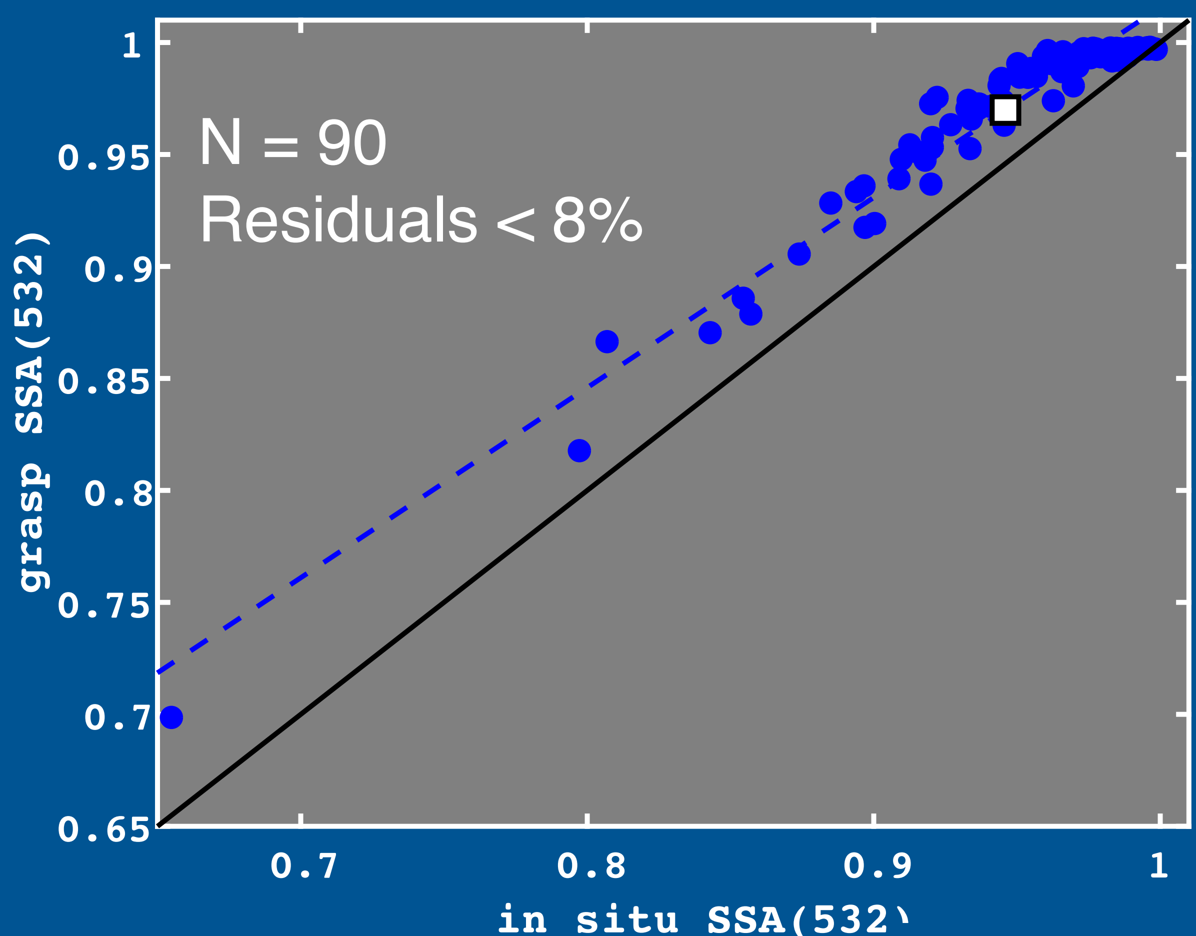

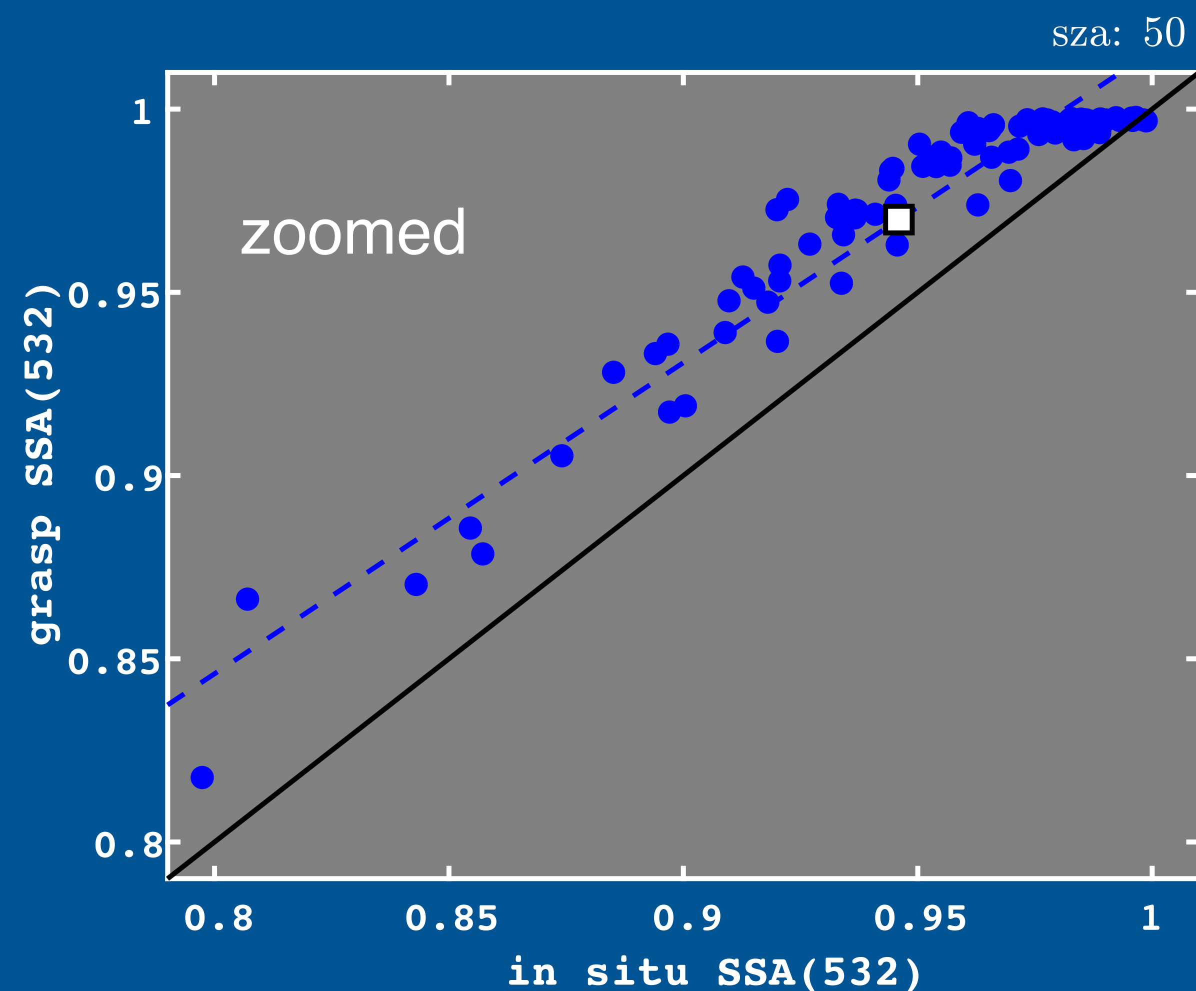

PSAP

	$\frac{(EXT - ABS_{psap})}{EXT}$
corr. coef.	0.973
slope	0.860
intercept	0.155
abslt bias	0.023

EXT:
Extinction via Cavity Attenuated Phase Shift Spectrometer (CAPS)

Single Scatter Albedo

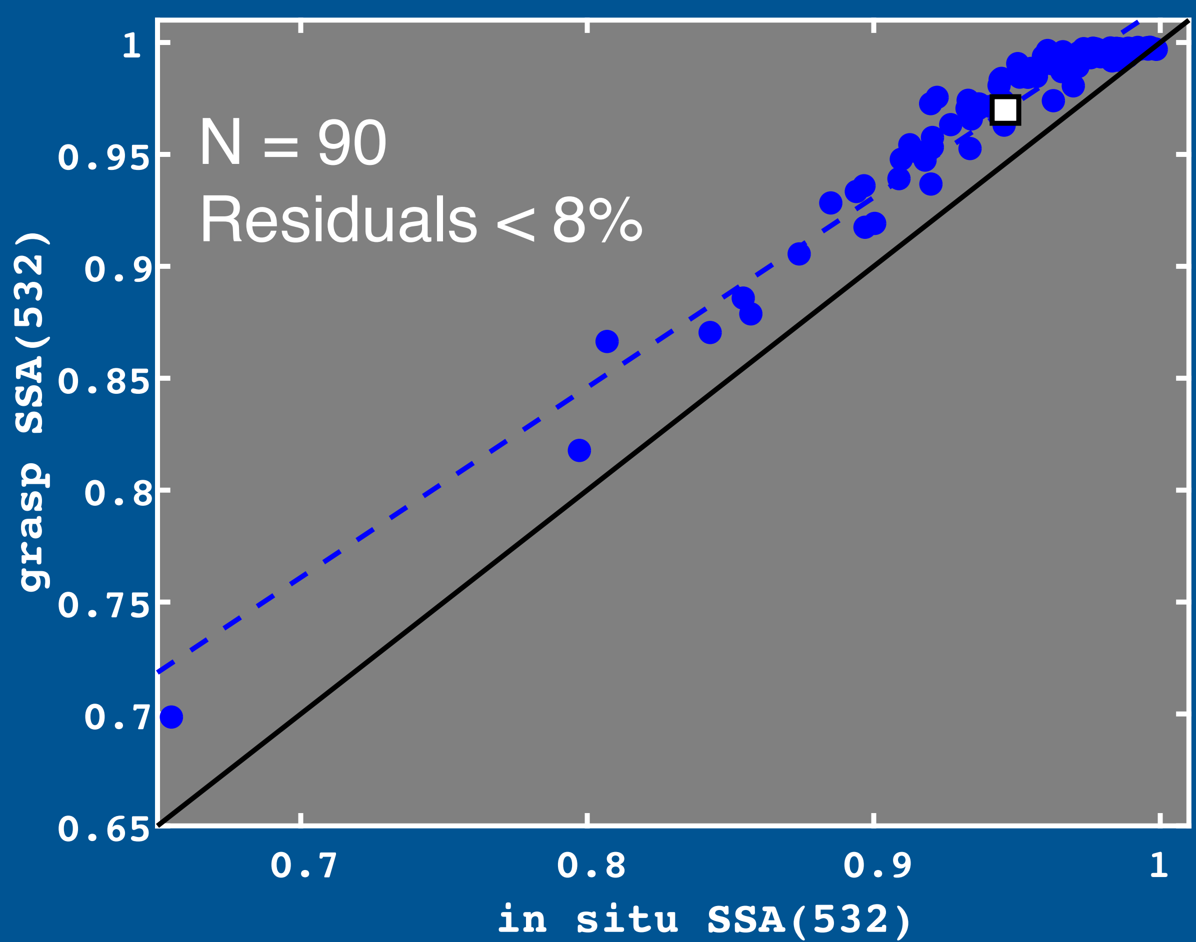

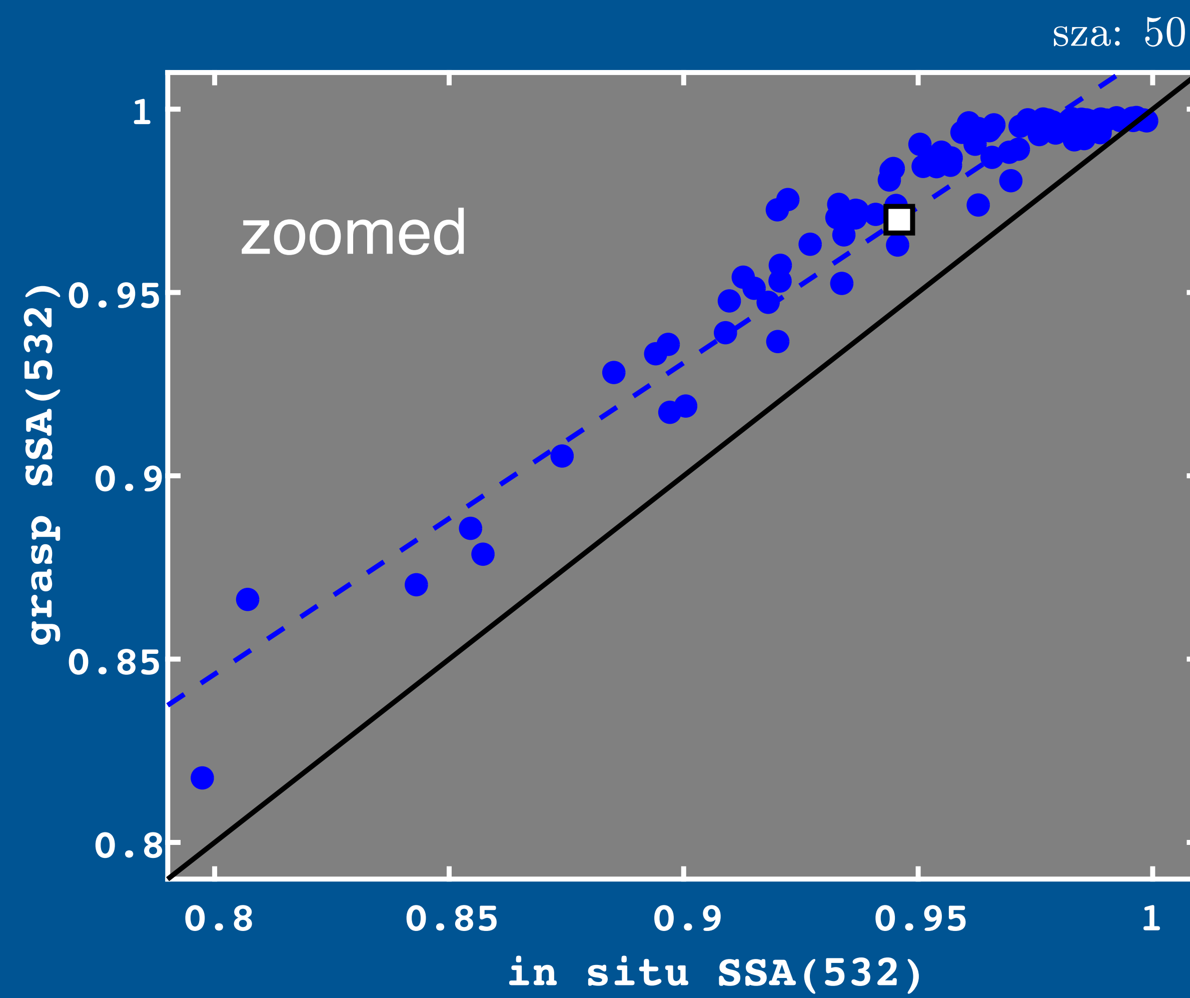

	PSAP	PASS	Neph
	$\frac{(EXT - ABS_{psap})}{EXT}$	$\frac{(EXT - ABS_{pass})}{EXT}$	$\frac{SCA}{EXT}$
corr. coef.	0.973	0.976	0.955
slope	0.860	0.871	0.895
intercept	0.155	0.146	0.131
abslt bias	0.023	0.026	0.036

EXT:
Extinction via Cavity Attenuated Phase Shift Spectrometer (CAPS)

Solar Zenith Angle effects on Absolute Bias

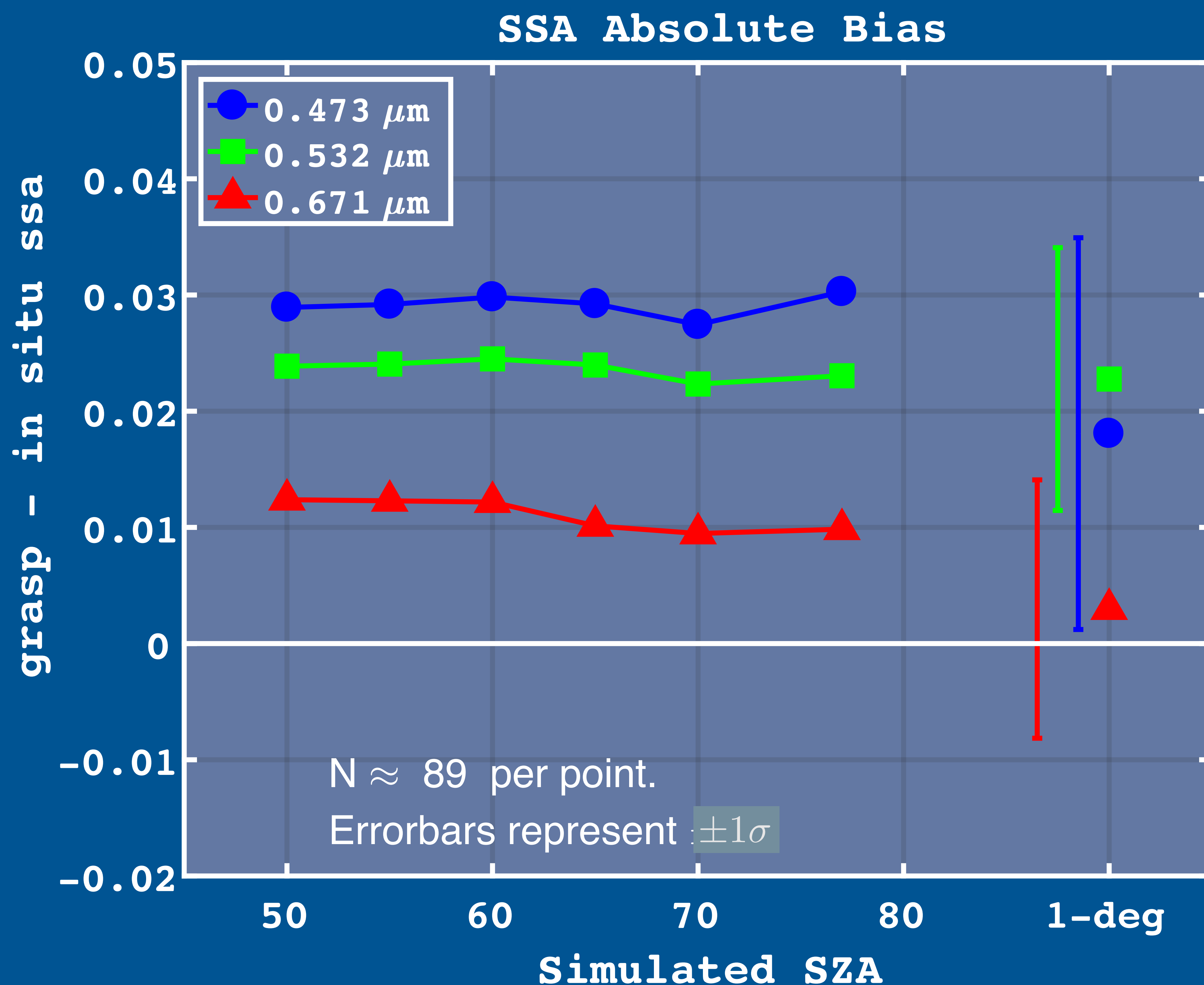

AERONET Retrievals at Low AOT

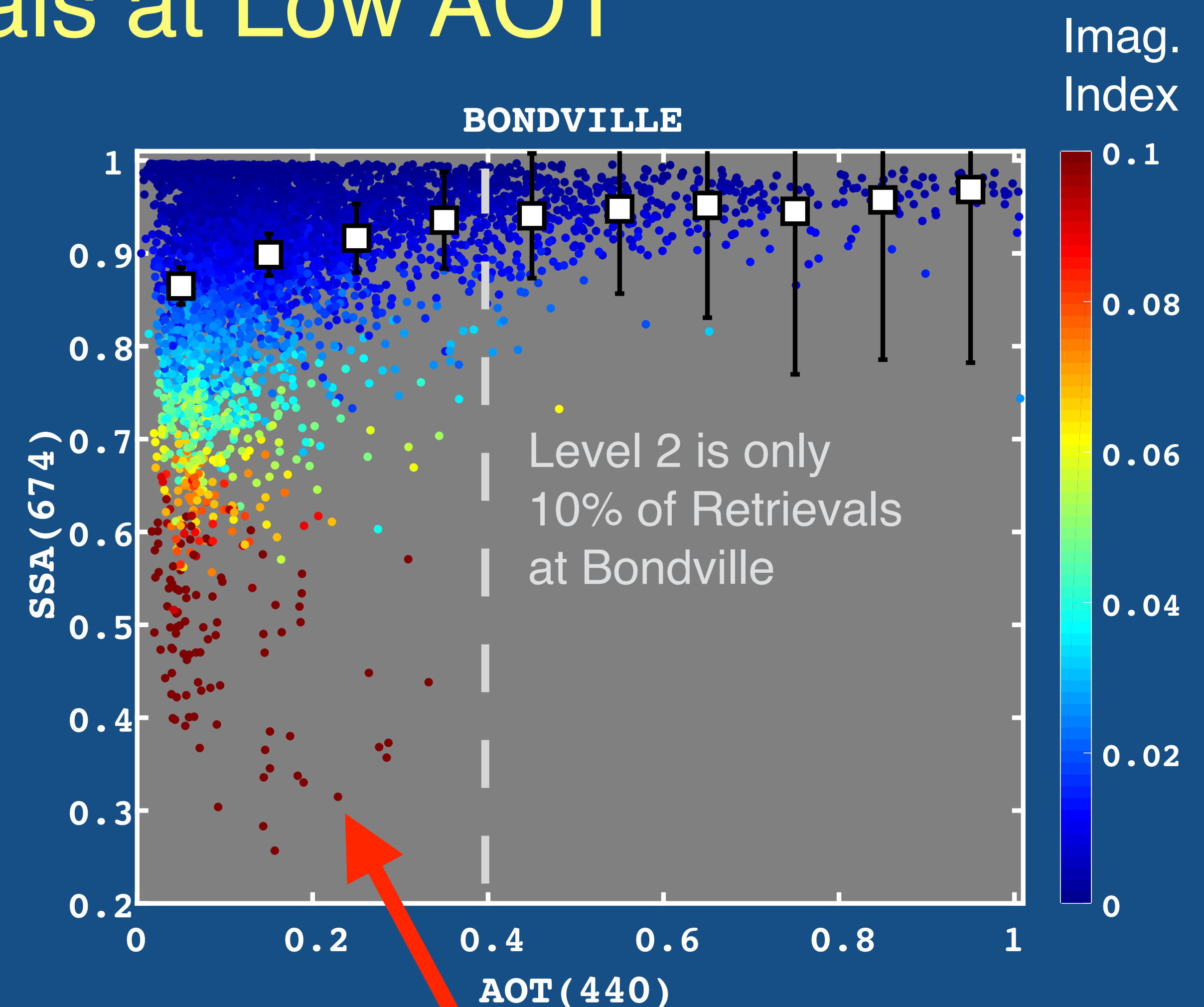

Important: Only use Lev 1.5 when corresponding Lev 2 size distribution exists

AERONET Retrievals at Low AOT

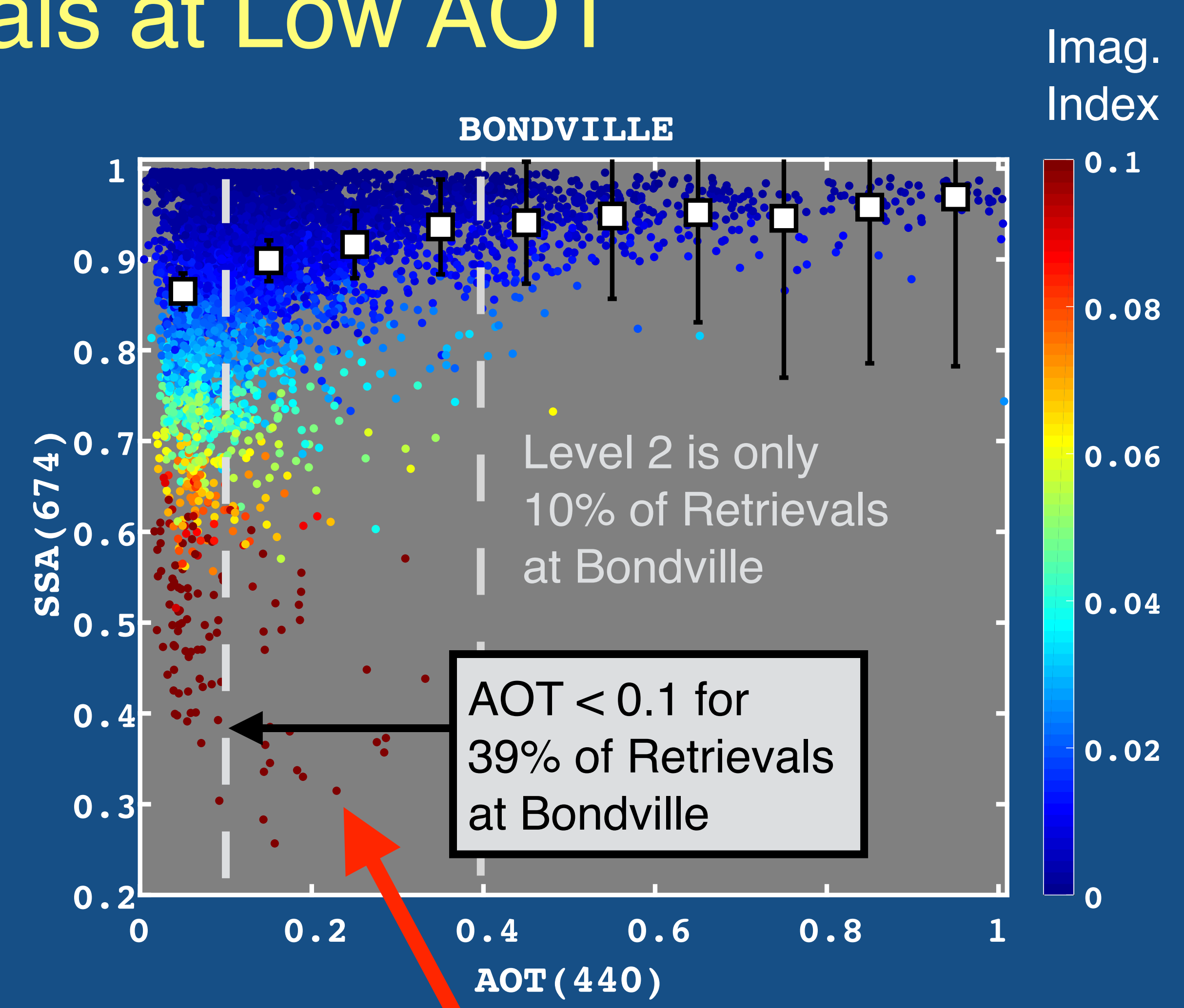

Important: Only use Lev 1.5 when corresponding Lev 2 size distribution exists

AERONET Retrievals at Low AOT

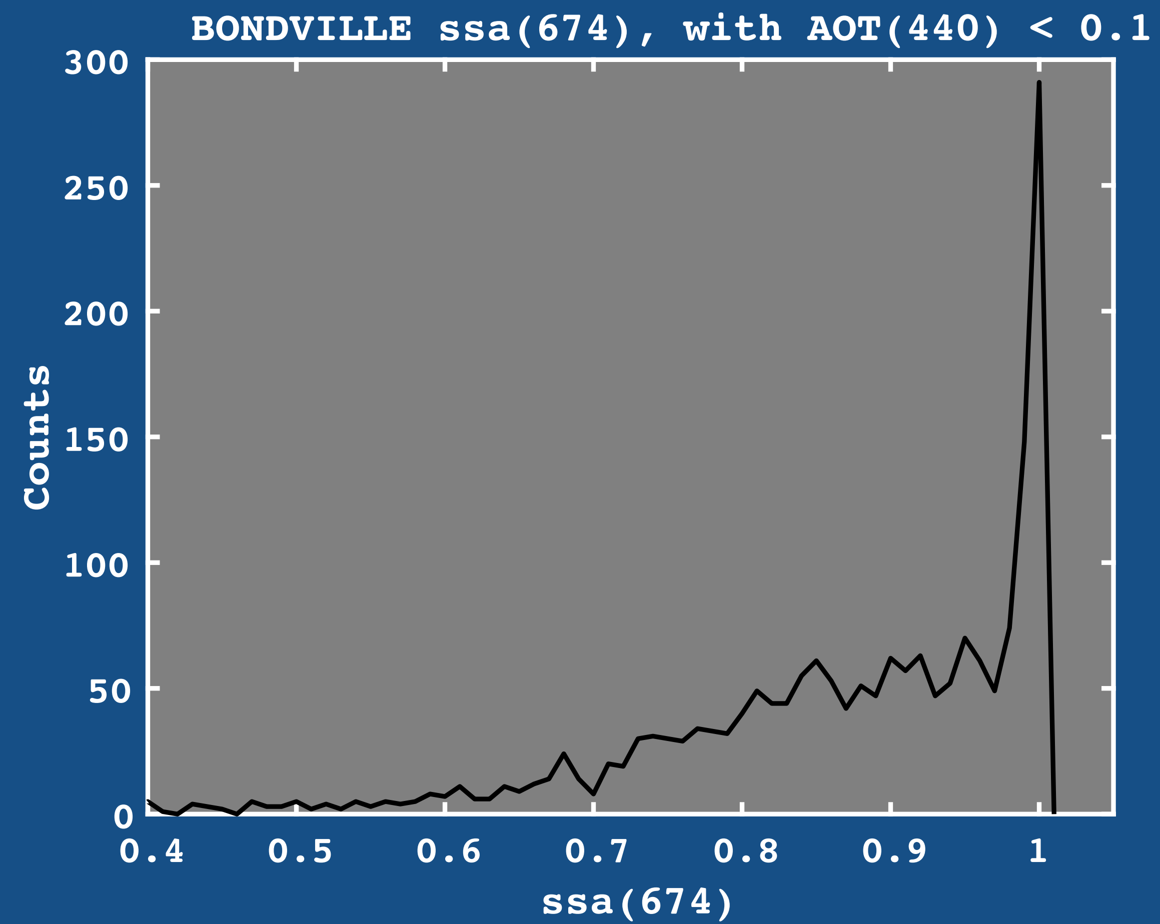

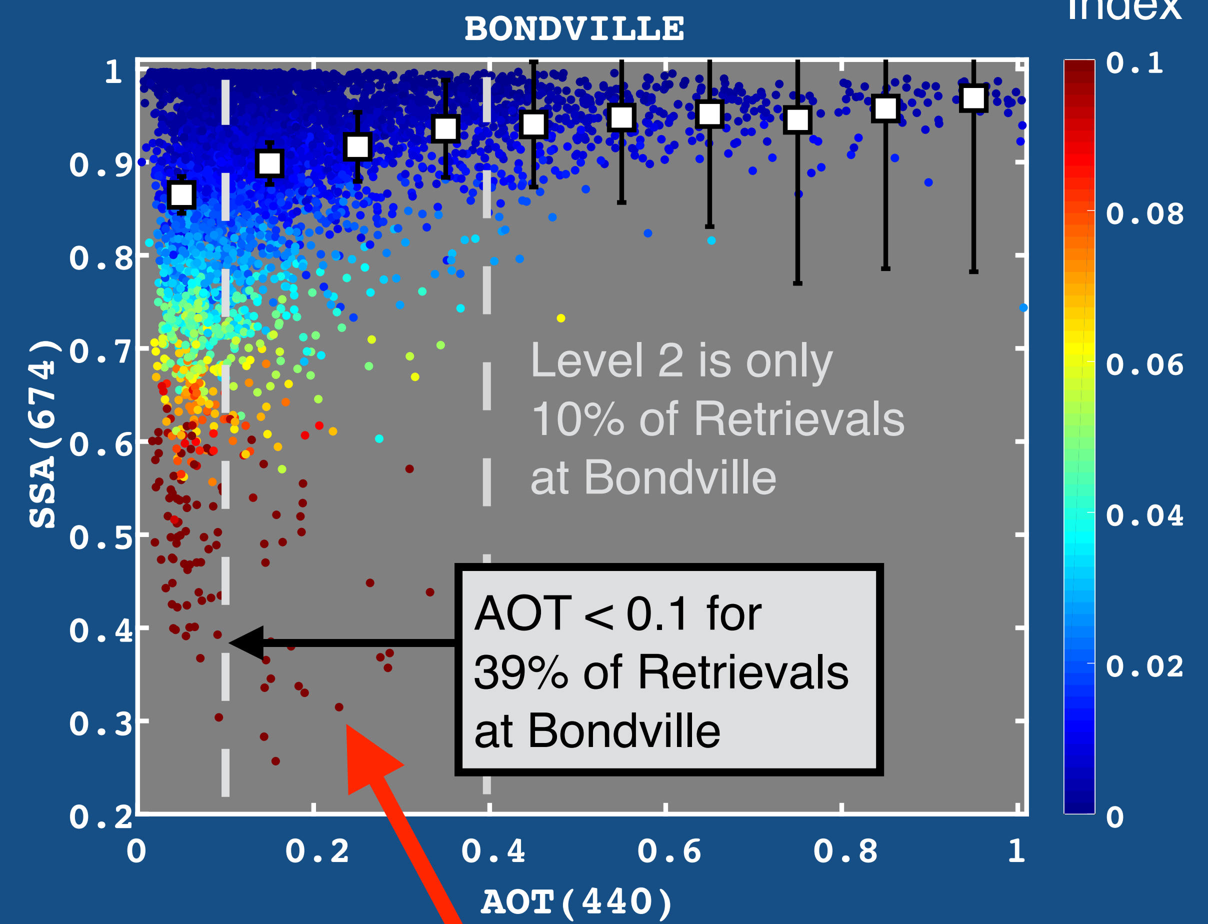

Important: Only use Lev 1.5 when corresponding Lev 2 size distribution exists

AERONET Retrievals at Low AOT

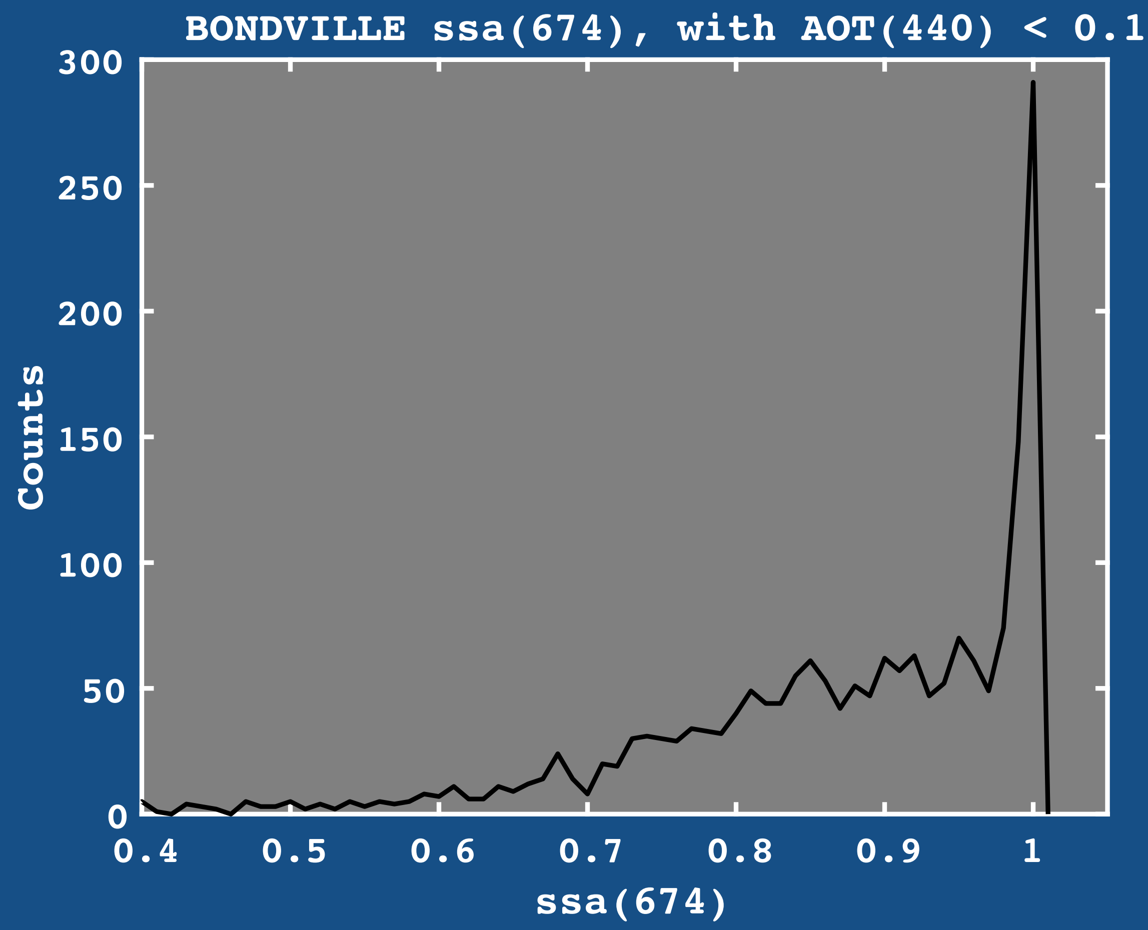

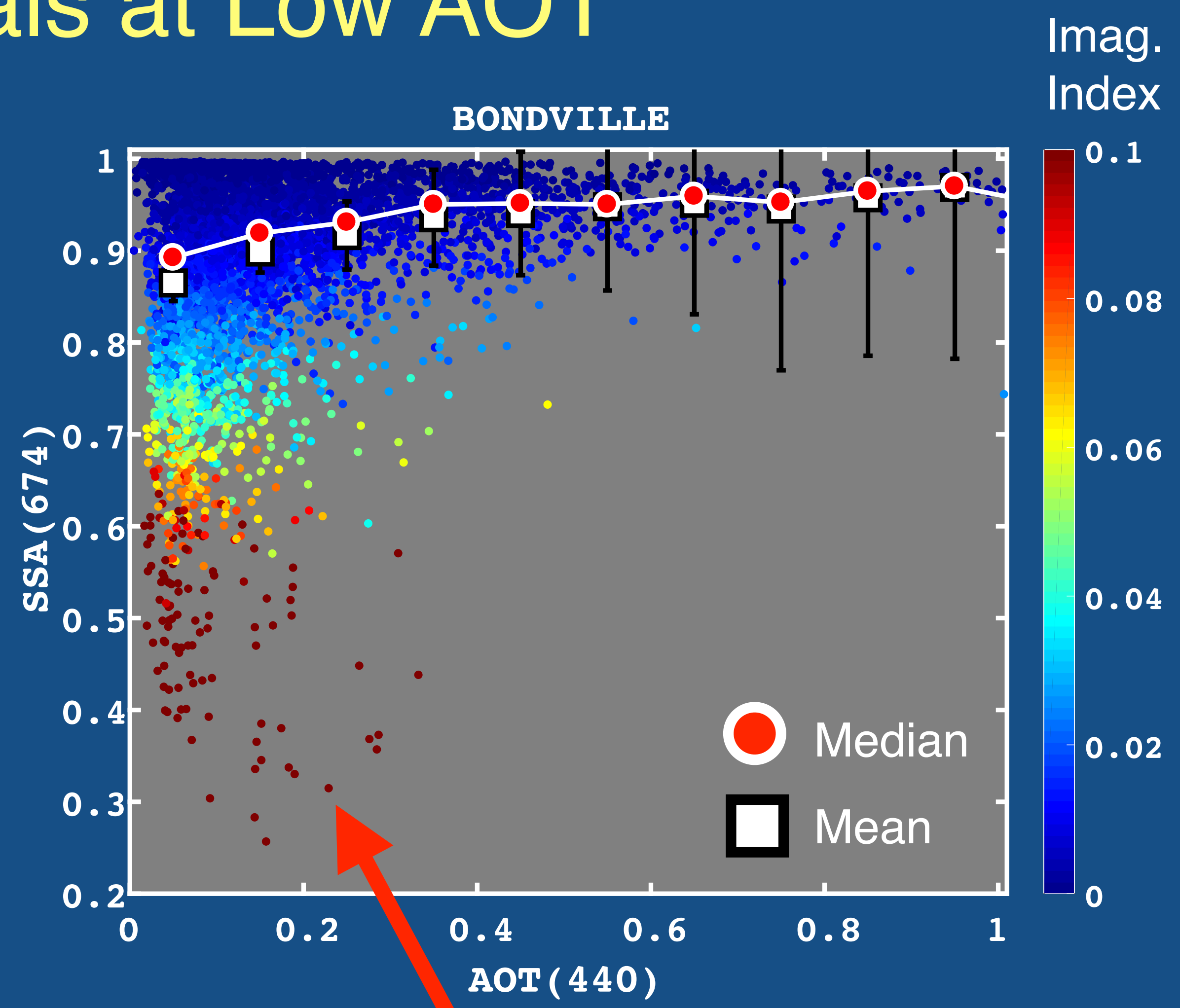

Important: Only use Lev 1.5 when corresponding Lev 2 size distribution exists

AERONET Retrievals at Low AOT

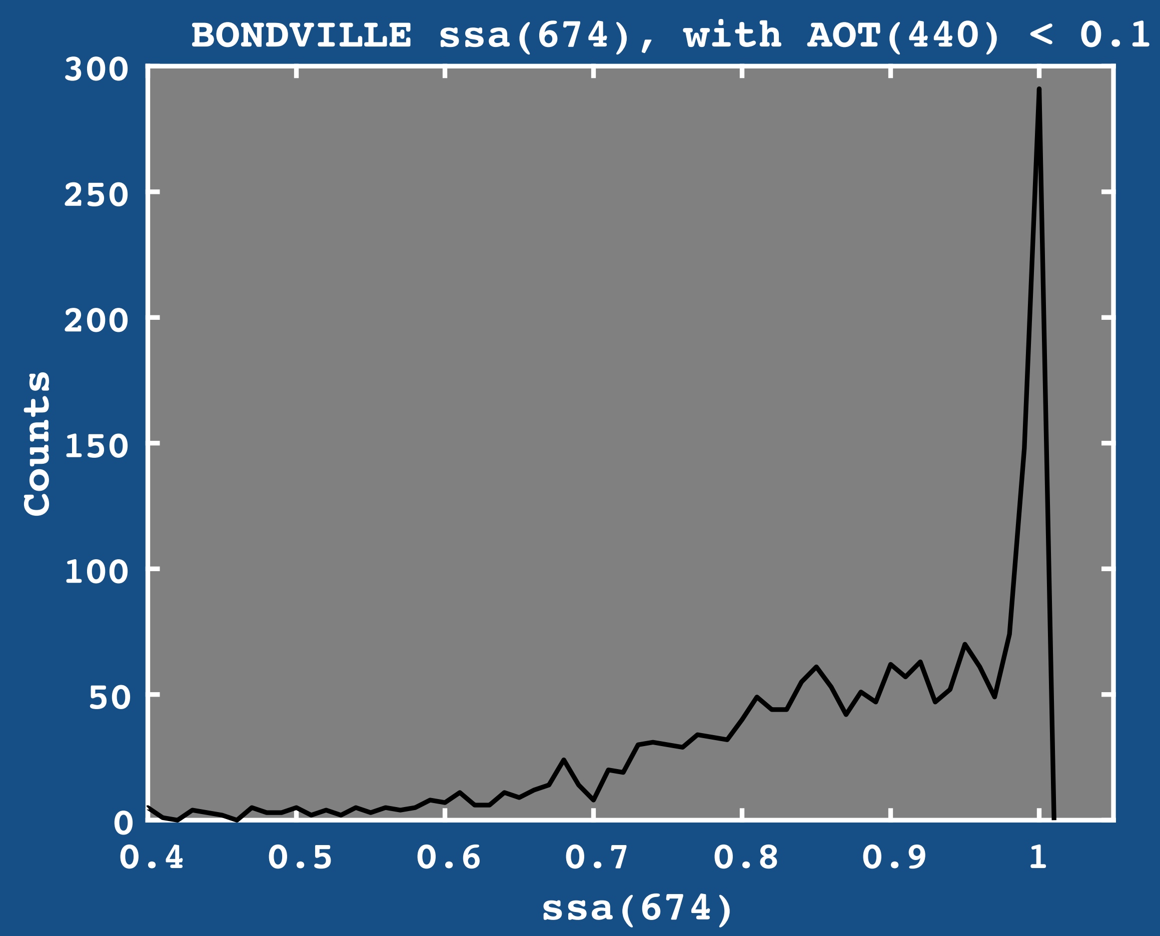

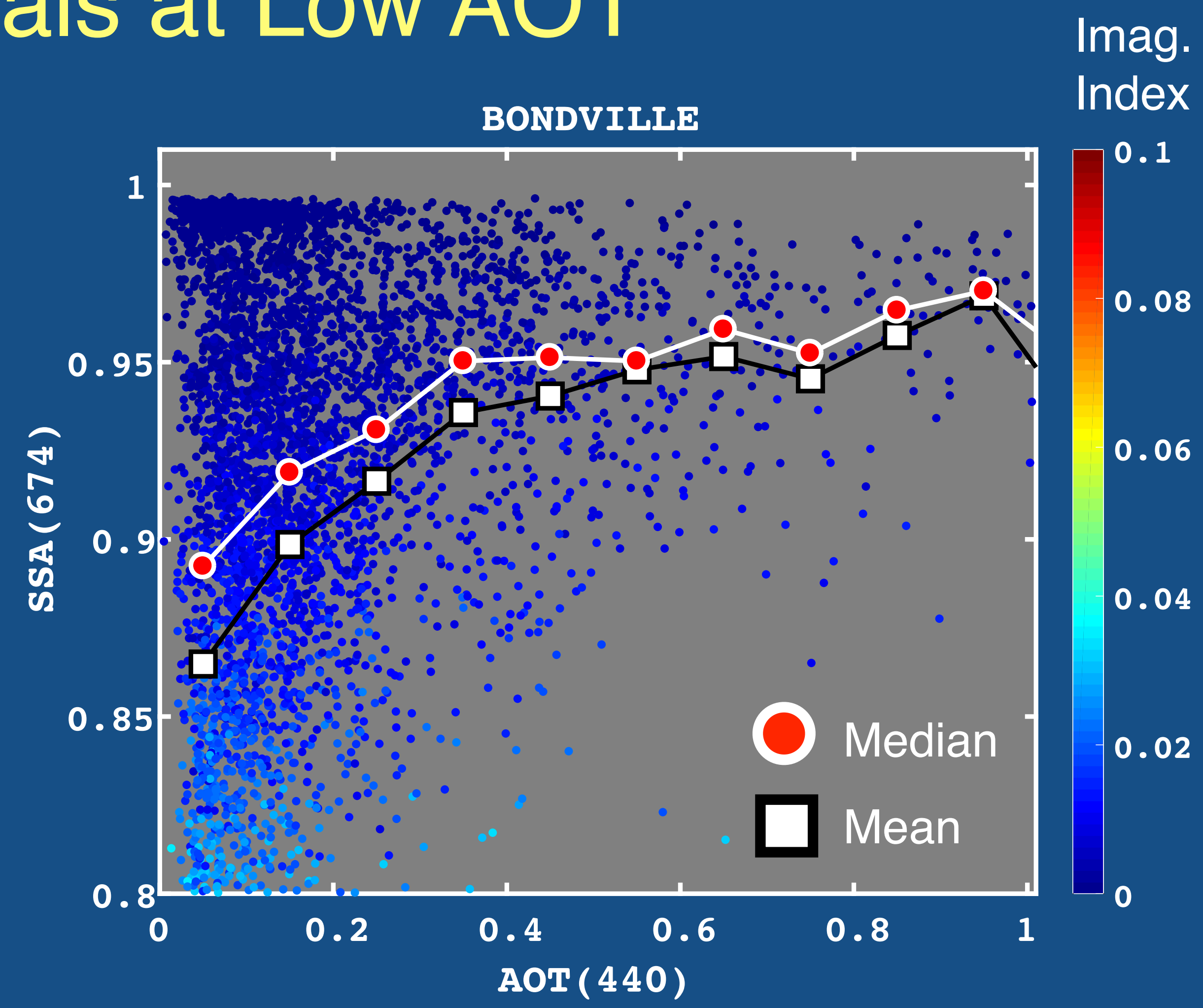

	AOT(440) < 0.1	ALL AOT	
mean ssa	0.865	0.895	
median ssa	0.892	0.926	Bondville
difference	0.033	0.031	

AERONET Retrievals at Low AOT

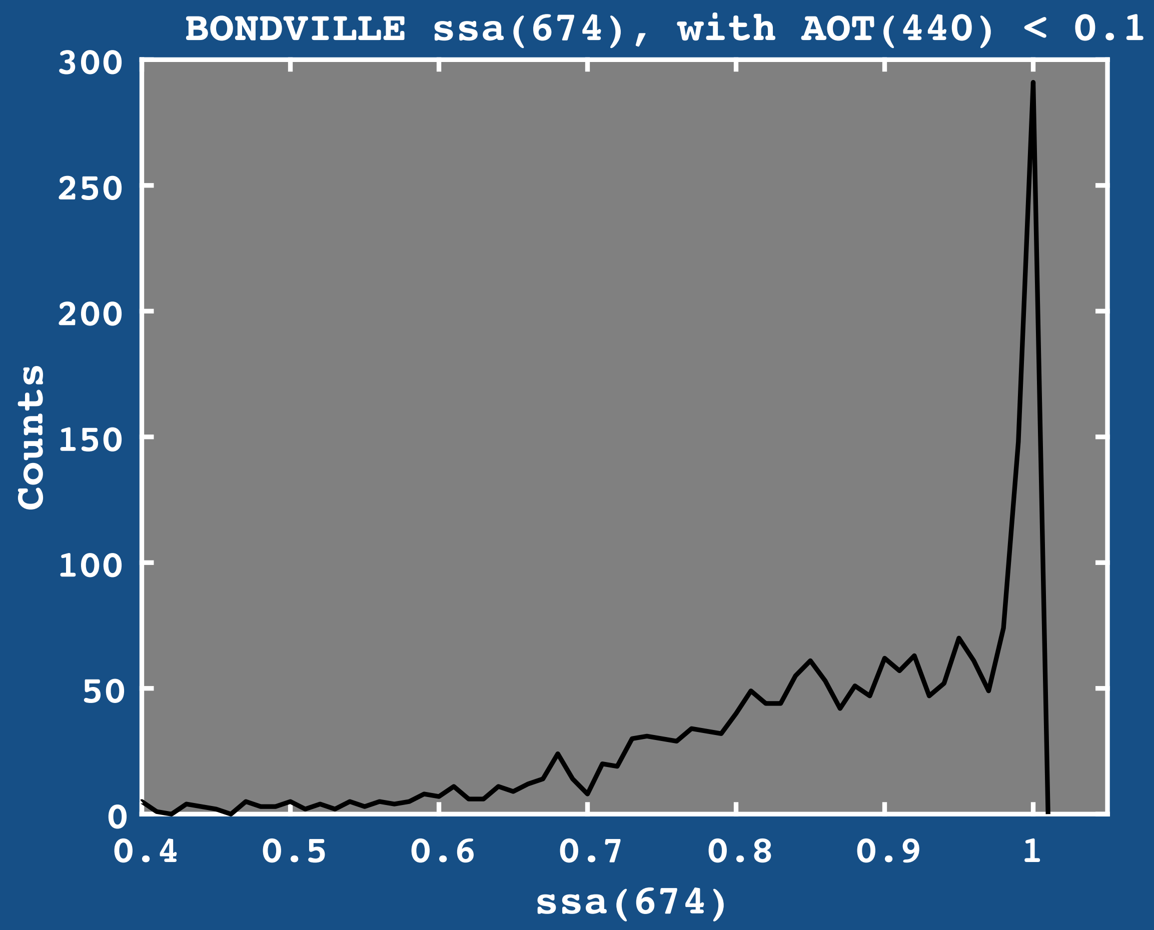

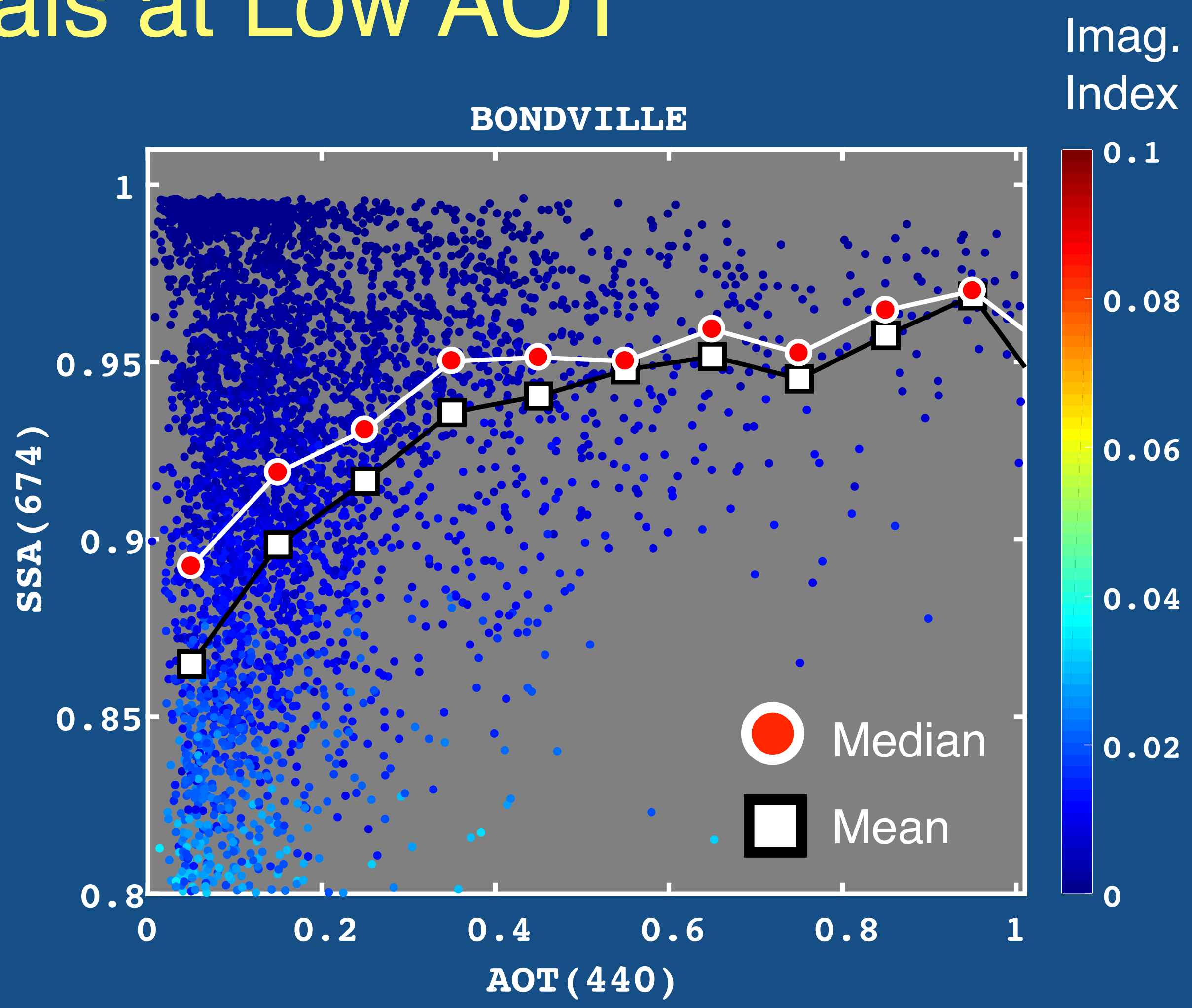

$$co\text{-}ssa = (1-\omega_o)$$
$$AAOD = (1-\omega_o) \times AOD$$

	AOT(440) < 0.1	ALL AOT	
mean ssa	0.865	0.895	
median ssa	0.892	0.926	Bondville
difference	0.033	0.031	

AERONET Retrievals at Low AOT

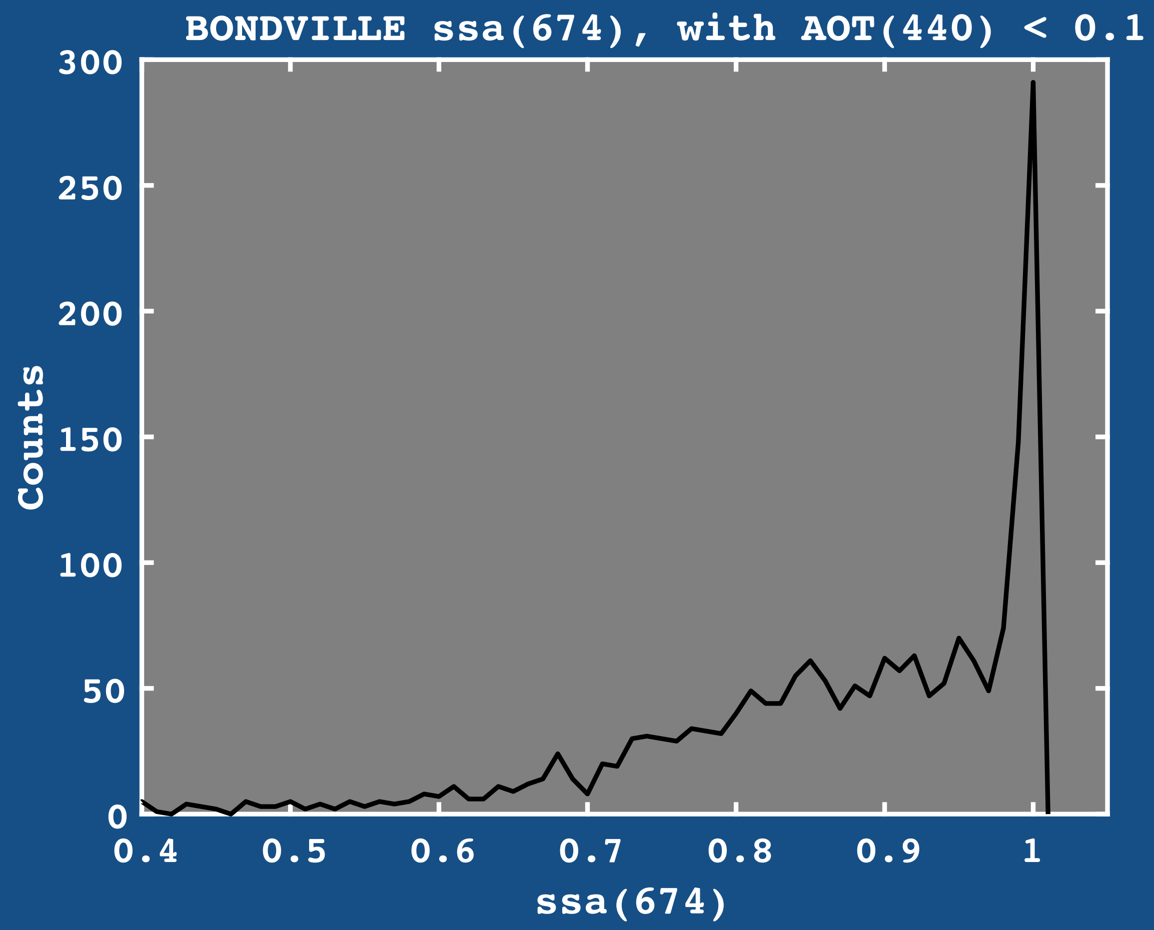

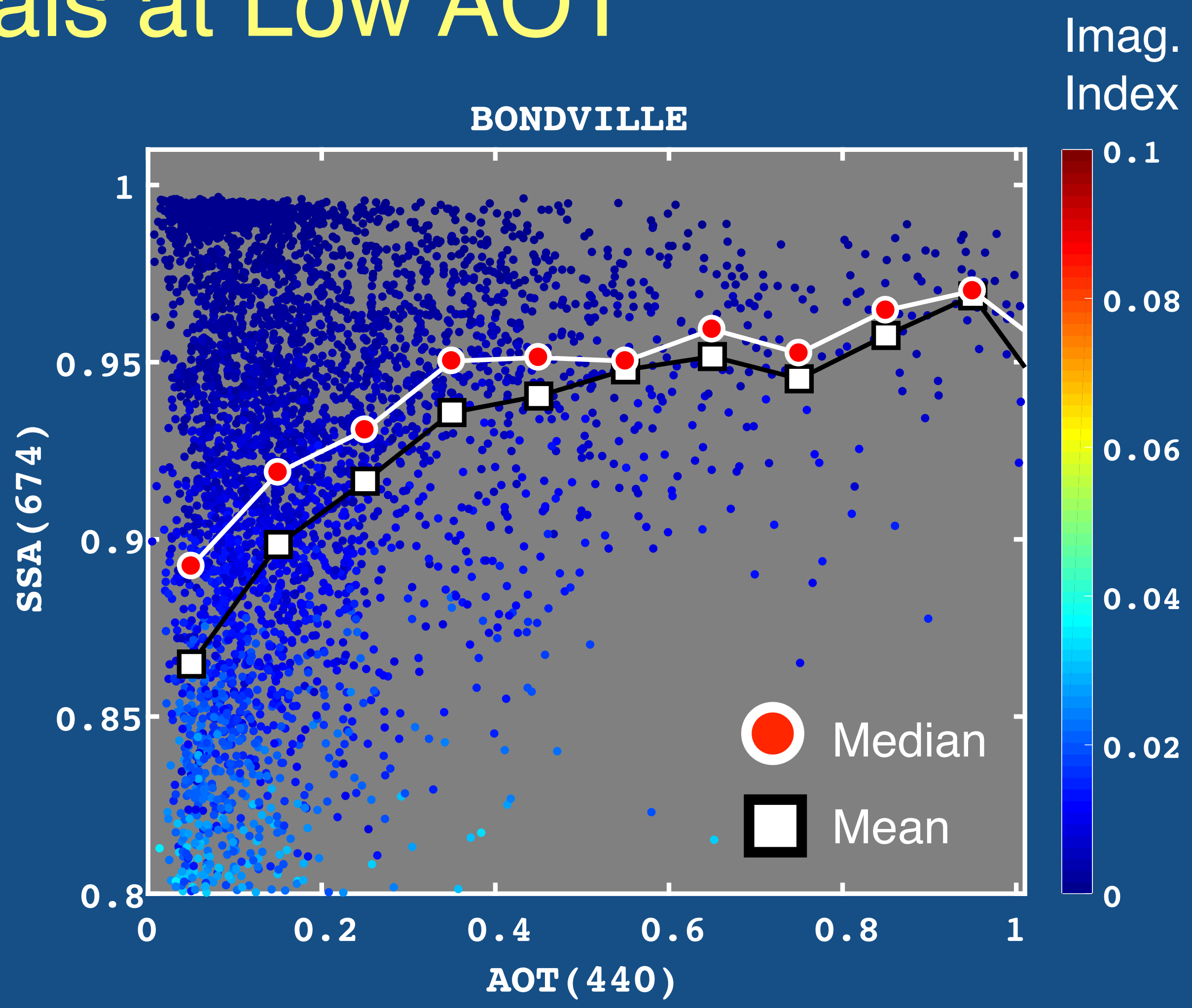

$$co\text{-}ssa = (1 - \omega_o)$$
$$AAOD = (1 - \omega_o) \times AOD$$

	AOT(440) < 0.1	ALL AOT	
mean ssa	0.865	0.895	
median ssa	0.892	0.926	Bondville
difference	0.033	0.031	
co-ssa ratio Mean / Median	1.25	1.419	Bondville

AERONET Retrievals at Low AOT

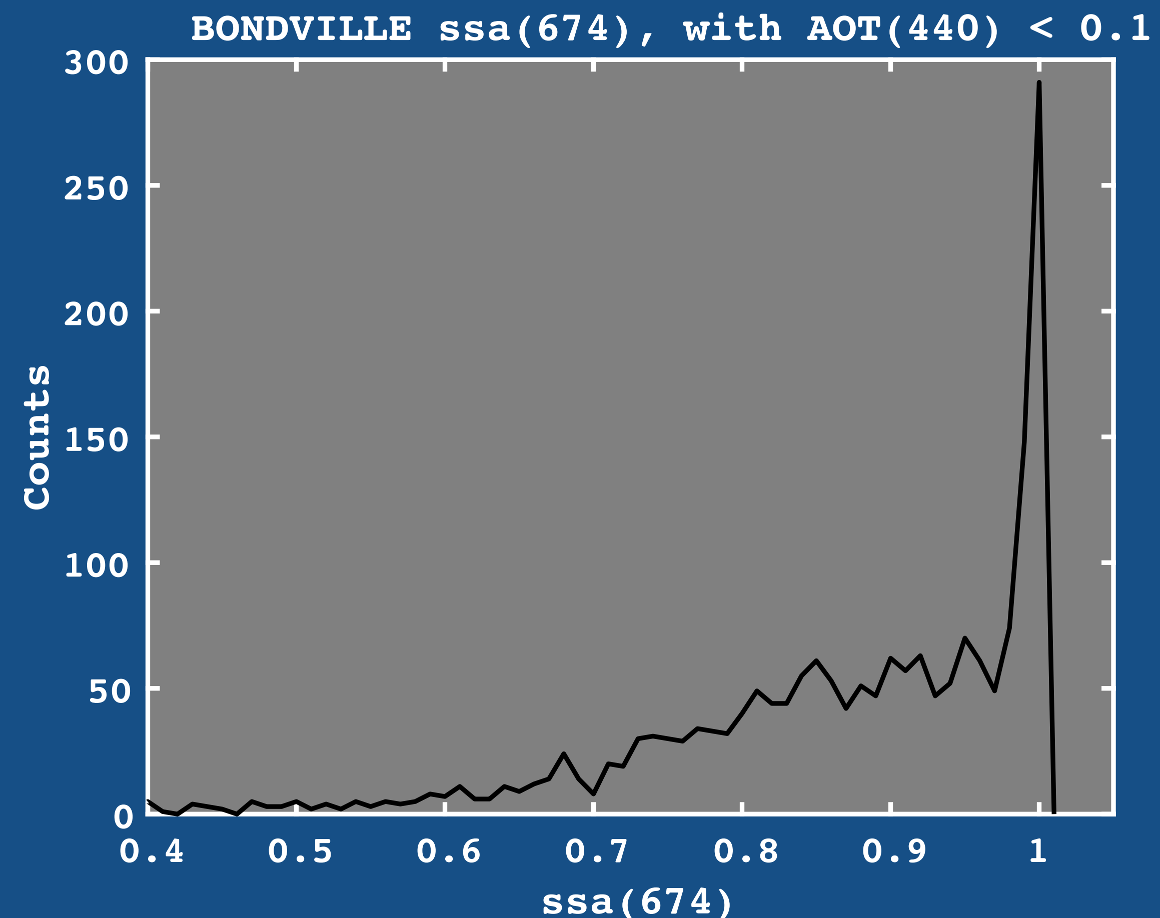

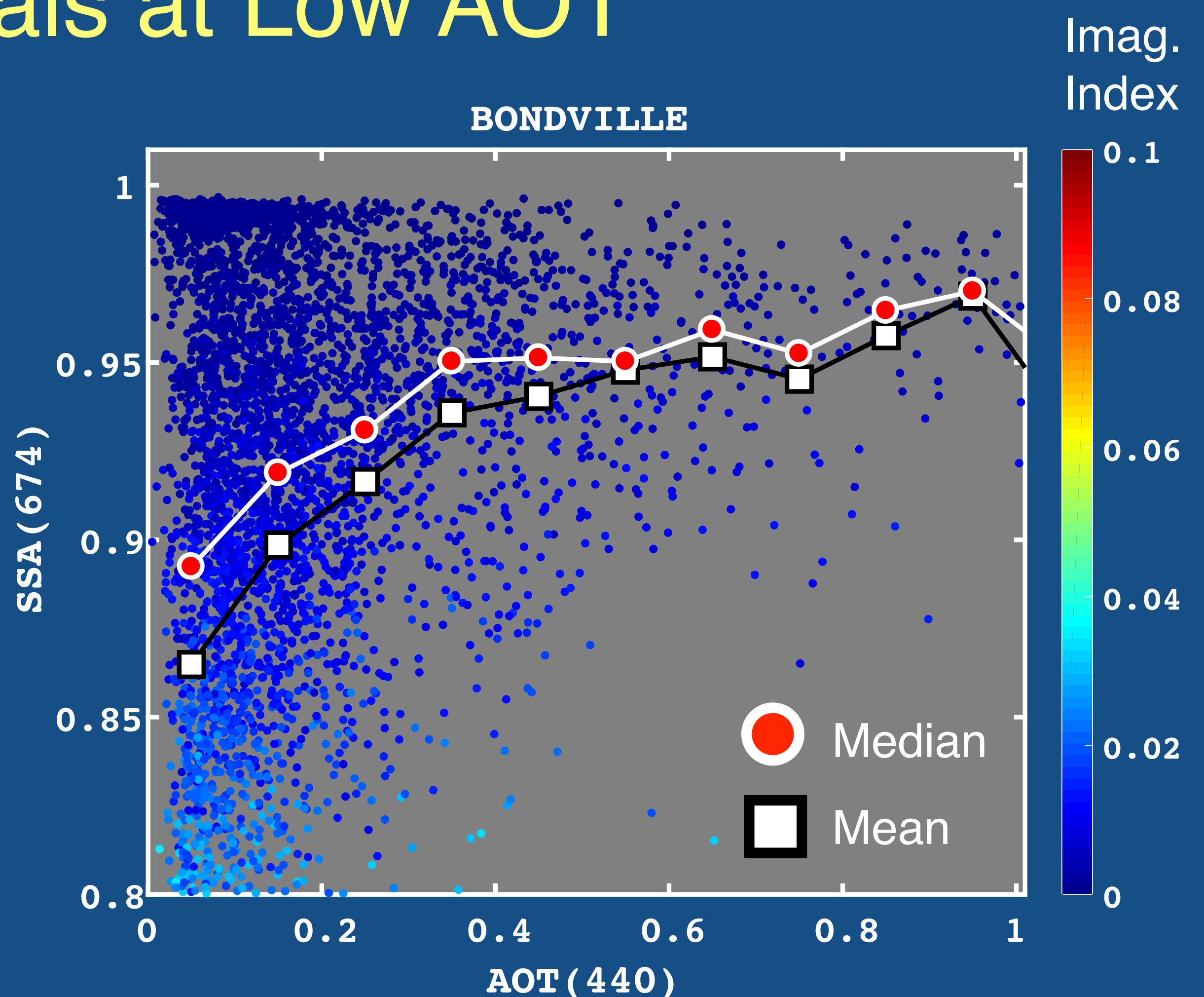

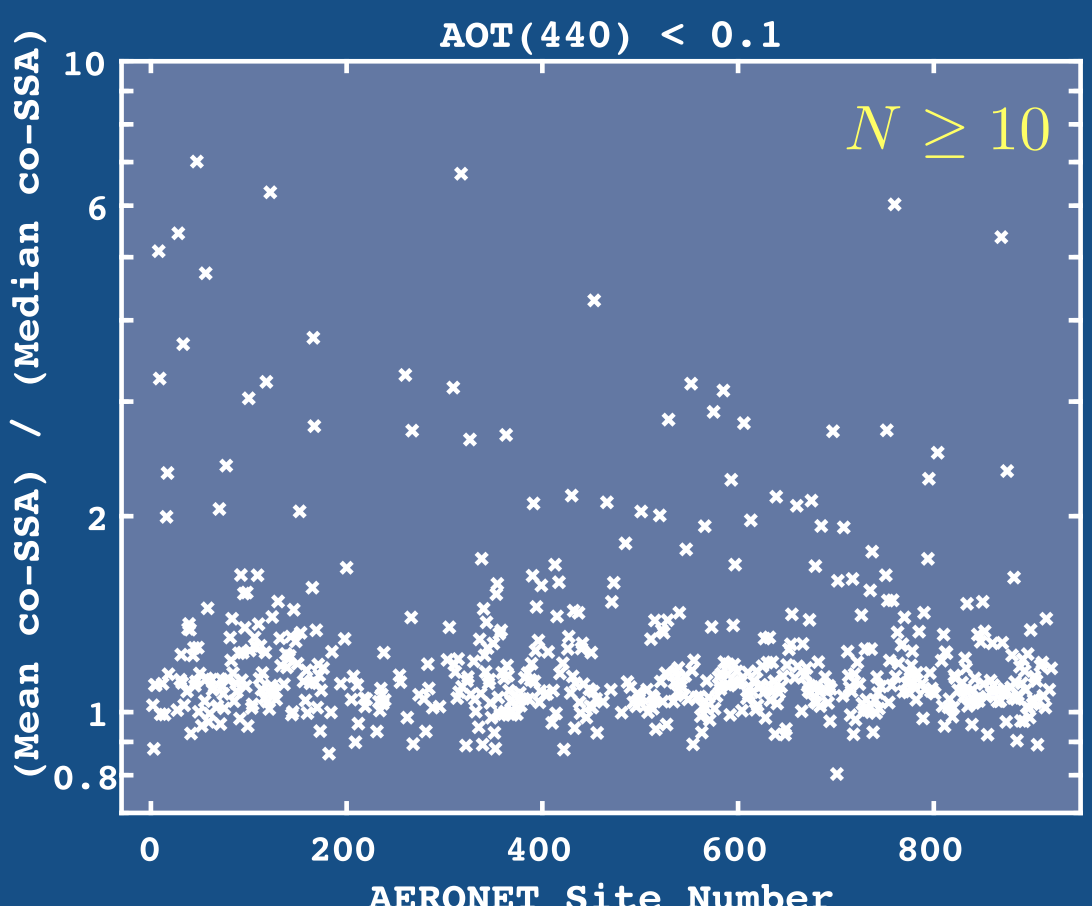

	AOT(440) < 0.1	ALL AOT	
mean ssa	0.865	0.895	
median ssa	0.892	0.926	Bondville
difference	0.033	0.031	
co-ssa ratio Mean / Median	1.25	1.419	Bondville

Conclusions

- Simulated AERONET measurements for 285 in situ sampling volumes.
- GRASP provided quality retrievals (residuals of < 8%) for ~90 samples.
- Relative bias for effective radius is 1% when dynamic shape factor is constrained by extinction.
- Relative bias for the effective variance of size distributions is 116%.
- Absolute bias for single-scatter albedo is +0.023 at 532 nm via PSAP, +0.026 via photo-acoustic, and +0.036 via nephalometer.
- Biases do not vary significantly for SZA = 50-77 degrees.
- Use median instead of mean SSAs to better neutralize noise of low AOT AERONET retrievals.

Acknowledgements

This material was supported by NASA through the ROSES Atmospheric Composition: Laboratory Research program, issued through the Science Mission Directorate, Earth Science Division. We acknowledge the efforts of the AERONET principal investigators and the entire AERONET team.

APPENDIX

Aerodynamic-Optical Size Conversion

Require closure with extinction measurements

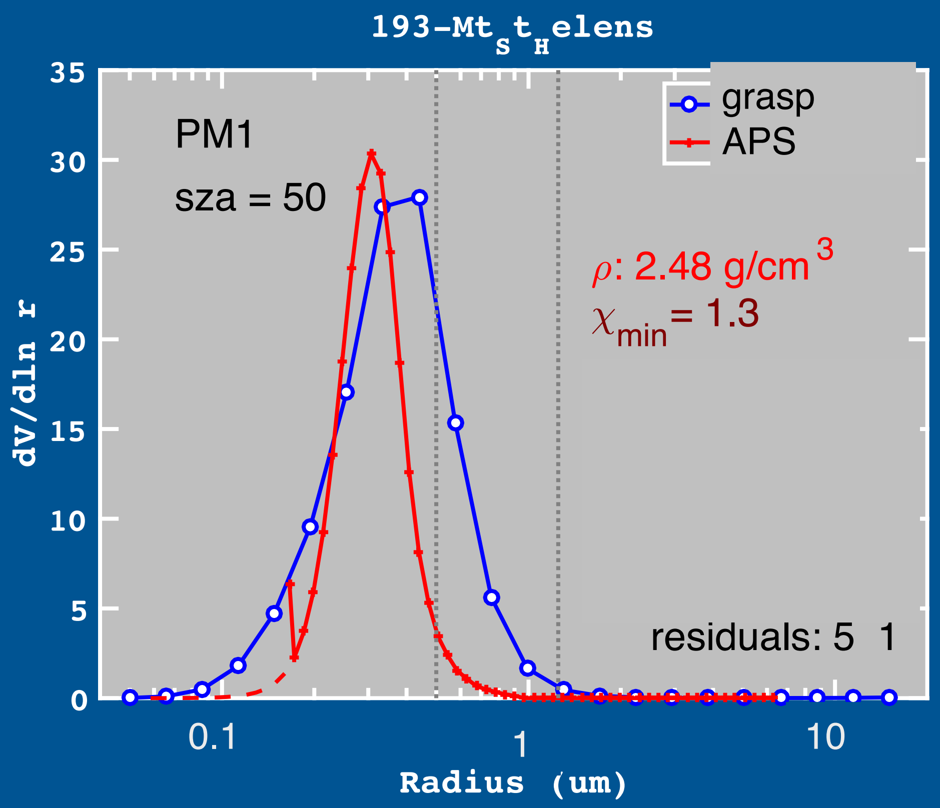

Aerodynamic-Optical Size Conversion

Require closure with extinction measurements

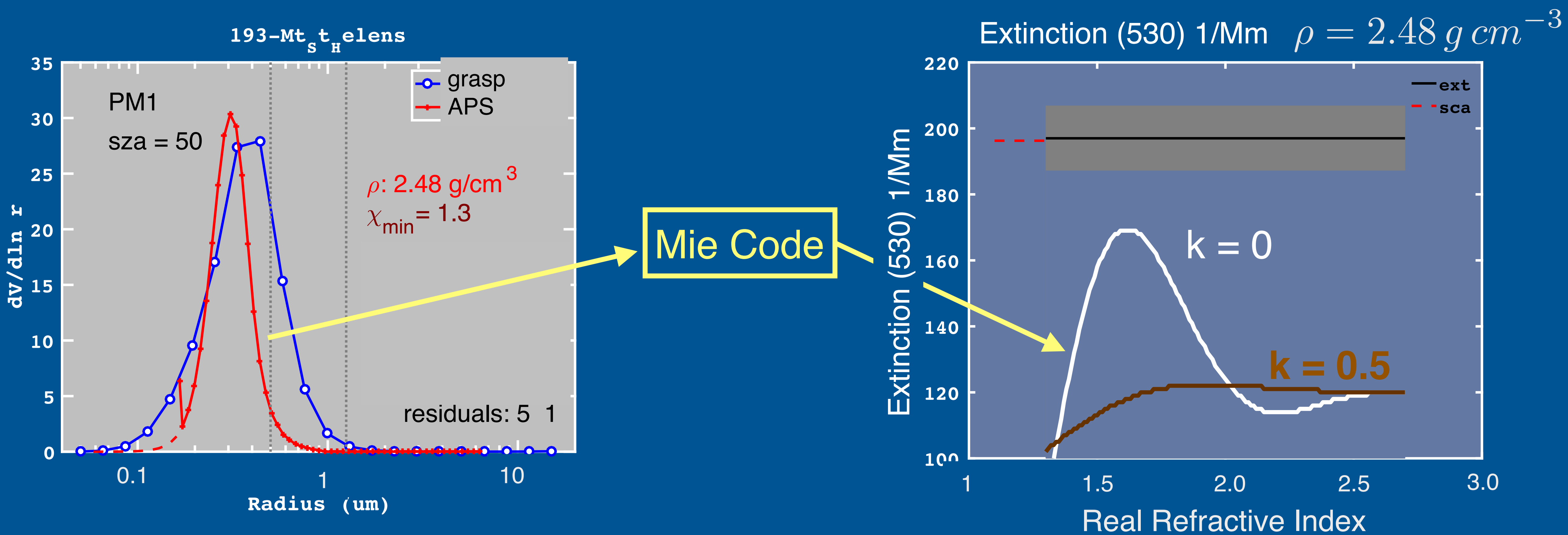

$$Extinction = \int Q(n, k, r, \lambda)\pi r^2 n(r) dr$$

Aerodynamic-Optical Size Conversion

Require closure with extinction measurements

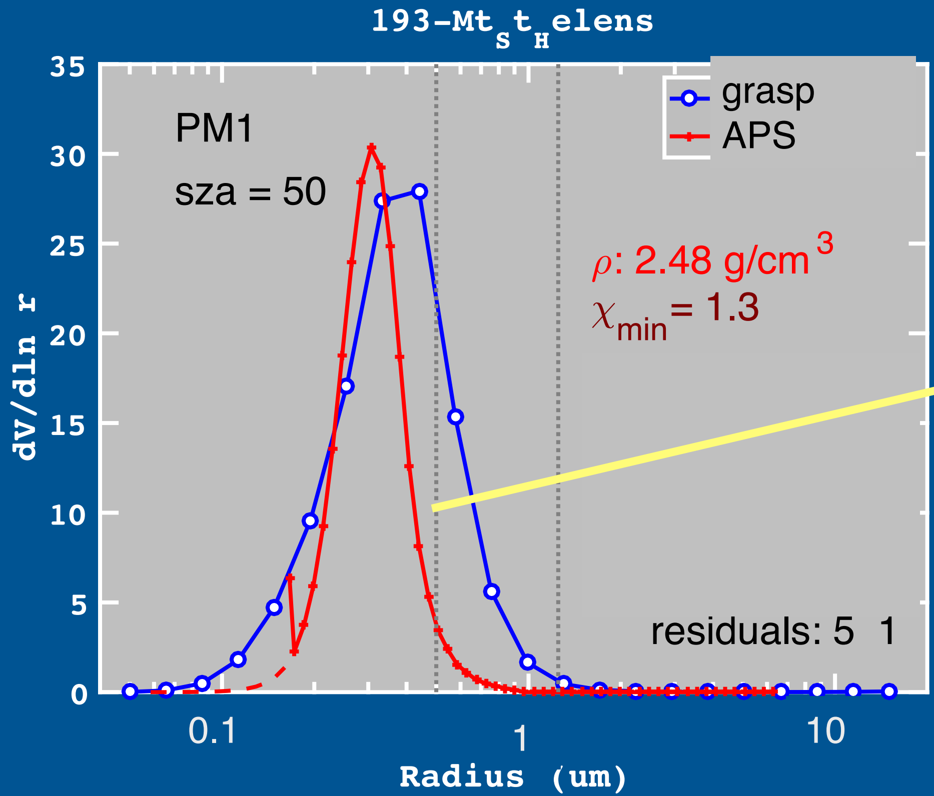

Mie Code

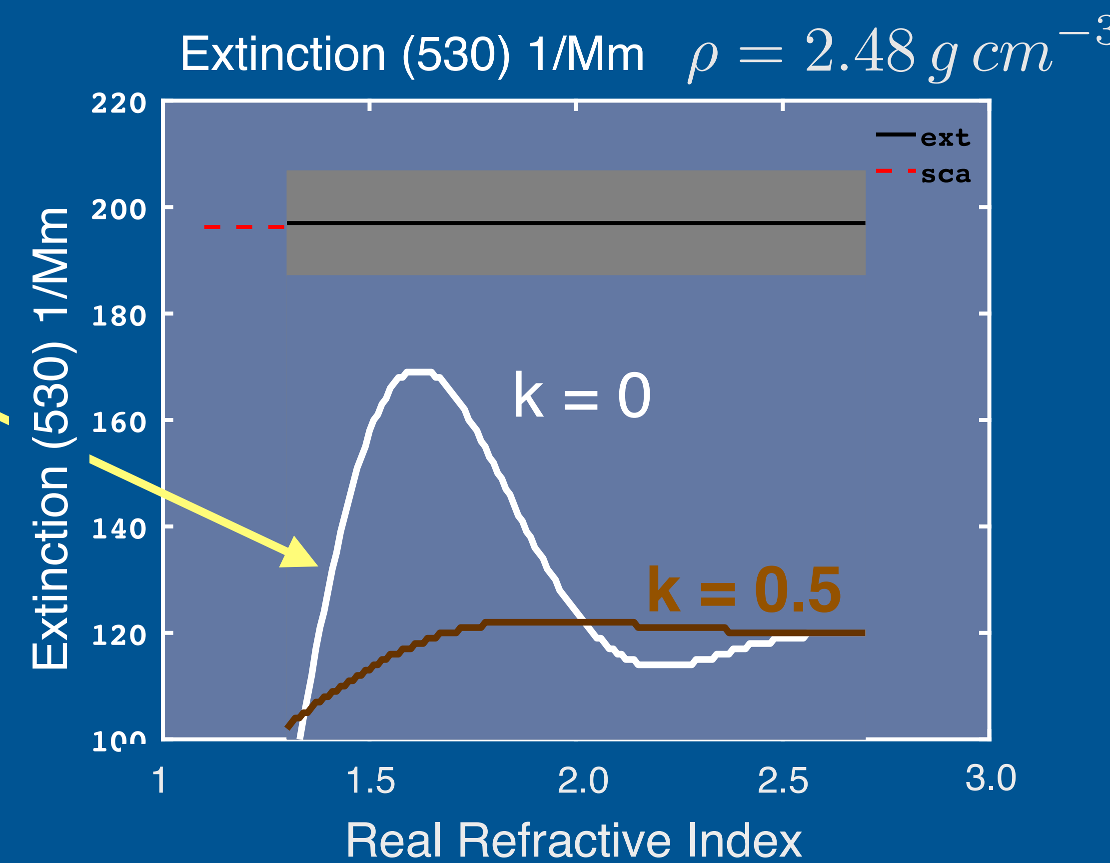

Decrease Density

$$Extinction = \int Q(n,k,r,\lambda)\pi r^2 n(r) dr$$

$$R_{vol} = R_{aero}\sqrt{\frac{\chi}{\rho}} = \frac{R_{aero}}{\sqrt{\rho^*}}$$

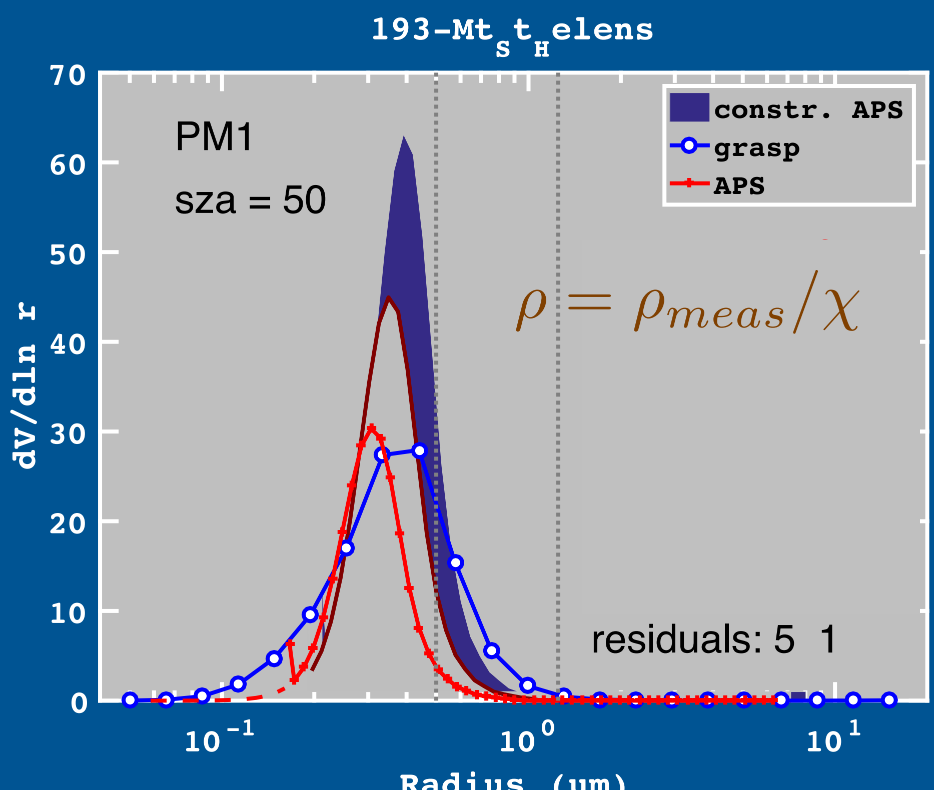

Aerodynamic-Optical Size Conversion

Require closure with extinction measurements

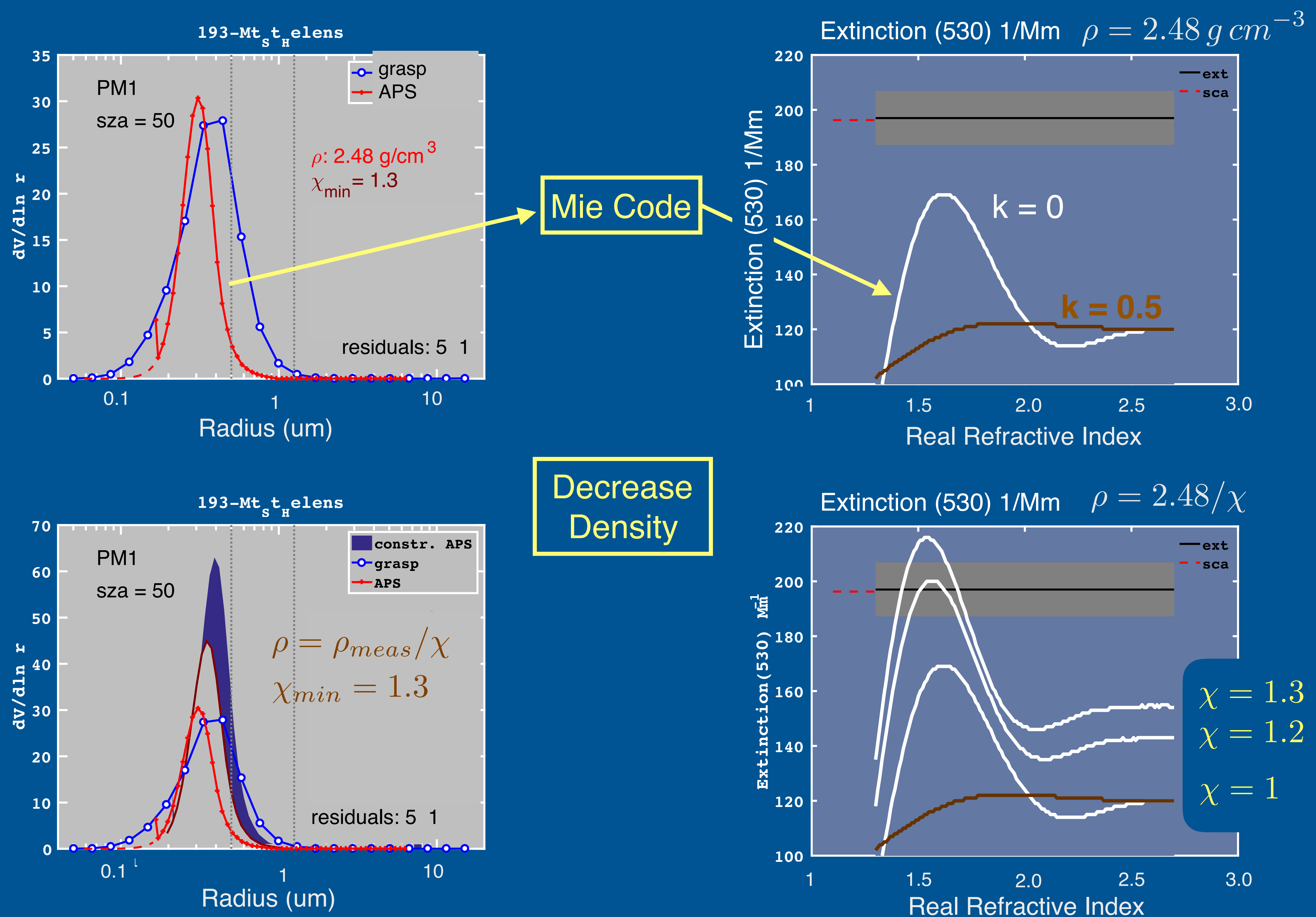

The Importance of Residuals

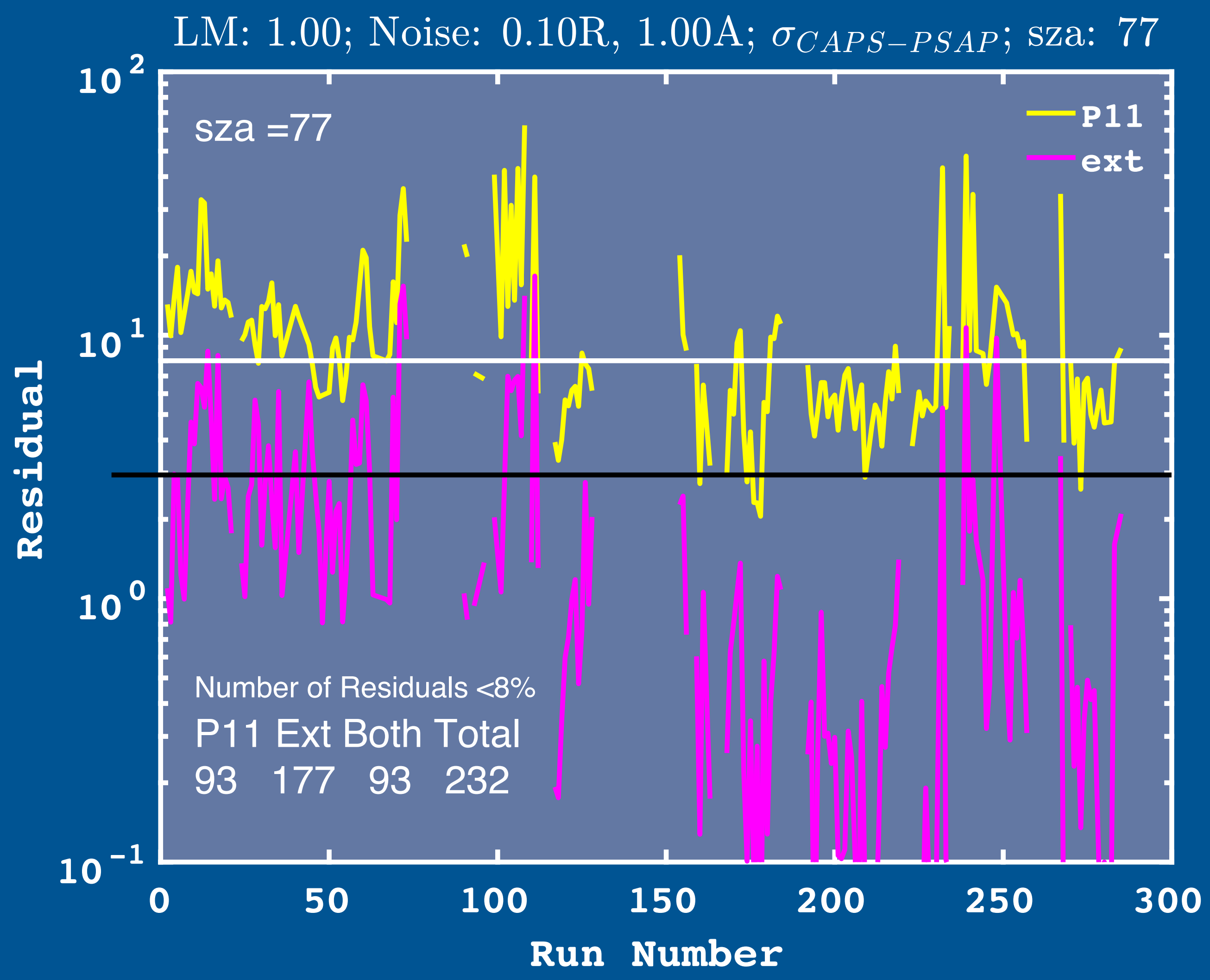

The Importance of Residuals

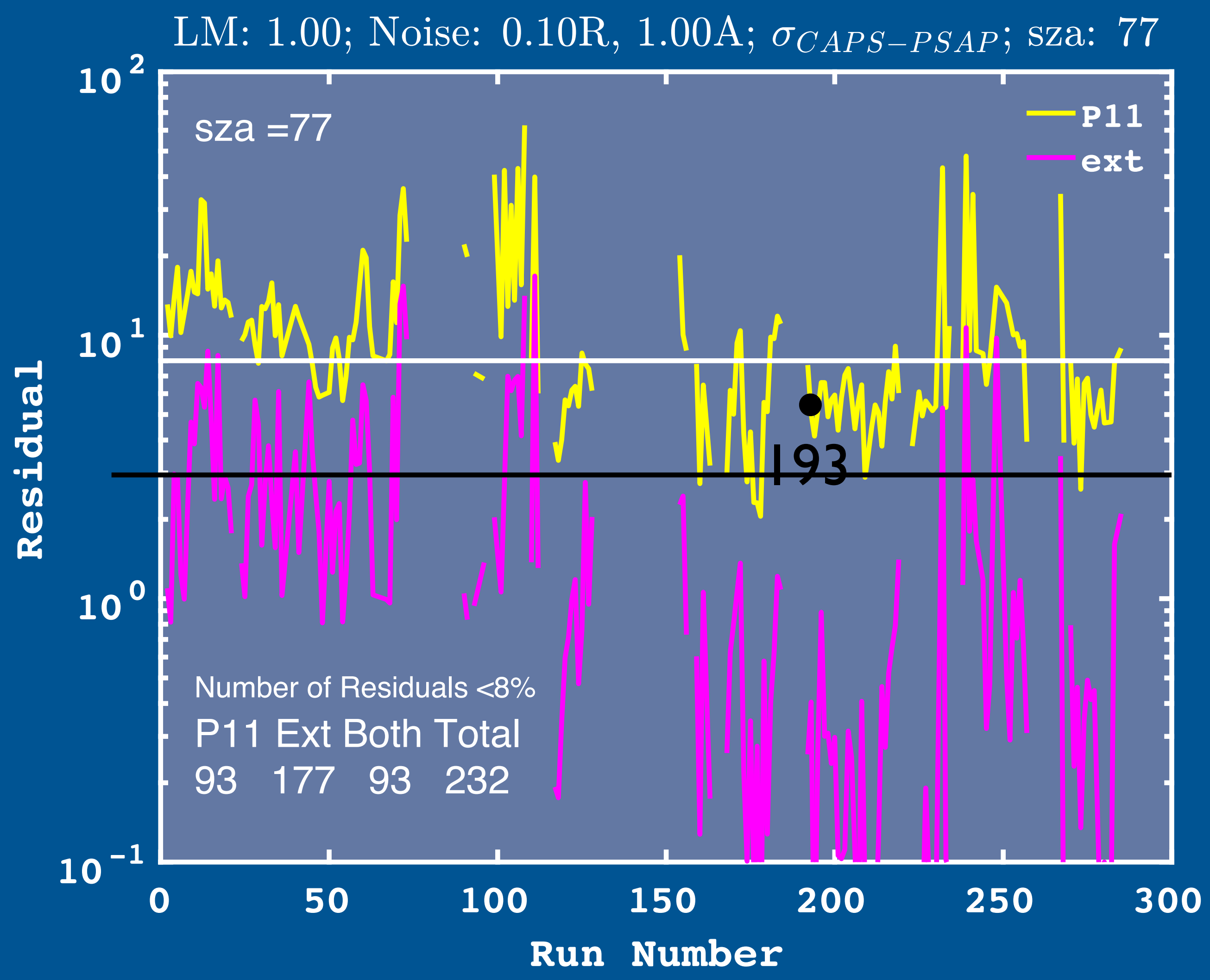

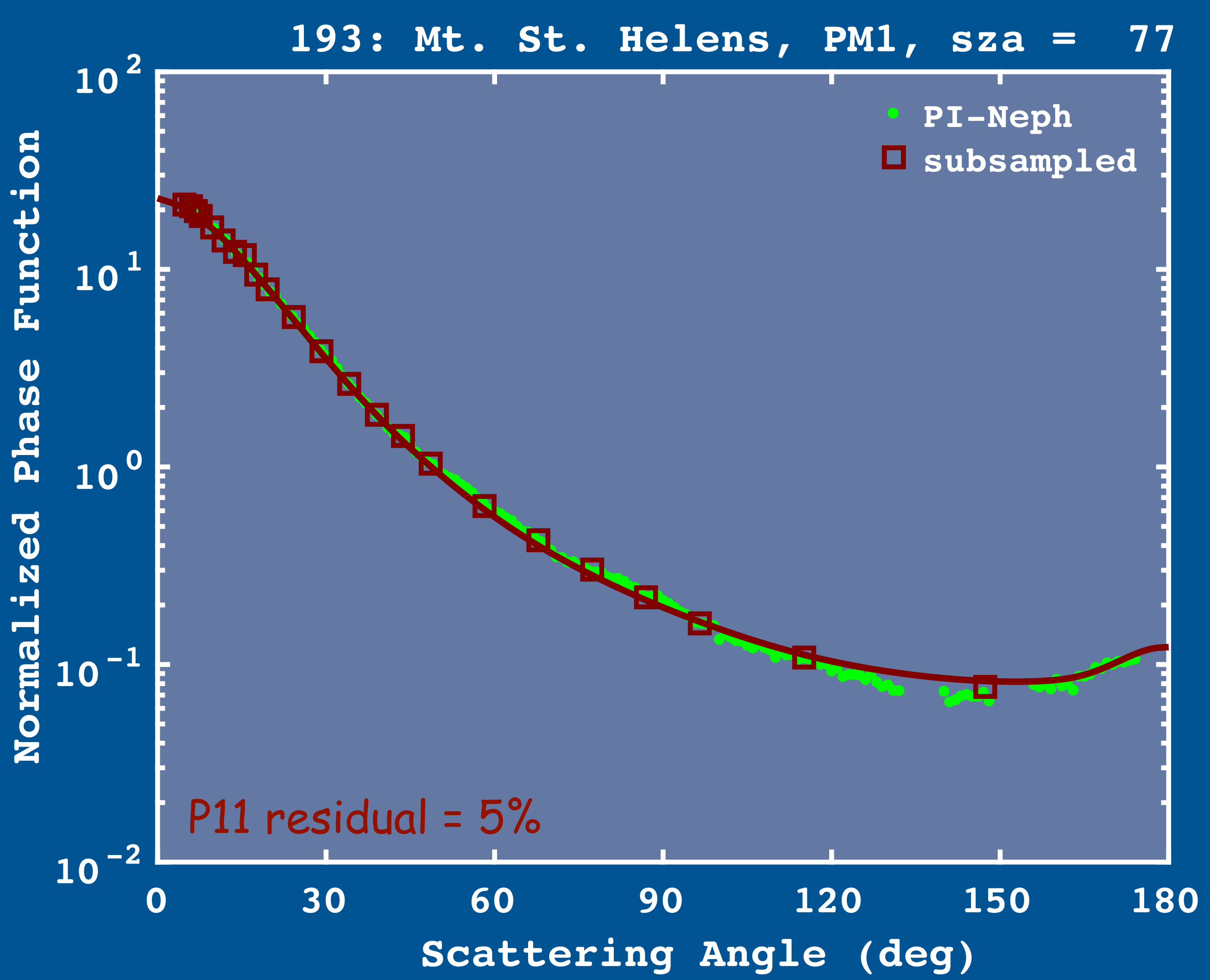

The Importance of Residuals

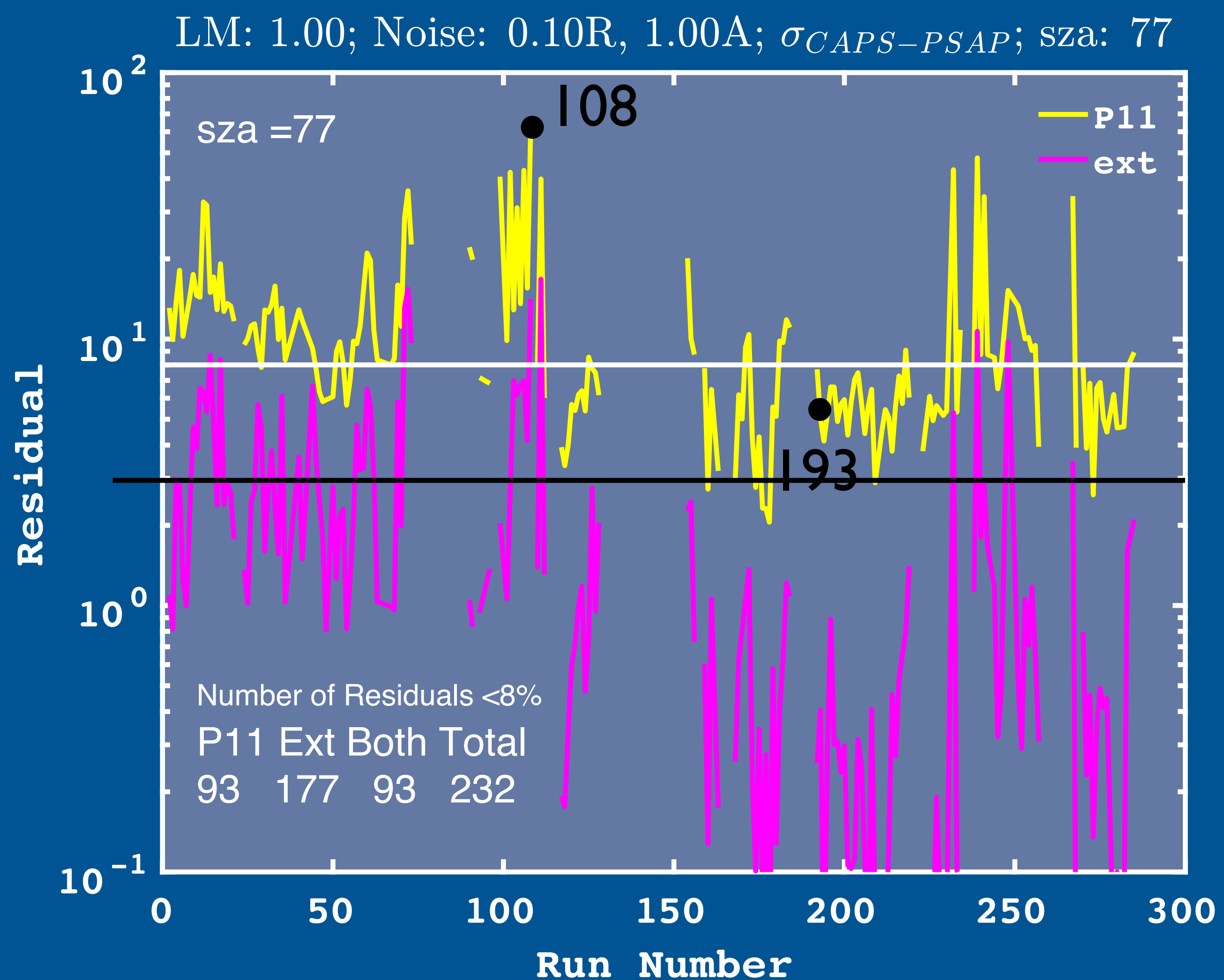

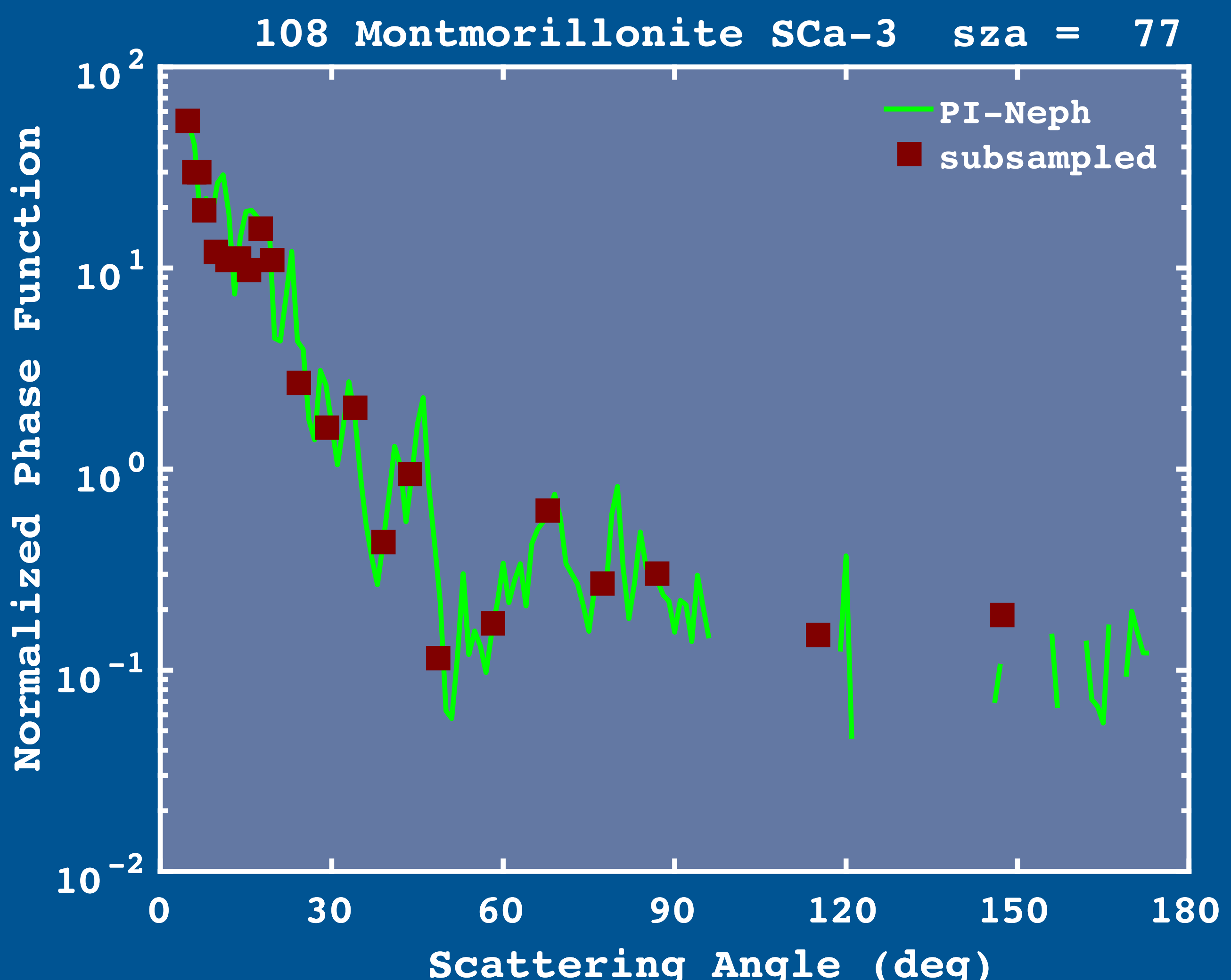

The Importance of Residuals

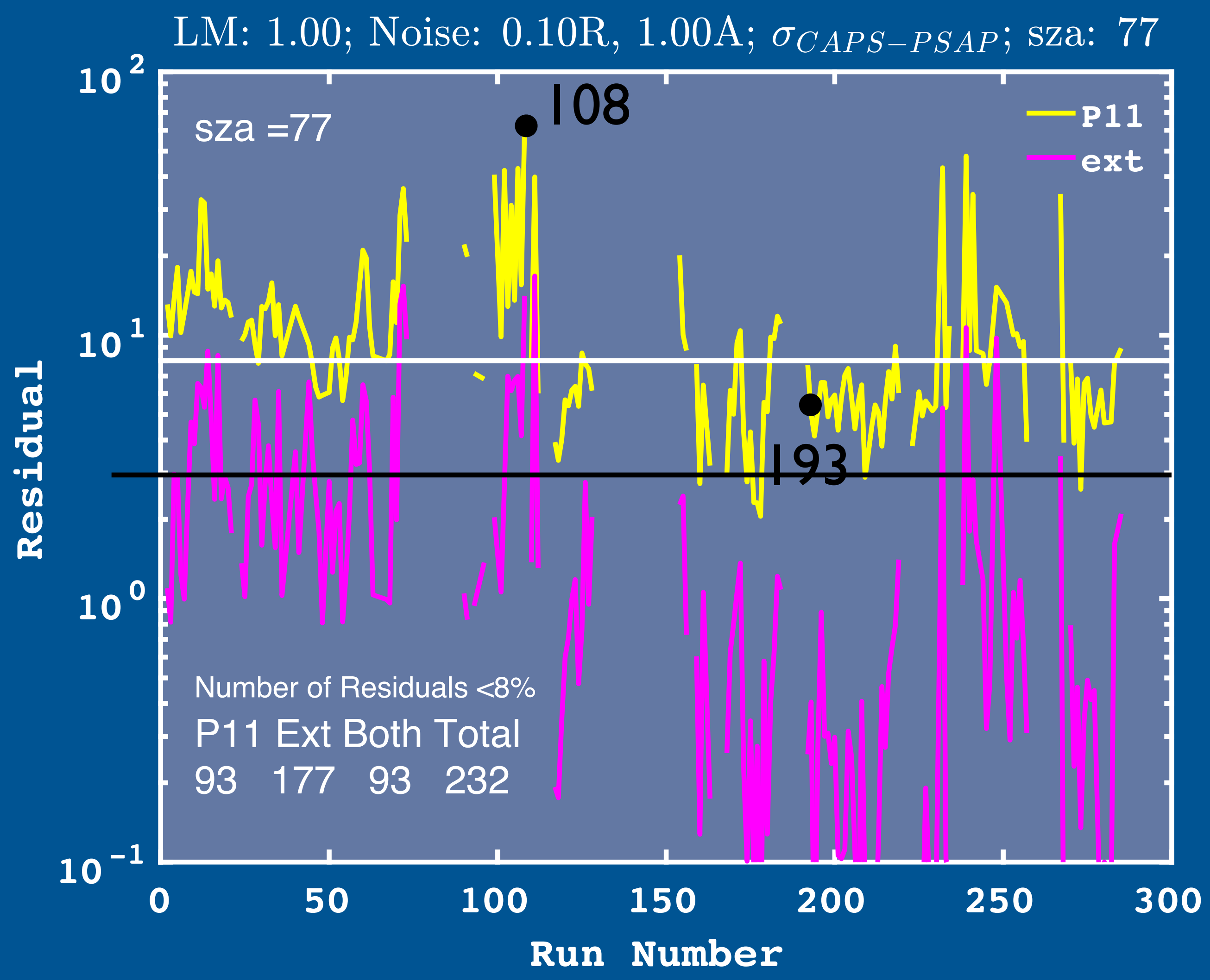

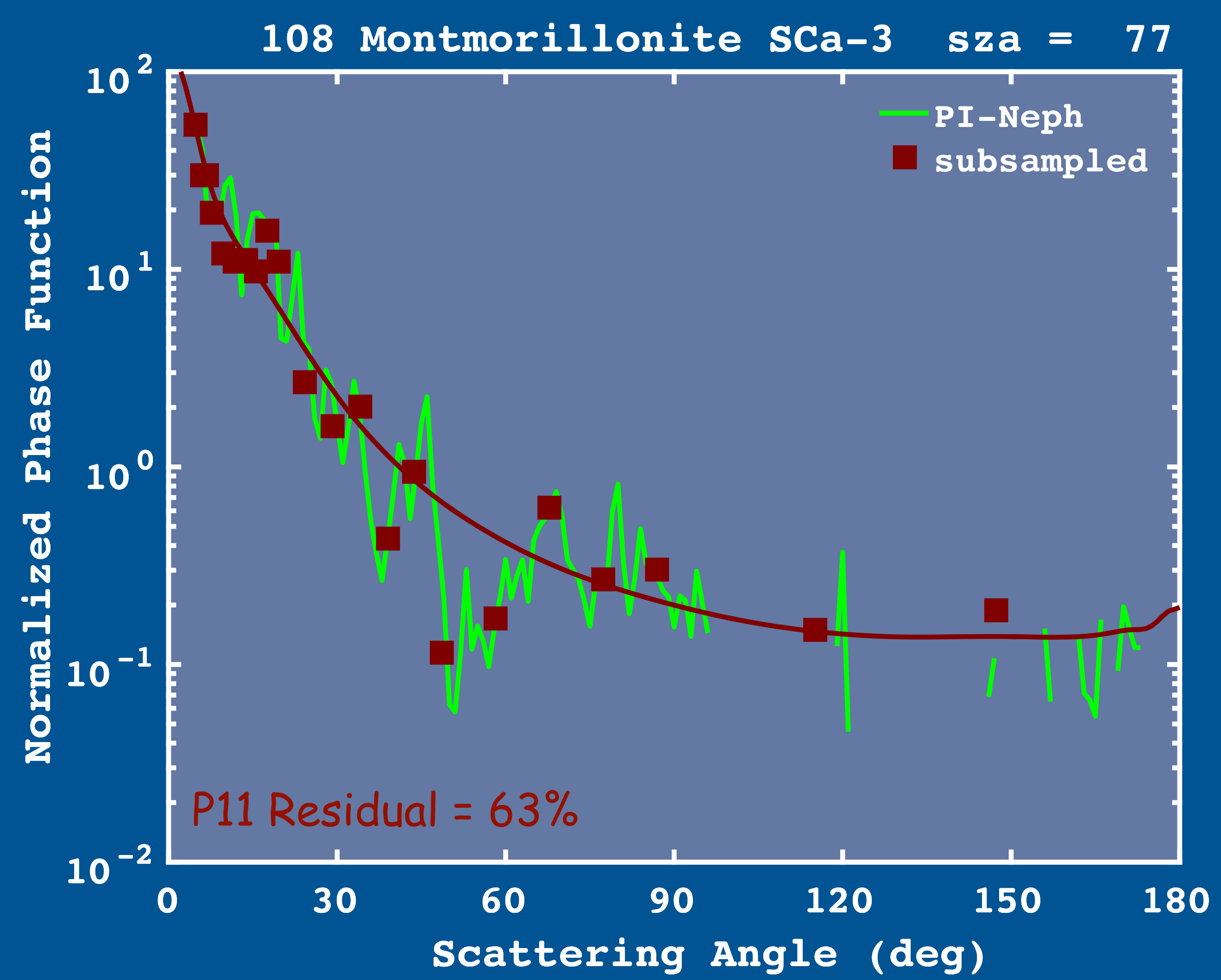

The Importance of Residuals

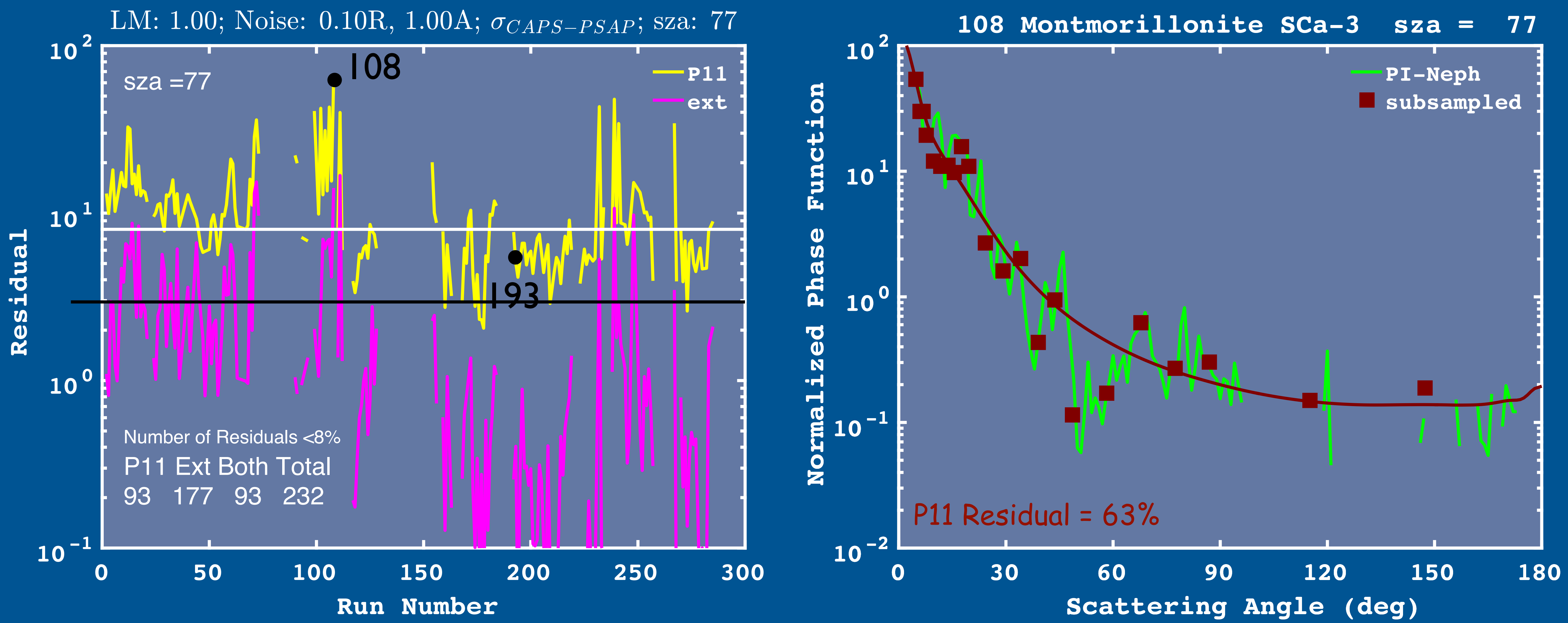

Note: AERONET Level 2 require residuals less than 5-8%, depending upon AOD.
AERONET Level 1.5 reports all retrievals, regardless of residuals.

The Importance of Residuals

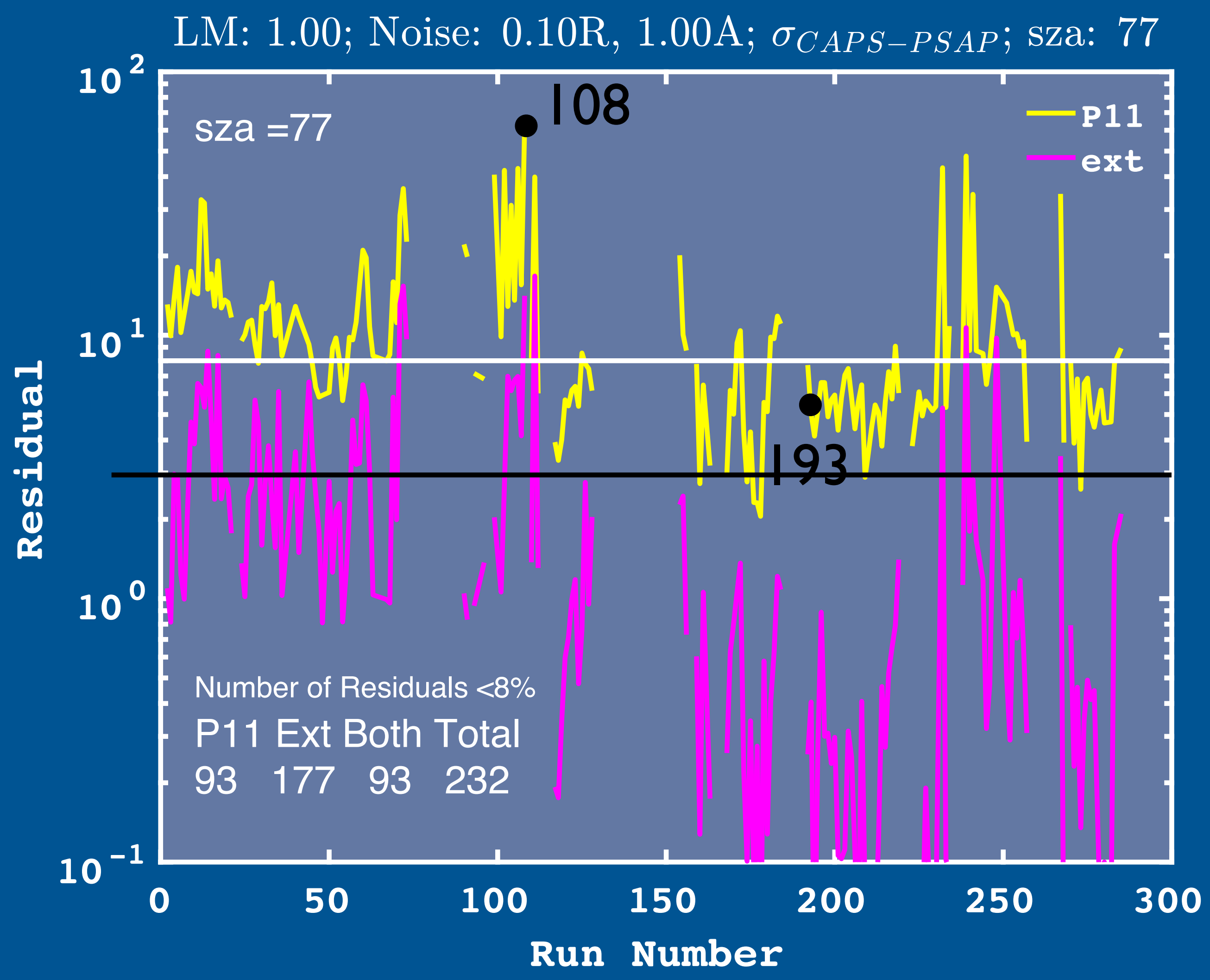

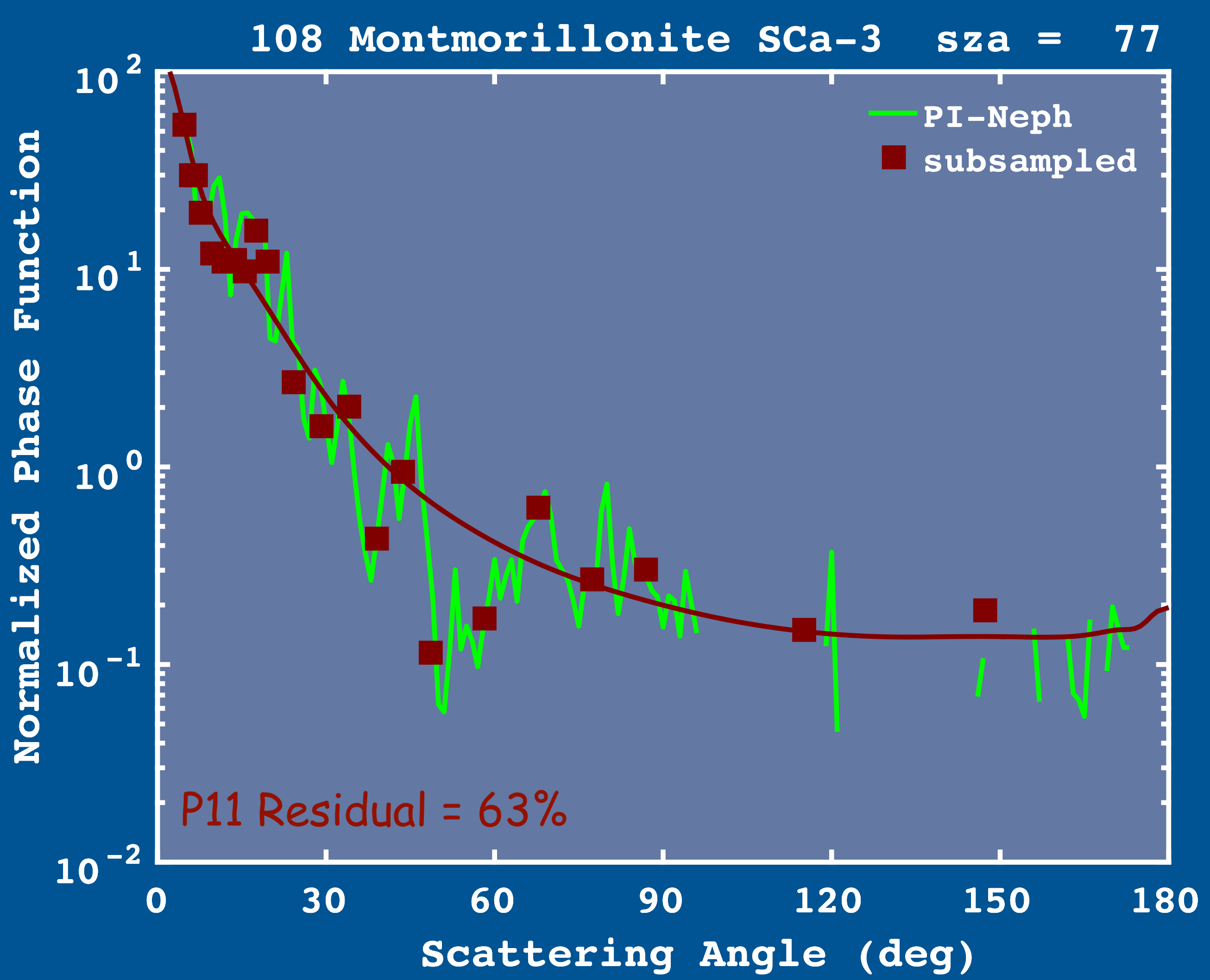

Note: AERONET Level 2 require residuals less than 5-8%, depending upon AOD.
AERONET Level 1.5 reports all retrievals, regardless of residuals.

➡ See Bond (JGR, 2013) for the "proper" way to use AERONET Level 1.5 data.

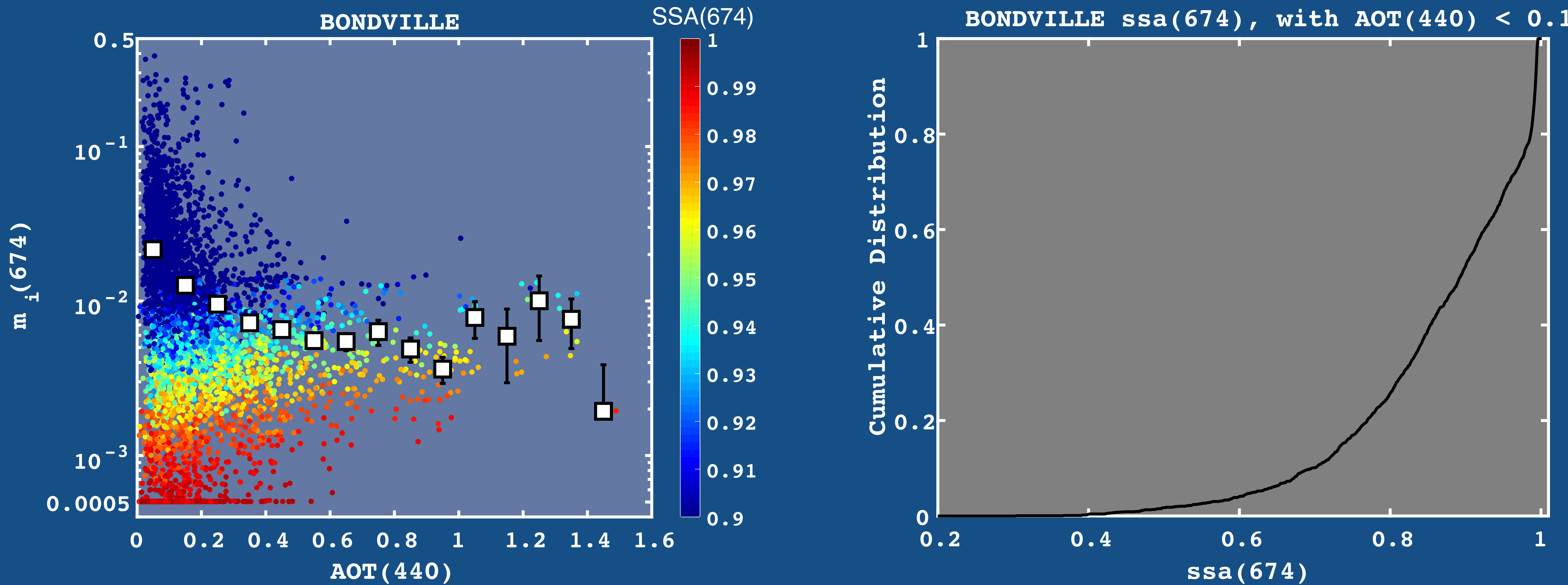

BONDVILLE
SSA(674)
m_i(674)
AOT(440)
0.5
10^-1
10^-2
10^-3
0.0005
0
0.2
0.4
0.6
0.8
1
1.2
1.4
1.6
1
0.99
0.98
0.97
0.96
0.95
0.94
0.93
0.92
0.91
0.9
BONDVILLE ssa(674), with AOT(440) < 0.1
Cumulative Distribution
ssa(674)

Bistatic Lidar Ratio at 173 degrees

Mt. St. Helens, PM1, sza = 77 deg

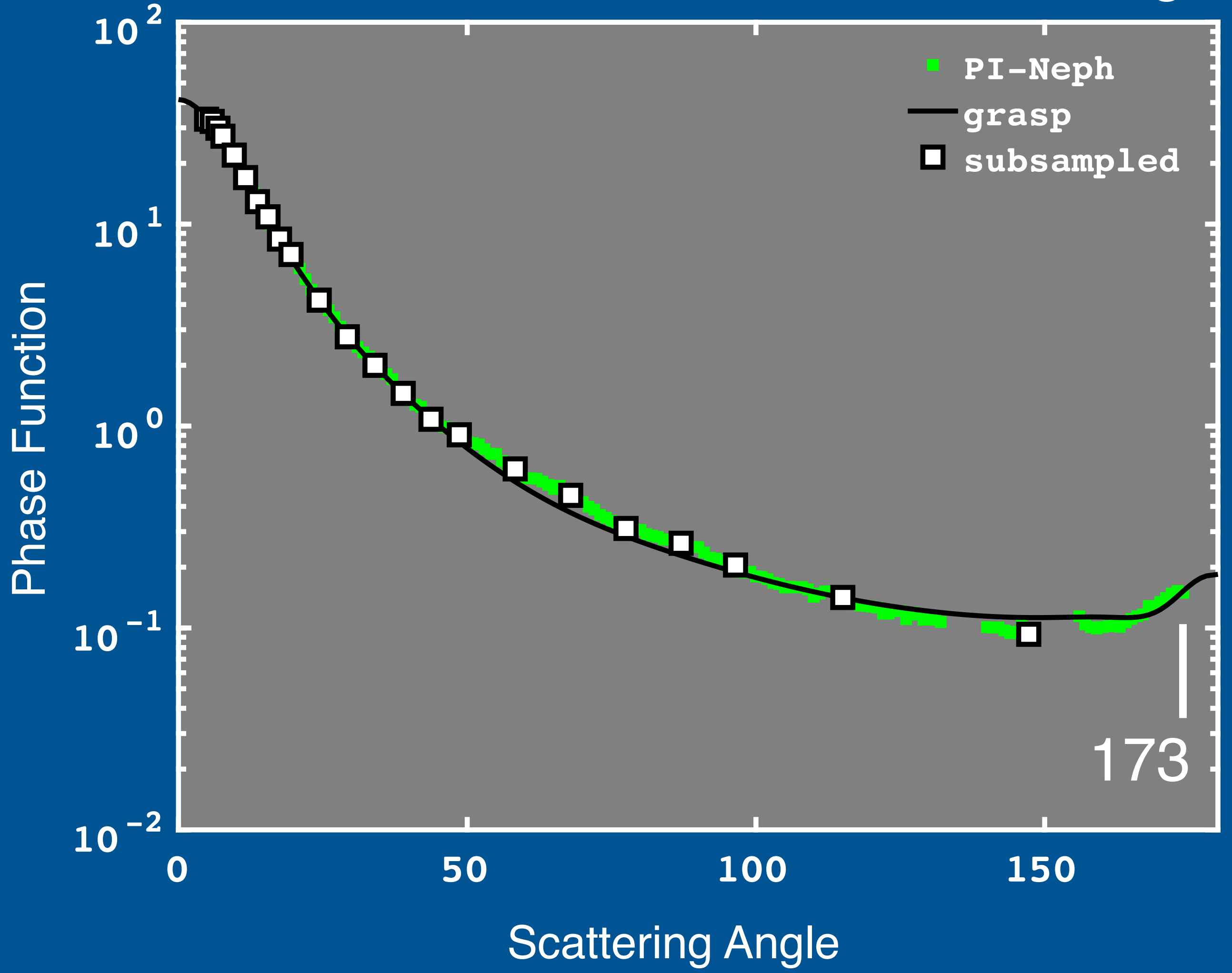

sza = 77 deg

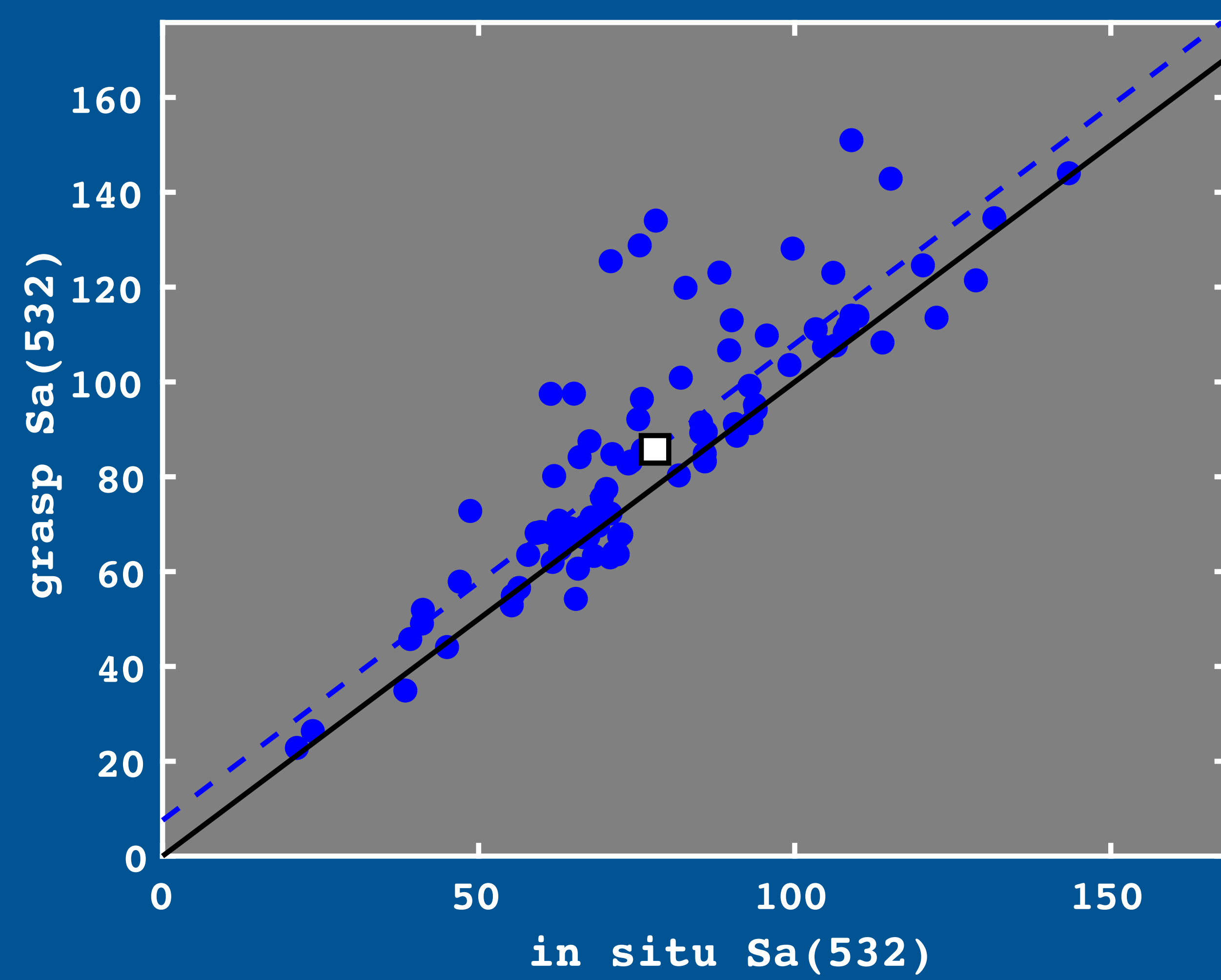

$$S_a = \frac{\text{ext}}{\text{sca}} \frac{4\pi}{P(173)}$$

Bistatic Lidar Ratio at 173 degrees

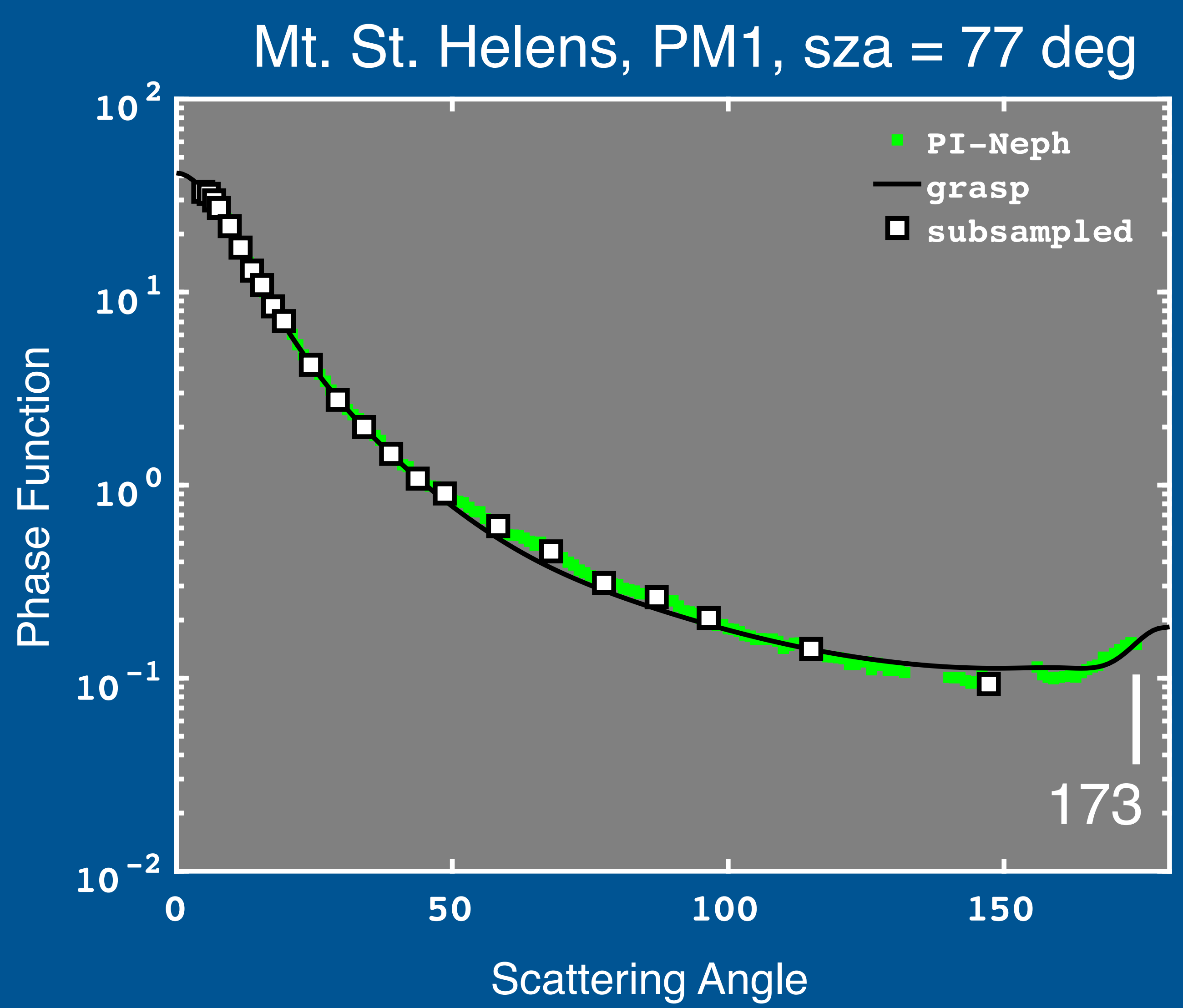

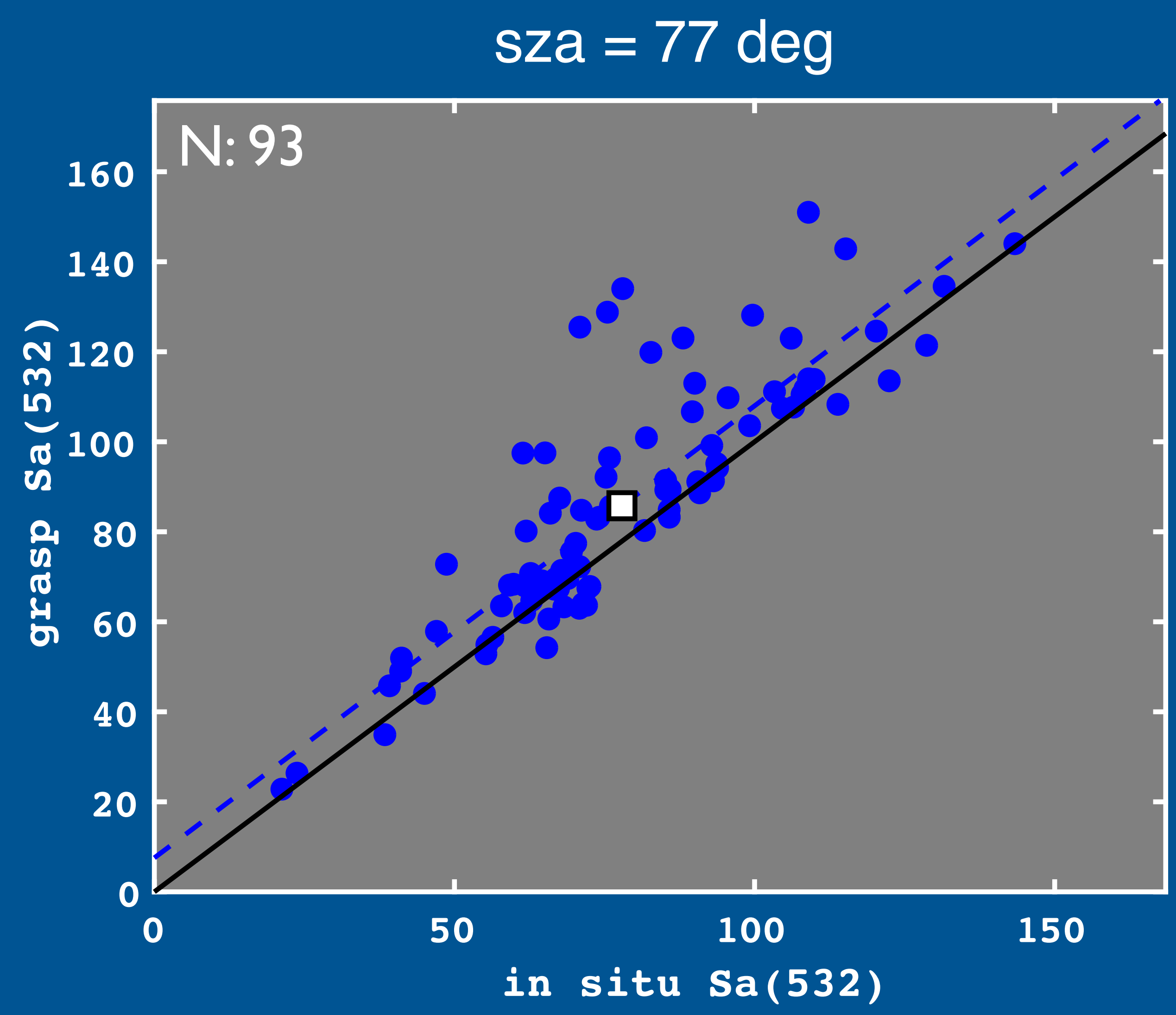

$$S_a = \frac{\text{ext}}{\text{sca}} \frac{4\pi}{P(173)}$$

sza	50	77
correlation coef	0.714	0.860
slope	0.774	1.004
Intercept	19.8 sr	7.5 sr
Absolute bias	1.8 sr	7.9 sr
Relative Bias	1.02	1.10

Comparing Retrieved Size Distributions to Aerodynamic Size

Evaluate size distribution retrievals using the effective variance and effective radius.

$$r_{eff} = \frac{\int r \times \pi r^2 n(r) dr}{\int \pi r^2 n(r) dr}$$

$$v_{eff} = \frac{\int (r - r_{eff})^2 \times \pi r^2 n(r) dr}{r_{eff}^2 \int \pi r^2 n(r) dr}$$

$\chi = 1$

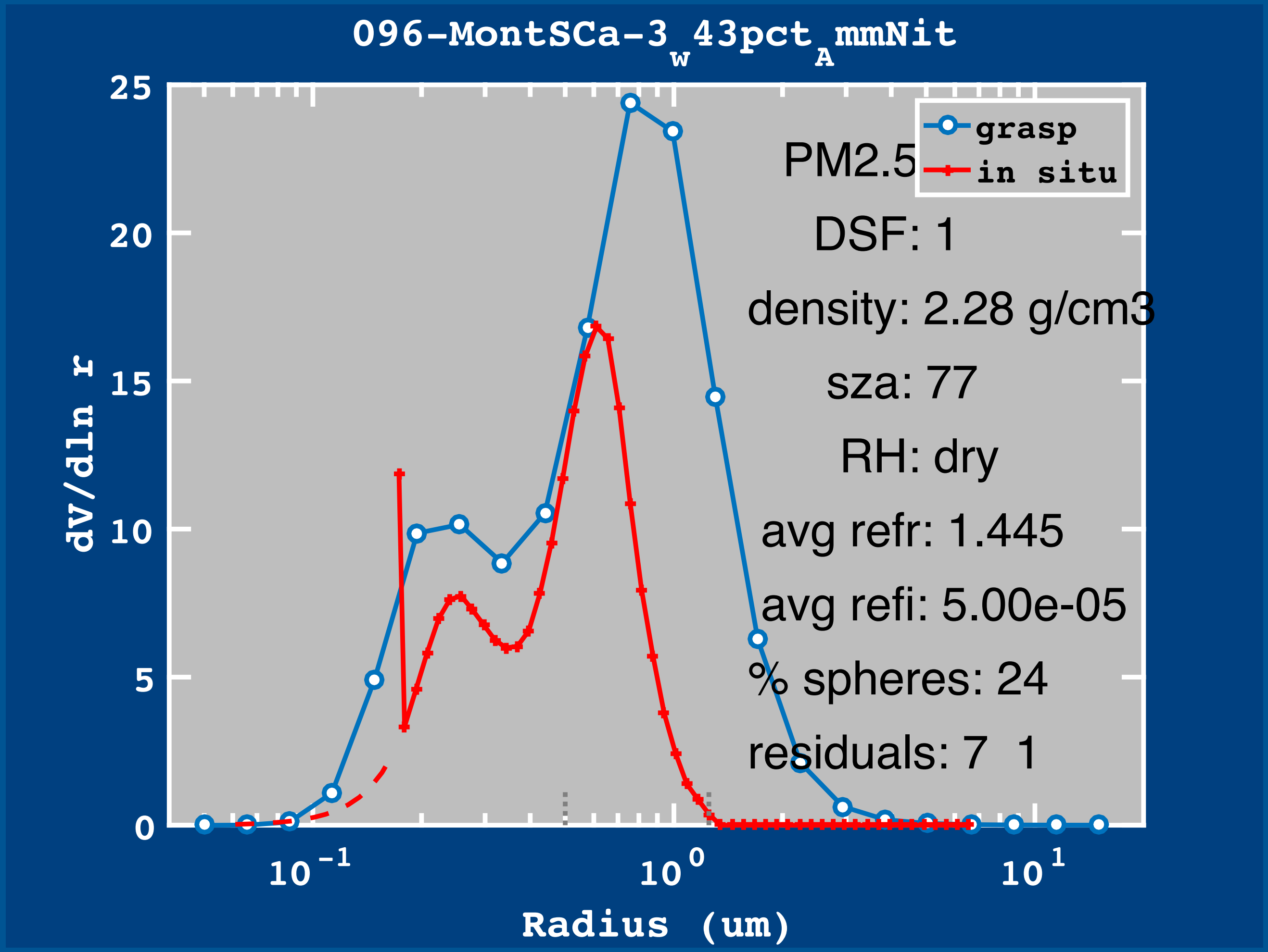

Comparing Retrieved Size Distributions to Aerodynamic Size

Evaluate size distribution retrievals using the effective variance and effective radius.

$$r_{eff} = \frac{\int r \times \pi r^2 n(r) dr}{\int \pi r^2 n(r) dr}$$

$$v_{eff} = \frac{\int (r - r_{eff})^2 \times \pi r^2 n(r) dr}{r_{eff}^2 \int \pi r^2 n(r) dr}$$

$\chi = 1$

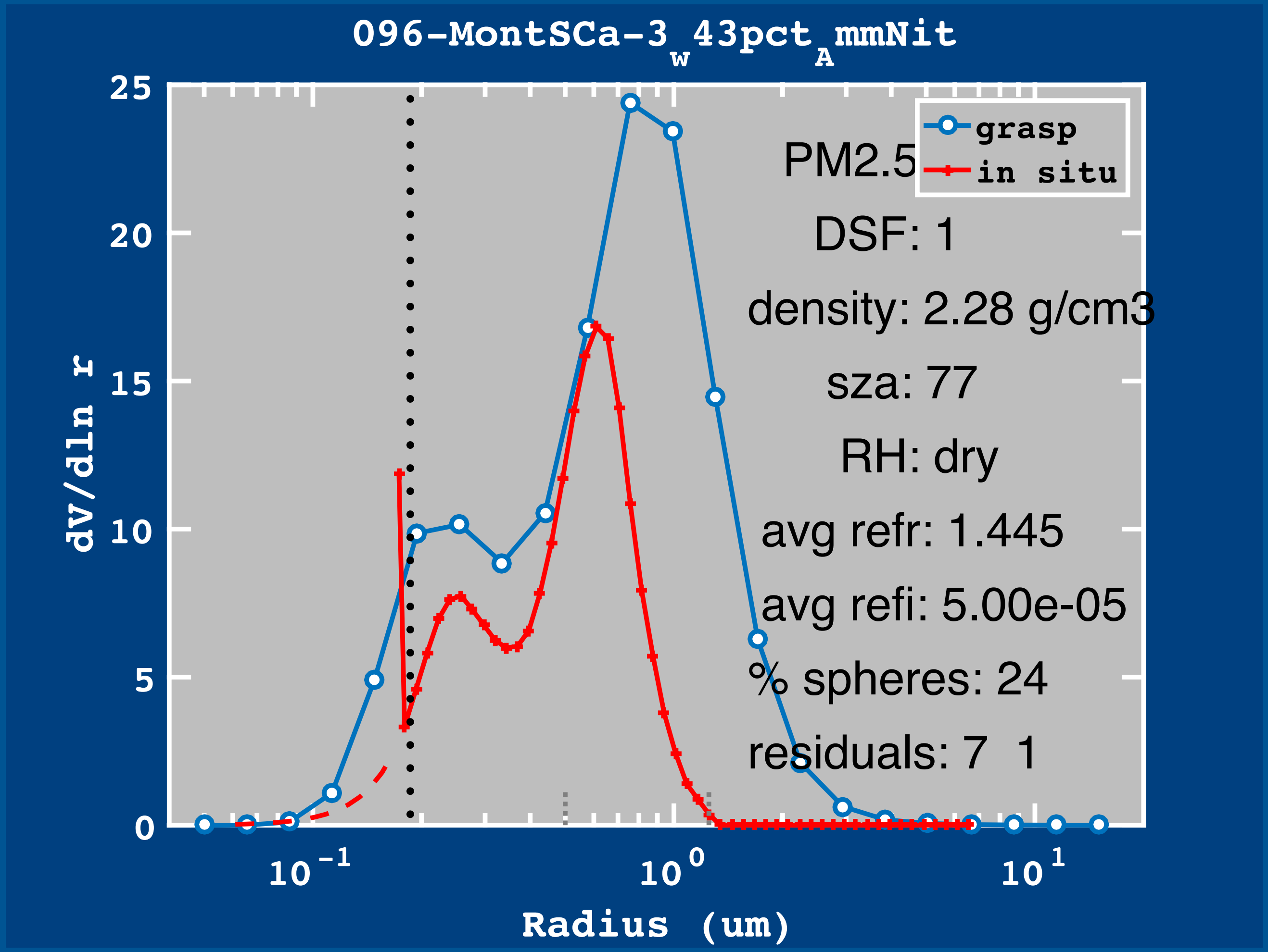

Comparing Retrieved Size Distributions to Aerodynamic Size

Evaluate size distribution retrievals using the effective variance and effective radius.

$$r_{eff} = \frac{\int r \times \pi r^2 n(r) dr}{\int \pi r^2 n(r) dr}$$

$$v_{eff} = \frac{\int (r - r_{eff})^2 \times \pi r^2 n(r) dr}{r_{eff}^2 \int \pi r^2 n(r) dr}$$

$$\chi = 1$$

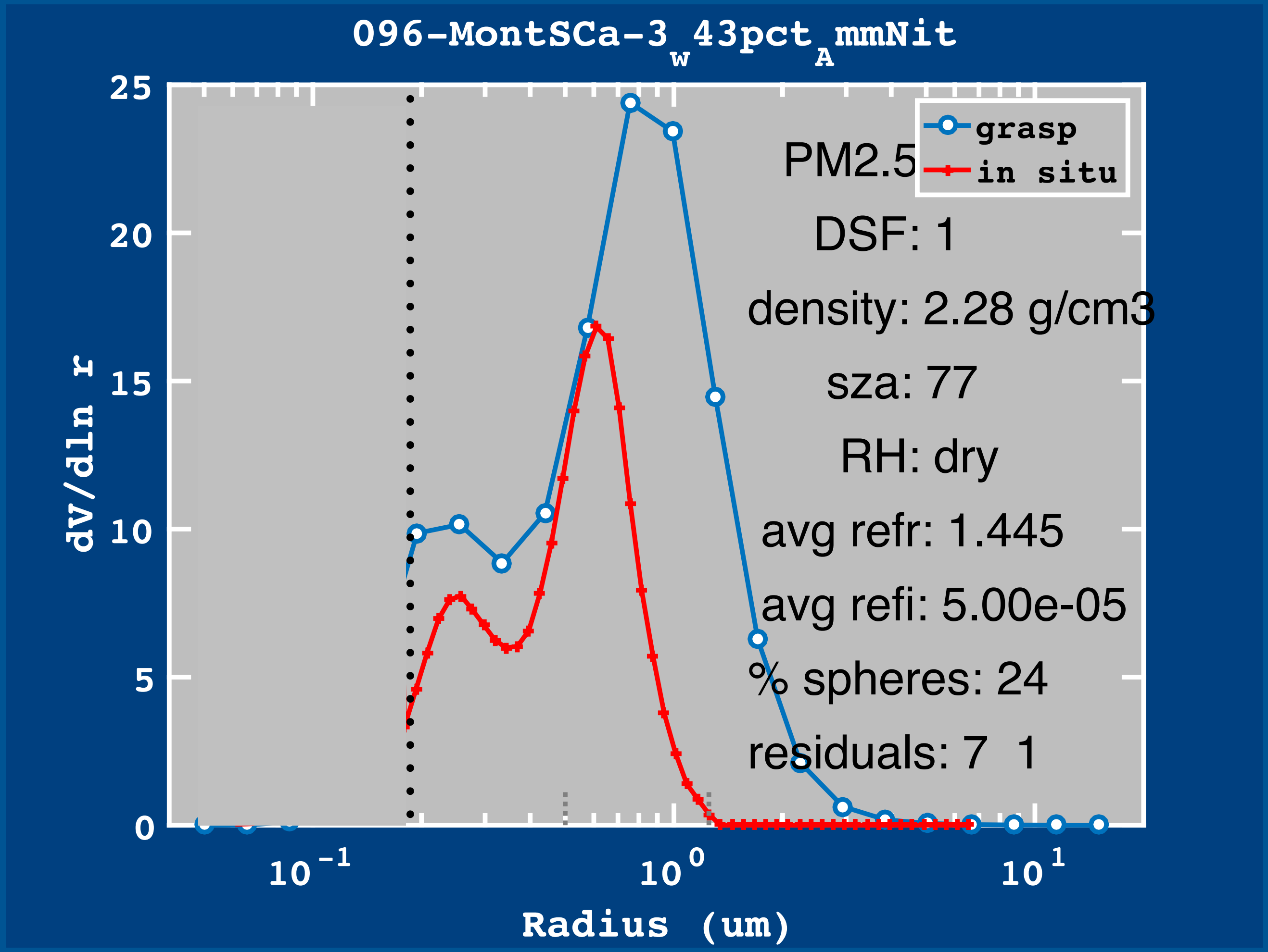

Comparing Retrieved Size Distributions to Aerodynamic Size

Evaluate size distribution retrievals using the effective variance and effective radius.

$$r_{eff} = \frac{\int r \times \pi r^2 n(r) dr}{\int \pi r^2 n(r) dr}$$

$$v_{eff} = \frac{\int (r - r_{eff})^2 \times \pi r^2 n(r) dr}{r_{eff}^2 \int \pi r^2 n(r) dr}$$

$$\rho^* = \rho/\chi = \rho/1.3$$

$\chi = 1$

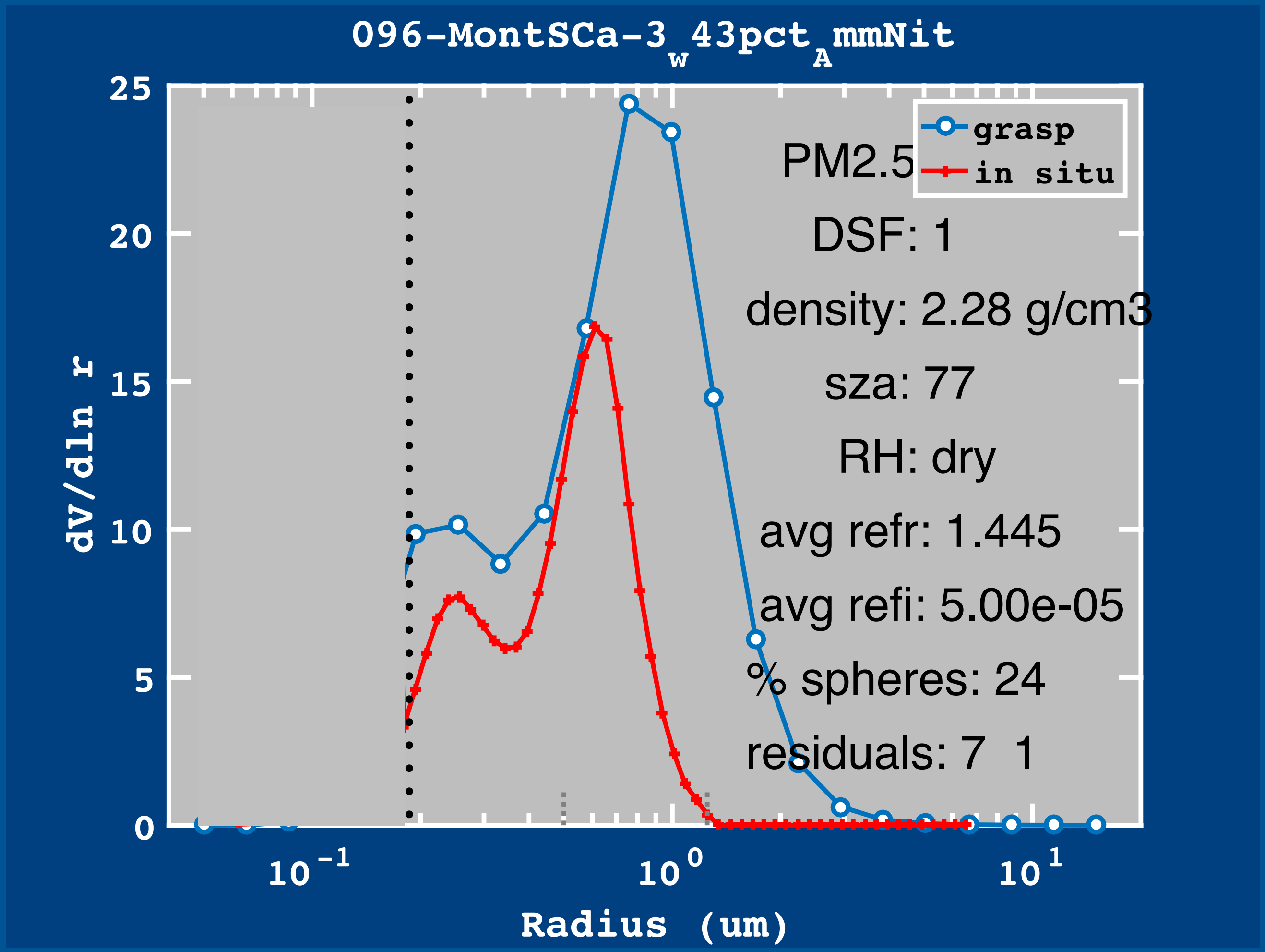

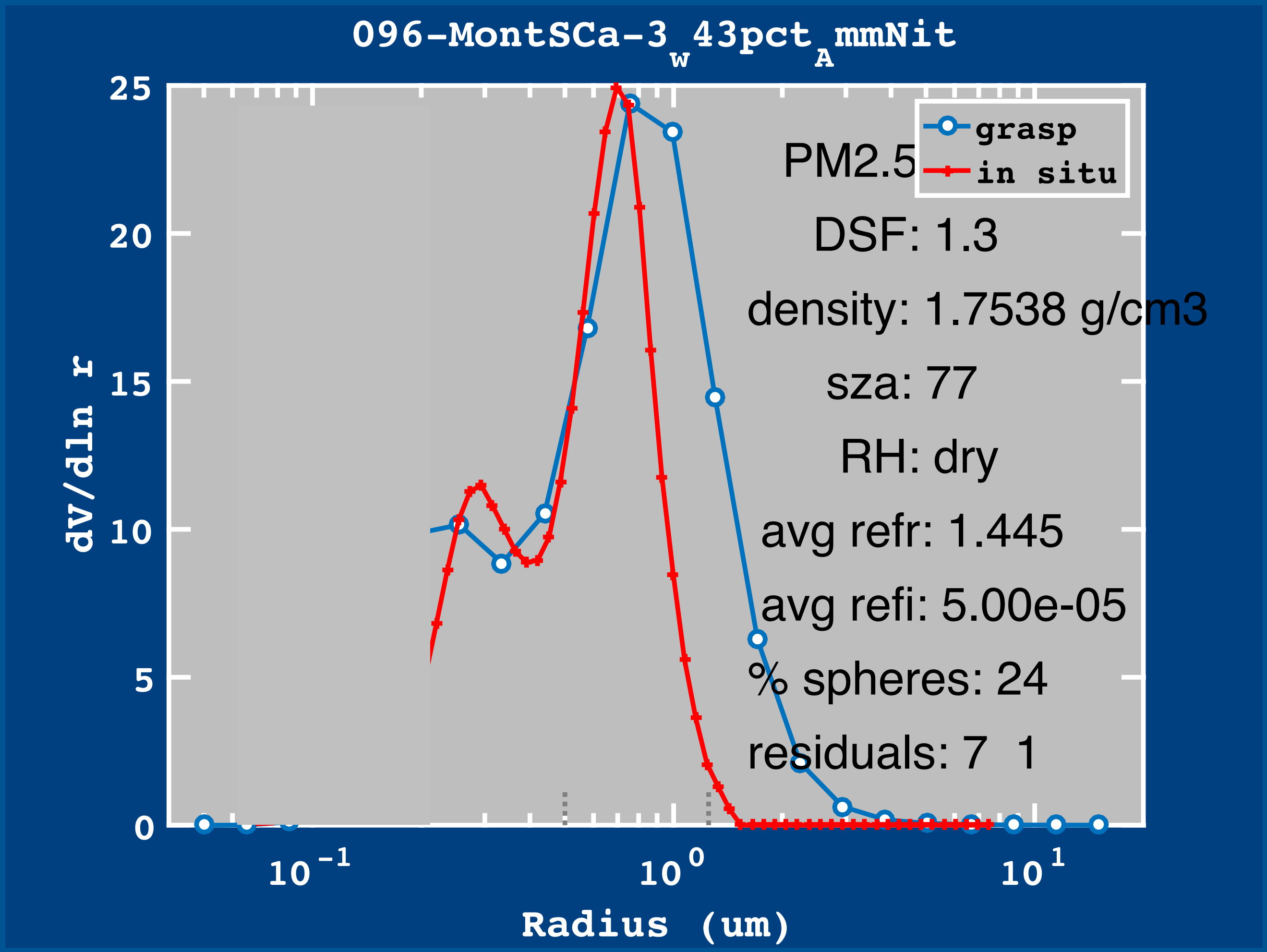

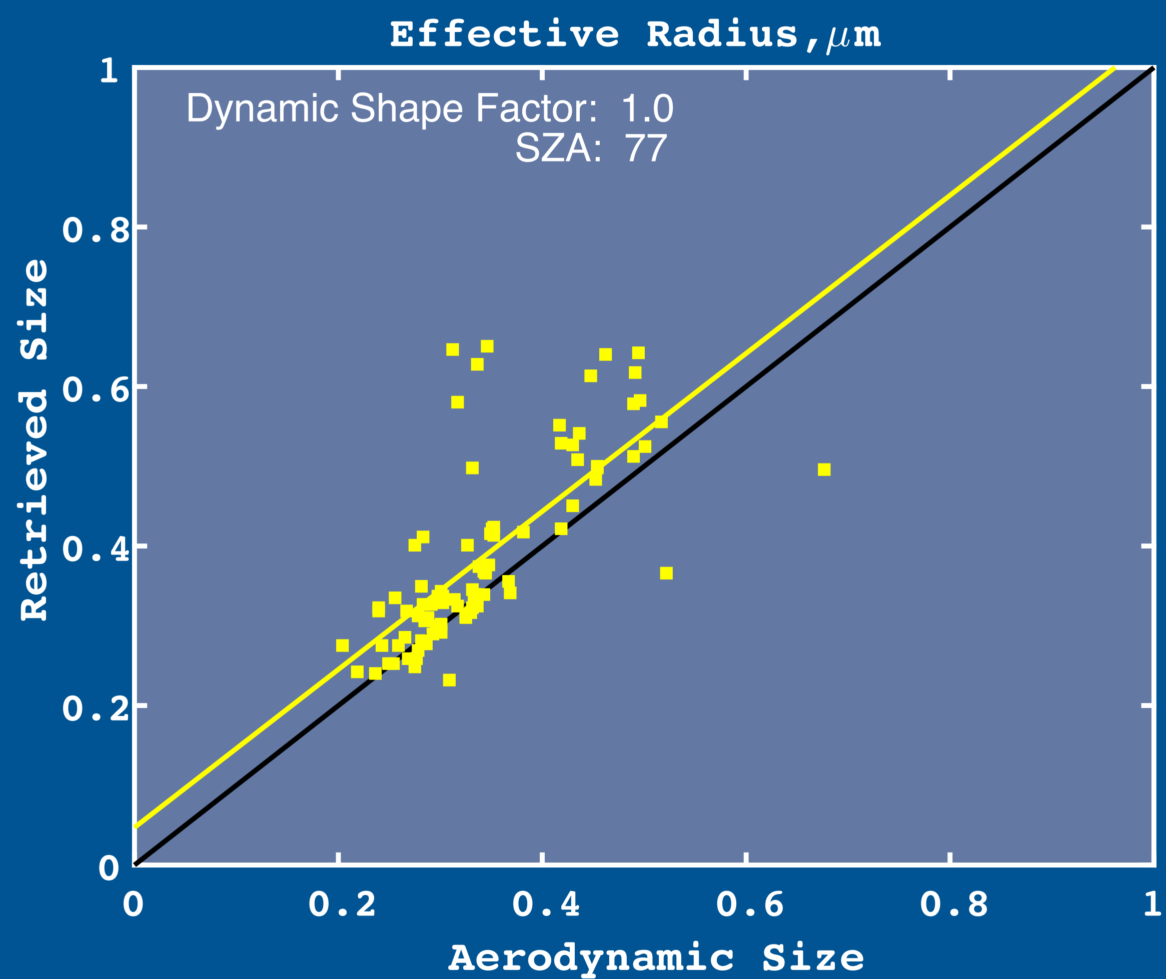

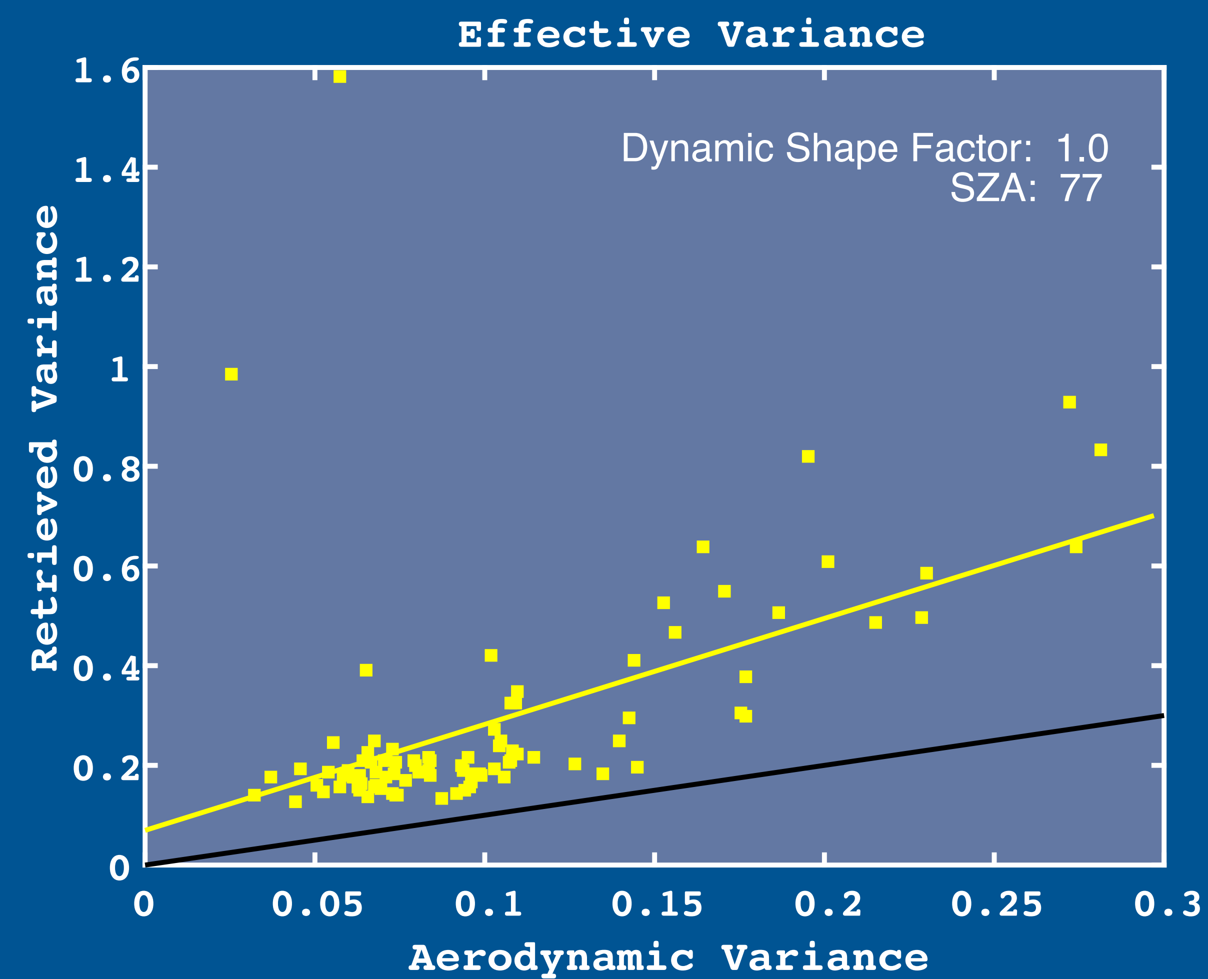

	slope	intcpt	cc	Absolute Bias	Relative Bias	RMS	N	SZA	DSF
R_eff	0.9908	0.0471	0.7227	0.0440	1.1283	0.0898	92	77	1.0
V_eff	2.1260	0.0696	0.5126	0.1863	2.7979	0.2757	92	77	1.0

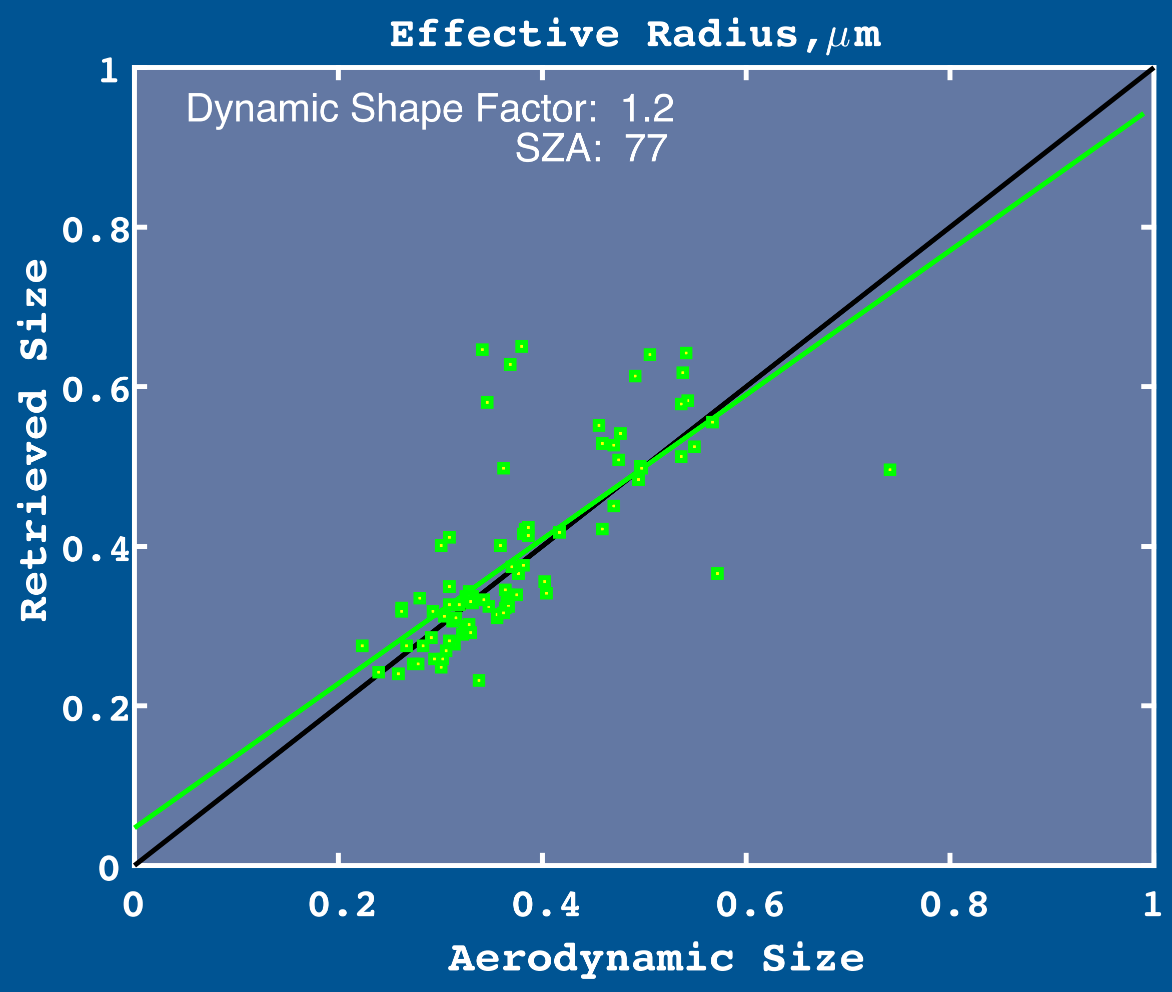

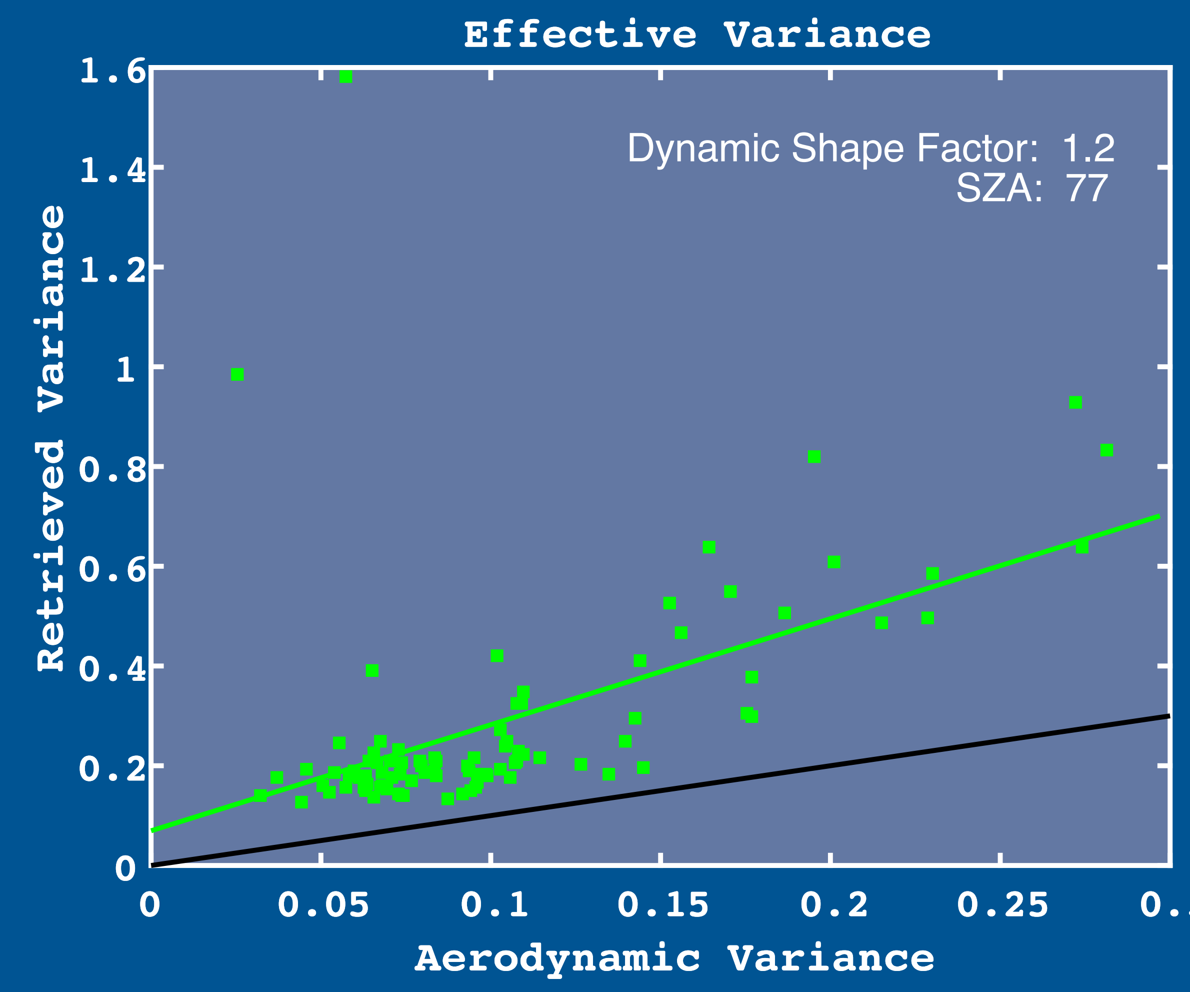

	slope	intcpt	cc	Absolute Bias	Relative Bias	RMS	N	SZA	DSF
R_eff	0.9908	0.0471	0.7227	0.0440	1.1283	0.0898	92	77	1.0
R_eff	0.9044	0.0471	0.7227	0.0113	1.0300	0.0796	92	77	1.2
V_eff	2.1260	0.0696	0.5126	0.1863	2.7979	0.2757	92	77	1.0
V_eff	2.1260	0.0696	0.5126	0.1863	2.7979	0.2757	92	77	1.2

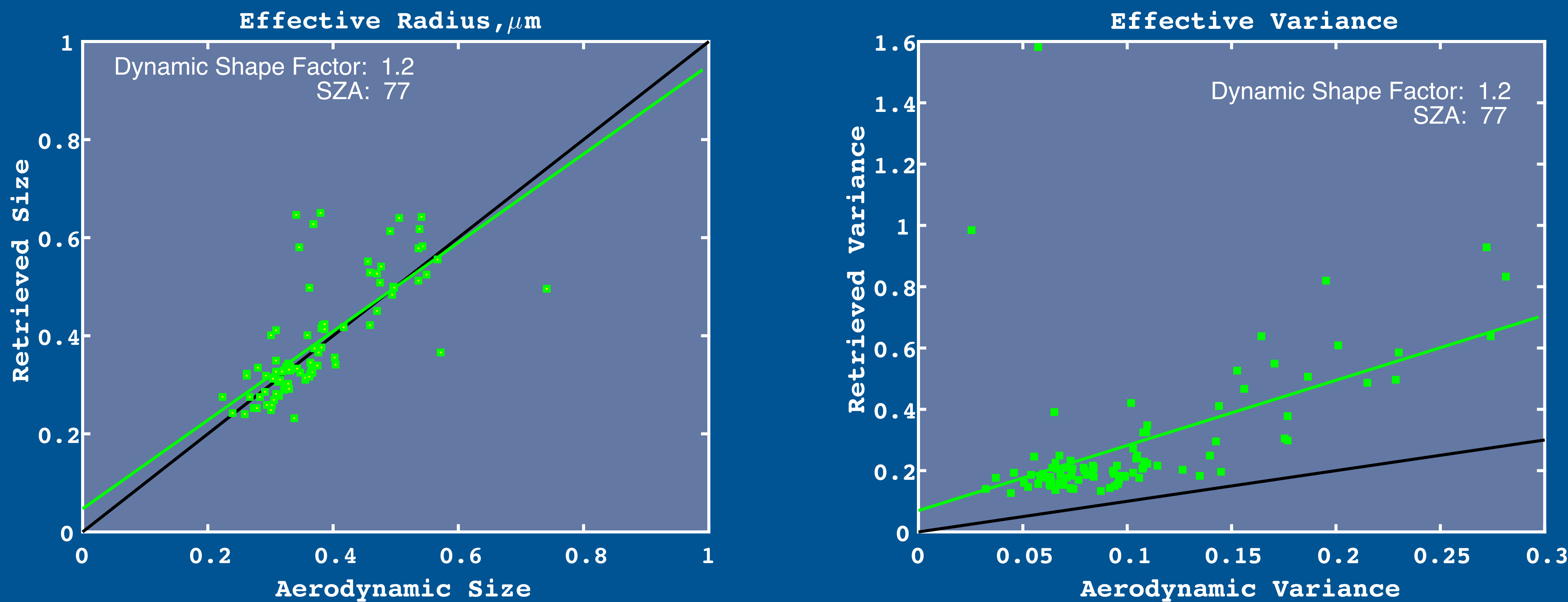

	slope	intcpt	cc	Absolute Bias	Relative Bias	RMS	N	SZA	DSF
R_eff	0.9908	0.0471	0.7227	0.0440	1.1283	0.0898	92	77	1.0
R_eff	0.9044	0.0471	0.7227	0.0113	1.0300	0.0796	92	77	1.2
R_eff	0.8689	0.0471	0.7227	-0.0041	0.9896	0.0794	92	77	1.3
V_eff	2.1260	0.0696	0.5126	0.1863	2.7979	0.2757	92	77	1.0
V_eff	2.1260	0.0696	0.5126	0.1863	2.7979	0.2757	92	77	1.2